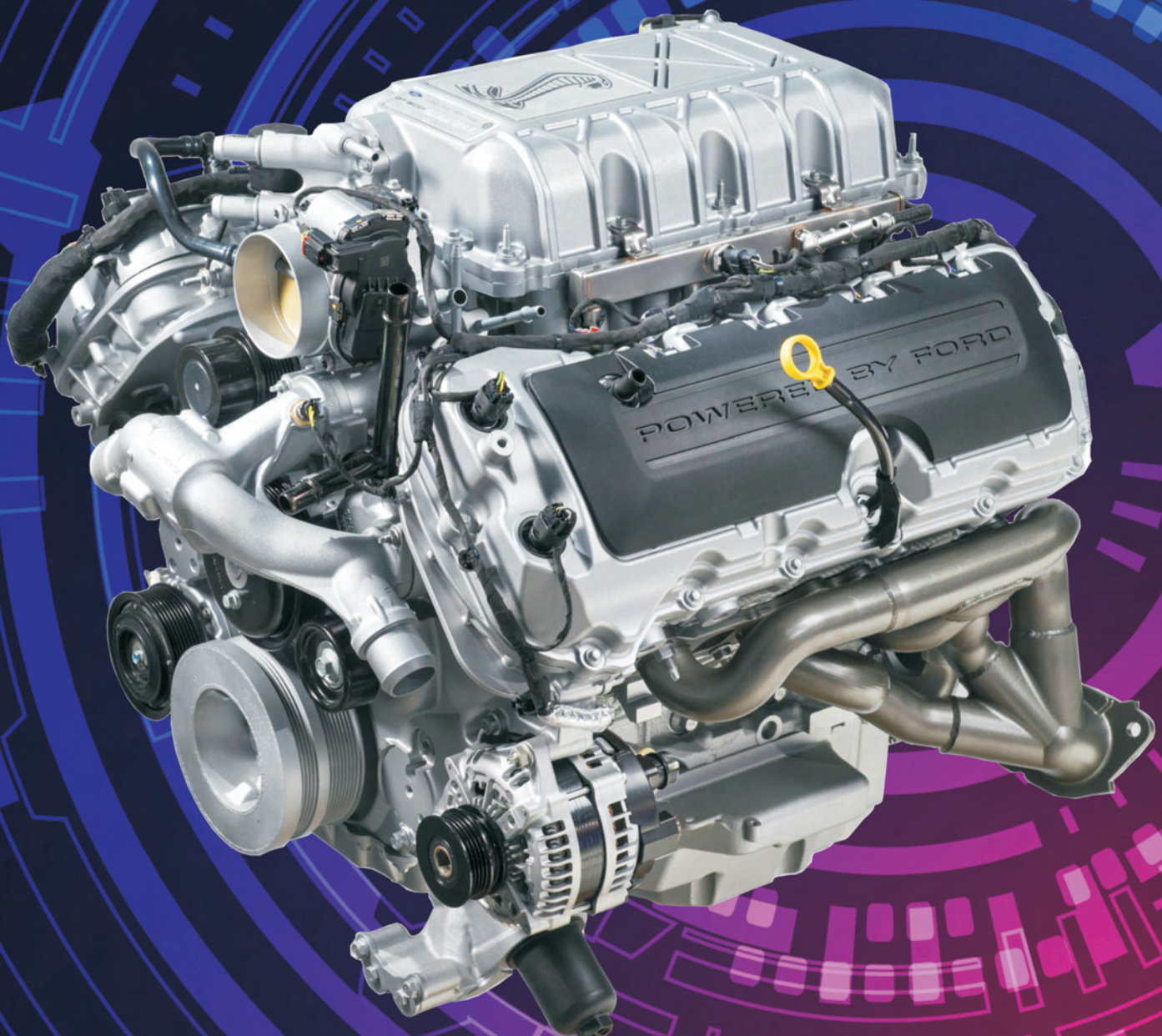




181(2), 2020



COMBUSTION ENGINES



SAMOŁADUJĄCY
ELEKTRYCZNY
NAPĘD
HYBRYDOWY

NADJEŻDŻA HYBRYDOWA REWOLUCJA



Toyota Business
Plus

PTNSS Supporting Members
Członkowie wspierający PTNSS

BOSMAL Automotive Research and Development Institute Ltd
Instytut Badań i Rozwoju Motoryzacji BOSMAL Sp. z o.o.

Motor Transport Institute
Instytut Transportu Samochodowego

Institute of Aviation
Instytut Lotnictwa

Automotive Industry Institute
Przemysłowy Instytut Motoryzacji

The Rail Vehicles Institute TABOR
Instytut Pojazdów Szynowych TABOR

Institute of Mechanised Construction and Rock Mining
Instytut Mechanizacji Budownictwa i Górnictwa Skalnego

Industrial Institute of Agricultural Engineering
Przemysłowy Instytut Maszyn Rolniczych

AVL List GmbH

Solaris Bus & Coach S.A.

Air Force Institute of Technology
Instytut Techniczny Wojsk Lotniczych

Toyota Motor Poland Ltd. Sp. z o.o.

Military Institute of Armoured & Automotive Technology
Wojskowy Instytut Techniki Pancernej i Samochodowej




COMBUSTION ENGINES

A Scientific Magazine

2020, 181(2)

Year LIX

PL ISSN 2300-9896

Editor:

Polskie Towarzystwo Naukowe Silników Spalinowych

43-300 Bielsko-Biała, Sarni Stok 93 Street, Poland

tel.: +48 33 8130402, fax: +48 33 8125038

E-mail: sekretariat@ptnss.pl

WebSite: <http://www.ptnss.pl>

Papers available on-line: <http://combustion-engines.eu>

Scientific Board:

Krzysztof Wiślicki – chairman, Poland (*Poznan University of Technology*)

Yuzo Aoyagi – Japan (*Okayama University*)

Ewa Bardasz – USA (*National Academy of Engineering*)

Piotr Bielaczyc – Poland (*BOSMAL Automotive Research and Development Institute Ltd.*)

Zdzisław Chłopek – Poland (*Warsaw University of Technology*)

Tadeu Cordeiro de Melo – Brazil (*Petrobras*)

Jan Czerwinski – Switzerland (*CJ Consulting*)

Fridrich Dinkelacker – Germany (*Leibniz Universität Hannover*)

Hubert Friedl – Austria (*AVL*)

Barouch Giechaskiel – Italy (*European Commission, JRC Italy*)

Leslie Hill – UK (*Horiba*)

Timothy Jonson – USA (*Corning Inc.*)

Kazimierz Lejda – Poland (*Rzeszow University of Technology*)

Hans Peter Lenz – Austria (*AVL*)

Helmut List – Austria (*AVL*)

Toni Kinunen – Finland (*Proventia*)

David Kittelson – USA (*University of Minnesota*)

Christopher Kolodziej – USA (*Delphi Automotive Systems*)

Hu Li – UK (*University of Leeds*)

Federico Millo – Italy (*Politecnico Torino*)

Jeffrey D. Naber – USA (*Michigan Technological University*)

Andrzej Niewczas – Poland (*Motor Transport Institute*)

Marek Orkisz – Poland (*Rzeszow University of Technology*)

Dieter Peitsch – Germany (*TU Berlin*)

Stefan Pischinger – Germany (*FEV Germany*)

Andrzej Sobiesiak – Canada (*University of Windsor*)

Stanisław Szwaja – Poland (*Częstochowa University of Technology*)

Piotr Szymański – Nederlands (*European Commission, JRC*)

Leonid Tartakovsky – Israel (*Technion – Israel Institute of Technology*)

Andrzej Teodorczyk – Poland (*Warsaw University of Technology*)

Xin Wang – China (*Beijing Institute of Technology*)

Thomas Wallner – USA (*Argonne National Laboratory*)

Michael P. Walsch – USA (*International Council on Clean Transportation*)

Mirosław Wendeker – Poland (*Lublin University of Technology*)

Piotr Wolański – Poland (*Warsaw University of Technology*)

Mirosław Wyszyński – UK (*University of Birmingham*)

Contents

<i>Orkisz M., Kuźniar M.</i> 3E – A new paradigm for the development of civil aviation (CE-2020-201)	3
<i>Chwist M., Pyrc M., Gruca M., Szwaja M.</i> By-products from thermal processing of rubber waste as fuel for the internal combustion piston engine (CE-2020-202)	11
<i>Łoza Ł.</i> The analysis of vibrations in the vehicle with naturally aspirated and turbocharged gasoline engine (CE-2020-203)	19
<i>Kuryka K., Pielecha J.</i> Cold start emissions from gasoline engine in RDE tests at different ambient temperatures (CE-2020-204).....	24
<i>Pielecha I.</i> Numerical investigation of lambda-value prechamber ignition in heavy duty natural gas engine (CE-2020-205)	31
<i>Kniaziewicz T., Zacharewicz M.</i> Evaluation of adequacy of a model of a marine diesel engine based upon empirical research (CE-2020-206)	40
<i>Szwajca F., Wisłocki K.</i> Thermodynamic cycles variability of TJI gas engine with different mixture preparation systems (CE-2020-207).....	46

Declaration of the original version
The original version of the Combustion Engines journal
is the printed version.

Editorial:

Institute of Combustion Engines and Powertrains
Poznan University of Technology
60-965 Poznan, Piotrowo 3 Street
tel.: +48 61 2244505, +48 61 2244502
E-mail: papers@ptnss.pl

Prof. Jerzy Merkisz, DSc., DEng. (Editor-in-chief)
Mirosław Kozak, DSc., DEng. (Editorial Secretary for Science)
Prof. Ireneusz Pielecha, DSc., DEng.
Wojciech Cieślik, DEng. (Technical Editors)
Joseph Woodburn, MSci (Proofreading Editor)
Wojciech Serdecki, DSc., DEng. (Statistical Editor)
and Associate Editors

Editor

Polish Scientific Society

of Combustion Engines

43-300 Bielsko-Biała, Sarni Stok 93 Street, Poland

tel.: +48 33 8130402, fax: +48 33 8125038

E-mail: sekretariat@ptnss.pl

WebSite: <http://www.ptnss.pl>

The Publisher of this magazine does not endorse the products or services advertised herein.

The published materials do not necessarily reflect the views and opinions of the Publisher.

© Copyright by

Polish Scientific Society of Combustion Engines

All rights reserved.

No part of this publication may be reproduced, stored in a retrieval system or transmitted, photocopied or otherwise without prior consent of the copyright holder.

Subscriptions

Send subscription requests to the Publisher's address.

Cost of a single issue PLN 30 + VAT.

Preparation for print

ARS NOVA Publishing House
60-782 Poznań, Grunwaldzka 17/10A Street

Circulation: 150 copies

Printing and binding

Zakład Poligraficzny Moś i Łuczak, sp. j.,
Poznań, Piwna 1 Street

The journal is registered
in the Polish technical
journals content database
– BAZTECH www.baztech.icm.edu.pl



The journal is listed
in the international
database

IC Journal Master List

– Index Copernicus www.indexcopernicus.com



Papers published in the

Combustion Engines

quarterly receive 20 points as stated
by the Notification of the Minister of Science
and Higher Education dated 31 July 2019.

Cover

I – Ford Mustang Shelby GT500 engine
([fot. us.motorsactu.com](http://us.motorsactu.com)); background (Modern background design –
Designed by Freepik, pl.freepik.com)

IV – Electric superchargers ([fot. www.autocar.co.uk](http://www.autocar.co.uk))

3E – A new paradigm for the development of civil aviation

Nowadays, in civil aviation, issues related to improving efficiency, reducing the costs of air operations as well as the negative impact of air transport on the environment are of increasing importance. These ideas allow the formulation of the paradigm relating to the development of air transport – ‘more Efficiently, more Economically, more Eco-friendly – 3E’. The article presents in a cross-sectional and synthetic way research conducted by leading scientific centres around the world as well as prototype aviation constructions designed by companies from the aviation industry. Benefits and disadvantages of future propulsions, such as purely electric, hybrid and distributed propulsions, were presented. Conclusions were formulated regarding further possible directions of civil aviation development, taking into account the improvement of its efficiency as well as economic and ecological indicators.

Key words: airplane, electric propulsion, hybrid propulsion, distributed propulsion, reduction of emission exhaust, reduction of noise, decrease of fuel consumption

1. Introduction

Aviation is the branch of transport that has significantly contributed to globalization of the world. Accompanying the development of aviation, until recently, the ‘Higher, Faster, Farther’ paradigm lost its significance in the last years. The currently noticeable trend of aviation development leads to the fulfilment of criteria more favourable to the protection of man and his ecosystem. Permanently emerging cognitive and utilitarian research programs try to redefine the existing solutions for the needs of the new paradigm. Among the examples of these activities there are studies on improving the airspace capacity and more efficient airspace management, as well as the works on improving and optimizing the operation parameters of internal combustion engines as well as programs aimed at determining the design assumptions for propulsions based on hybrid, combined or all-electric systems. The effect of such solutions is the possibility to reduce journey costs by reducing fuel consumption, as well as noise and toxic emissions to the atmosphere.

Due to the above, the authors propose to replace the paradigm mentioned above with a new, more timely one, taking into account current trends – the 3E’ paradigm – ‘more Efficiently, more Economically, more Environment’.

The pro-environmental trend is reflected in the regulations developed and constantly improved in the scope of reducing the negative impact of air transport on the natural environment. The first international regulations regarding the reduction of fuel consumption, pollutants and noise emissions entered into force in 1972 (Annex 16 to the ICAO Convention) [29], and in March 2018 the new wording of Annex 16 entered into force. It regulates emission of pollutants and noise limits for newly designed aircraft structures in accordance with the recommendations of CAEP (ICAO Technical Committee for Environmental Protection).

At the same time, there emerge declarations, international research programs and initiatives of international, governmental and non-governmental organizations, as well as aviation companies who aim at the sustainable and re-

sponsible development of aviation. Such a development is possible to achieve through the following tasks [29]:

- stabilizing CO₂ emissions in the aviation sector at the level of 2020 (through so-called carbon-neutral growth),
- reducing CO₂ emissions in aviation by 2050 by 50% (compared to 2005),
- reducing the carbon footprint in air freight,
- fleet rejuvenation and modernization,
- investing in bio jet fuels (biofuels for aircraft turbine engines),
- reducing mass of aircraft,
- developing e-freight (called paperless cargo),
- developing lightweight ULDs.

Many research works are being currently carried out in line with the above-mentioned tasks, such as works related to increasing the efficiency of air traffic, e.g. the SESAR program. Within its framework, attempts are being made to develop a new approach to flight planning and to make more efficient use of cargo and passenger spaces in aircraft. In addition, research related to the optimization of flight trajectory in terms of minimizing flight time or fuel consumption indicate that it is possible to achieve a decrease in pollutants emissions and fuel consumption on a given route [24-29].

However, the goals assumed in the longer term (for the year 2050) require developing new technical solutions. Composite materials have a growing share in newly emerging aviation constructions, which clearly affect the decrease in flying vehicles mass. Propulsion efficiency has been increased by developing new propeller aerodynamic systems [31], as well as by increasing the exhaust gas temperature before the high pressure turbine in the case of turbine engines [5].

In order to increase further the efficiency of aircraft constructions, new aerodynamic solutions (e.g. the flying wing shown in Fig. 1) are being sought [21], as well as propulsion systems envisaged in future aircraft, such as distributed propulsion [4].

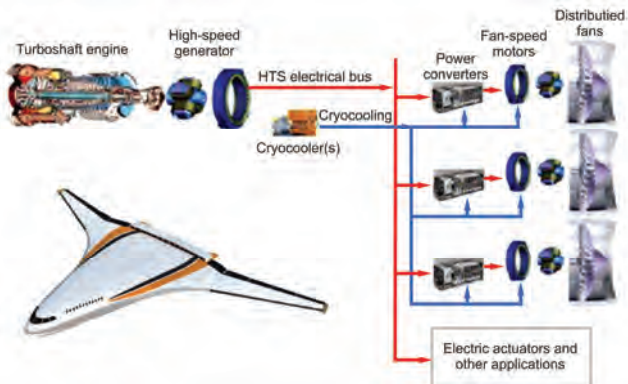


Fig. 1. Airplane in a flying wing configuration with a hybrid, distributed propulsion [21]

The distributed propulsion is characterized by the use of a number of electric motors (EM) together with propellers of a small diameter [31] or flow engines of the low thrust class [4]. They are usually placed on the wing leading edge or at the fuselage. This division and location of the propulsion is aimed at improving the propulsion efficiency, improving the aerodynamic parameters of the aircraft and a better balance of energy consumption during the flight [7, 11, 20].

In the presented publication, the authors focused on the analysis and synthesis of the last of the above-mentioned research problems – the possibility of using propulsion systems in aviation based on hybrid, combined or all-electric drive.

2. Research problem

The current trend combining activities increasing the efficiency and effectiveness as well as the environmental performance (3E) of aircraft propulsions forces the development of new technical solutions or improvement of current ones.

One concept is to use an electric propulsion to propel aircraft. Electric motors are characterized by high efficiency, reaching up to 95% [10, 15, 34], and in relation to piston engines of the same power they show a better power-to-weight ratio. For comparison, the Emrax 268 engine, which weighs 11 kg, generates 110 kW of peak power and 500 Nm of peak torque [34]. In contrast, the Wankel AG 807 tgi piston rotary engine, which weighs 35 kg, for 75 kW of power, generates 80 Nm of torque [37]. In the case of an electric motor, attention should also be paid to [2, 3, 18]:

- lack of complicated equipment, nor heavy cooling and oil system,
- lower vibrations generated by the propulsion system, which, combined with the lower mass of the engine, allows building simpler and lighter systems integrating the propulsion with the plane,
- high reliability,
- simple operation.

Among other things, these properties have caused the popularity of the use of electric propulsion in both amateur modelling aircraft and unmanned aerial vehicles (UAVs). Initial selection of the engine for driving an unmanned vehicle requires first of all determining the take-off mass of the vehicle [1]. Based on this information and aerodynamic

data, based on the known power method [6], the value of the power required for the aircraft flight is determined. The power of the propulsion system depends on the propeller efficiency for a given flight speed and the power received by the propeller.

It seems interesting to compare the performance of unmanned vehicles of short or vertical take-off (VTOL) presented, e.g. in [11], where the performance of combustion and electric vehicles with the same take-off mass is taken. It was shown that for the same take-off mass and same power generated at the start of the vehicle, the range of UAV equipped with electric propulsion is reduced threefold.

For short missions it is not necessary to construct complicated hybrid propulsion and purely electric propulsion is sufficient [14]. In addition, the authors show that all-electric propulsion systems are still too heavy, and the combustion-electric hybrid systems do not offer noticeable benefits over conventional configurations. However, they state that for a greater flight distance, hybrid technology constitutes a more advantageous propulsion system compared to a purely combustion system, even with the energy density for the battery of 500 Wh/kg. The authors also show that electric VTOL aircraft will not be able to cover a distance of 500 km, even with a minimum take-off mass. In addition, based on their computational research, the authors state that the use of distributed propulsion allows more efficient use of energy stored on board.

Among the studies on current trends in aviation technology, the use of electric and hybrid propulsions in small and passenger aviation is described, which was presented in the doctoral dissertation [23]. An interesting concept presented in the dissertation is the propulsion using ducted fans driven by electric motors. These fans generate up to 80% of the thrust necessary to flight. The electricity needed for the fans to operate and the missing value of thrust for the flight is generated by the turbine engine. This work also describes the concept of a by-pass turbine-electric engine. A traditional turbine engine would work in the internal channel of this engine and there would be no power turbine to drive the fan. Due to this arrangement, it would be possible to save fuel during the flight. The impact of this type of propulsion on reducing NO_x and CO₂ emissions during aircraft operation was also described.

Based on the cited research, it can be concluded that the main disadvantage of electric propulsion systems used in aircraft constructions is their high mass. The high mass of the batteries together with their relatively small capacity results in a low value of the energy density stored on board – compared to e.g. the energy density stored in the hydrocarbon fuel. These properties affect the limited range or duration of the flight, which are affected by increased requirement for power during manoeuvres, such as take-off or climb. Therefore, it seems interesting (until an energy source with sufficient energy density is developed) to develop a hybrid propulsion that would allow to increase the usable parameters of the aircraft.

A hybrid system is the one where the energy necessary for the flight of an aircraft comes from more than one source. The most common solutions are electric-combustion systems, where energy comes from both the combustion of

hydrocarbon fuel and the energy accumulated in batteries. The system in which fuel cells are used to replace the combustion engine is also called hybrid. An important energy indicator determining the type and design of the propulsion system is so-called degree of hybridization [3, 10, 15, 16]. The degree of hybridization is the ratio of energy from the battery to the total energy accumulated on board the aircraft, and can be described by the formula (1):

$$H = \frac{E_{\text{Bat}}}{E_{\text{Tot}}} \quad (1)$$

where: H – degree of hybridization, E_{Bat} – the amount of energy stored in batteries, E_{Tot} – total energy accumulated on board the aircraft.

At low values of the degree of hybridization, the amount of energy stored in the batteries is small compared to energy coming from a combustion engine or fuel cell. For high values of the degree of hybridization, it is the combustion engine or the fuel cell that takes over the role of an auxiliary energy source.

The hybrid propulsion can be constructed in series or in parallel and their schematic diagrams are presented in Fig. 2.

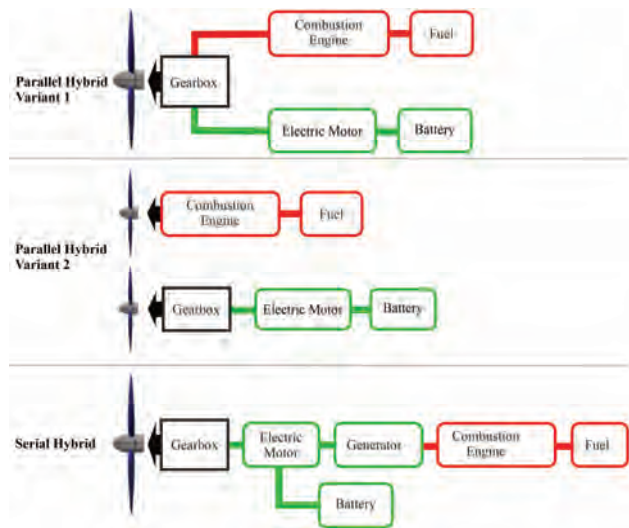


Fig. 2. Schematic diagrams of hybrid propulsion [8]

The serial propulsion is characterized by the fact that the propeller is driven exclusively by an electric motor [7–11]. The energy needed for flight in systems with a low degree of hybridization is generated by a piston or turbine combustion engine, e.g. APU engines or other solutions presented in [3, 28, 33].

The electrical system is complemented by the battery to provide energy when the combustion engine or fuel cell is not generating electricity. In systems with a high degree of hybridization, the combustion unit and electric generator are used to recharge the battery and maintain its capacity, thereby increasing the range and flight duration. The combustion engine-generator system is called a range extender. In this case, the role of the range extender can be taken over by a fuel cell, e.g. a hydrogen fuel cell, as in the AOS H2 motor glider [20].

In a hybrid serial propulsion system, the propeller is driven solely by an electric motor of dimensions adapted to

the maximum energy requirements – energy consumption depends on the aerodynamic performance of the propeller and the requirements of the aircraft performing a given flight mission. A multi-propeller system, where each propeller is driven by its own electric motor, is also possible. Depending on the system layout and degree of hybridization, the combustion engine can work at a constant speed and constant level of developed power, which enables optimizing it for one specific design point, i.e. set the operating range of the internal combustion engine to work at its highest thermal efficiency. This will ensure the highest power obtained on the propeller shaft with the lowest specific fuel consumption of the engine. The engine drives a mechanically coupled generator that generates electricity, which is then fed into the energy management system. The power can be directed directly to the electric motor that drives the propeller or the power is divided between the battery (to charge it) and the motor driving the propeller. Such a system is safer due to the fact that the battery is a safety buffer in case of a failure of the charging system or running out of the fuel [10]. The energy management system also enables to supply additional energy from the battery to the aircraft's propulsion if the required power is higher than that which the charging system can provide. Thus, if the combustion generator or fuel cell possesses the parameters (obtained electric power) enabling efficient flight, the electric generator and battery can provide the excess power used for take-off and climb of the aircraft.

If the battery pack is properly selected for the airframe in terms of energy and mass, the aircraft with serial hybrid propulsion system can also operate in all-electric mode. This may be desirable from the point of view of noise and pollutants emissions reduction [29], especially during the take-off and initial climb phase [26, 27].

A parallel hybrid is a configuration in which the internal combustion engine and electric motor operate in mechanical coupling [11, 12]. In the case of a parallel hybrid propulsion system, the electric motor and the internal combustion engine are mechanically connected to the propeller shaft, often via a gearbox. For a system with a low degree of hybridization, an electric (of low power) motor will support the internal combustion engine during the take-off and climb to achieve the assumed rotational speed of the propeller and the steady engine parameters of the most favourable performance characteristics (the ratio of developed power to fuel consumption).

It should be noted that an implementation in which an electric motor drives one propeller and an internal combustion engine drives another propeller [11] is also considered a parallel hybrid. The total required power is divided between internal combustion engine and electric motor, which corresponds to the designated degree of hybridization of the structure. This enables to optimize the construction by applying a smaller internal combustion engine, as well as a properly selected electric motor. Compared to the serial configuration of the hybrid propulsion, the electric motor in the parallel hybrid propulsion system can be smaller and lighter because it provides only a certain amount of the total power and constitutes in this regard an auxiliary engine. Since the power obtained by the internal combustion engine

is mechanically transferred to the propeller, there is no dedicated generator in such a system. This reduces the complexity and mass of the propulsion unit and positively affects its propulsion efficiency [31].

The application of this type of solutions in General Aviation (GA) aircraft was analysed in [9]. The authors point out that the use of traditional methods to determine aircraft geometry in the conceptual design phase is inadequate for hybrid or electric propelled aircraft. They propose to reduce the computed value of wing area obtained via computations using a traditional approach to design by increasing the power of the engine. The approach presented could be beneficial during the high-speed flight phase. When taking-off and flying at low speeds, the excess power needed may limit the overall range and duration of the flight. The authors rightly noticed that for the traditional configuration of the aircraft the most advantageous is the parallel system – an electric motor and internal combustion engine driving the propeller together. This is due to the characteristics of the combustion engine. The authors did not mention that the internal combustion engine achieves its greatest efficiency for the flight range, while in transient states it would be advisable to use an electric motor as a booster. This is because a serial propulsion or propulsion using range extender may be more advantageous when adopting propulsion using more than one propeller. The authors also state that hybrid and electric propulsion can be successfully used on light aircraft and GA.

Increasing efficiency (increasing range and reducing fuel consumption) and reducing environmental impact (reducing emissions) constitute the issue raised in [13]. The authors presented the possibilities of adopting aircraft structure optimization to reduce fuel consumption and increase the aircraft range. This issue is the foundation for multi-criteria optimization of the aircraft structure or flight parameters with the aim of improving the environmental and performance indicators of the aircraft. Optimization can relate to both the selection of aircraft flight trajectories and the reduction of aircraft mass. Properly designated flight path can significantly affect the performance of the aircraft and the propulsion system, such as fuel consumption or pollutants emission, as shown in [24–29]. On the other hand, the optimized mass of the aircraft significantly reduces fuel consumption, which is associated with lower power and thrust required for an aircraft's steady flight at a certain speed [20, 31]. Such an approach to aircraft design is inline with the '3E' paradigm.

The hybrid propulsion system combines the advantages of the systems based on hydrocarbon fuel and the systems powered by batteries [8]. It can contribute to more efficient operation of internal combustion engines assisted by an electric motor in transient states. In addition, hybrid designs offer greater flexibility for comprehensive aircraft design, such as distributed propulsion. This is possible because the power of an internal combustion engine can be transferred to light electric motors by means of wires instead of many heavy engines or drive shafts, as noted by the authors of [8]. The authors, after analysing various configurations of hybrid propulsion with different degrees of hybridization using a combustion generator, noticed the potential benefits

of this type of assembly. They state that hybrid-electric and all-electric aircraft can revolutionize the propulsion and construction of the aircraft. However, to take full advantage of these concepts, new and innovative aircraft design methods need to be developed. Best performance is only achieved through a comprehensive approach in aircraft design. It is an approach where the airframe and propulsion system are designed simultaneously, and the design is optimized in terms of aerodynamics taking into account the interference between the airframe and rotors or propellers. This can ensure the efficient use of energy stored on board the aircraft in its various types.

The result of work on electric and hybrid propulsions are flying vehicles, both manned and unmanned, built in recent years.

Airbus has been developing the E_Fan aircraft concept since 2014. It is the vehicle with a wingspan of 9.5 m and an aircraft length of 6.67 m. The propulsion is responsible for two ducted fans with a thrust of 0.75 kN each, powered by 30 kW electric motors. The take-off mass of this aircraft is 550 kg, 170 kg of which is the lithium-polymer battery (li-pol). The E_Fan is a platform used for testing the concept of zero emission jet propulsion. An extension of this concept is the aircraft with so-called range extender – a combustion engine driving an electric generator, which is expected to be presented in 2020. A further development of this project is the concept of the E_Fan X passenger aircraft (presented in Fig. 3), where three traditional turbine jet engines are supported by the engine tested in the E_Fan aircraft. The electricity needed to drive it, is generated by combustion engines.



Fig. 3. The E_Fan X aircraft [31]

Pipistrel company has presented the Panthera aircraft [35] (cf. Fig. 5 – it is worth paying attention to the refined silhouette in terms of minimizing aerodynamic drag force), which is available in three variants: combustion, hybrid and all-electric. Each version is designed for different target groups of customers. The internal combustion engine is dedicated to people who need fast long-distance travelling, while the electrical system, which is the most environment-friendly solution, is mainly used for local communication. The hybrid system is a combination of these two concepts, however, the complexity of design and operation can increase operating costs.



Fig. 4. Pipistrel Panthera aircraft [35]

Constructions equipped with eco-friendly propulsions are also: the Boeing Phantom aircraft equipped with a fuel cell to drive avionics, the German Antares 18E motor glider – a high performance aerobatic vehicle equipped with a small electric motor providing the possibility of an independent take-off and a safer flight. A fuel cell version has also been developed.

The AOS 71¹ (Fig. 5) and AOS H2² motor gliders are noteworthy. They were developed by a consortium of Rzeszow University of Technology, Warsaw University of Technology, AGH University of Science and Technology and The Glider Factory ‘Jeżów’–Henryk Mynarski. The first one is a purely electrical construction and the second one is a hybrid using a hydrogen fuel cell.



Fig. 5. The AOS 71 motor glider 71 [35]

Hybrid and electric propulsions have a significant disadvantage – it is the large mass of the propulsion system, which is particularly visible in the case of smaller aircraft. To increase aircraft propulsion performance, energy management on board an aircraft could be optimized [17].

Distributed propulsion constitutes an alternative to traditional propulsion systems. As previously mentioned, such

a system is based on the use of many small electric motors or combustion engines. Low-thrust jet engines, fans or propellers driven by electric motors can be used. These can be all-electric as well as hybrid or combustion units. Propulsion elements can be placed along the leading edge of the wings [31], on the fuselage and even on the aircraft stabilizers. The purpose of the research on this system is to demonstrate that having the same power of a small engine assembly as the power of a traditional ‘focused’ power unit, it is possible to achieve more favourable performance characteristics, such as increasing thrust with lower fuel consumption and lower pollutants emissions into the atmosphere. Many scientific and research centres worldwide undertake work on these issues.

The company JOBY Aviation together with NASA runs the LEAPTech research program, which aims to build an electric aircraft using the amount of electricity available on board the aircraft more efficiently. Additional goals are to remove internal combustion propulsion and to reduce noise emission significantly. Therefore, the construction of an aircraft equipped with all-electric distributed propulsion was undertaken. The Cirrus SR22 aircraft served as a comparative base for research. The results of the research conducted were published, e.g. in [31]. To validate the design assumptions, the performance of the Cirrus 22 aircraft with a traditional propulsion system was compared with its LEAPtech development equipped with distributed propulsion of the same take-off power. The analysis was carried out with the CFD simulations and laboratory ground tests of wing flow by air flow generated by electric motor-propeller assemblies. Table 1 contains basic technical data for both aircraft, and Fig. 6 shows the LEAPtech aircraft.

Table 1. Comparison of technical data for Cirrus and LEAPtech aircraft [2]

	Cirrus SR22	LEAPTech
Take-off mass	1542 kg	1361 kg
Seats	4	4
Wing span	11.7 m	9.45
Aspect ratio	10.1	17.4
Wing area	13.5 m ²	5.1 m ²
Wing loading	114.2 kg/m ²	266.86 kg/m ²
Cruise speed	340 km/h	320 km/h
C ₂ for cruise speed	0.3	0.77

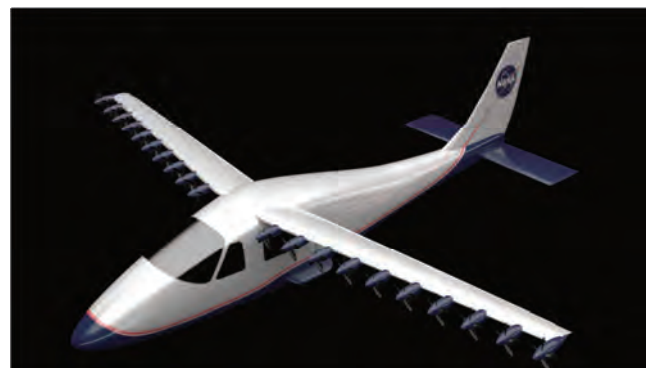


Fig. 6. LEAPTech concept aircraft [21]

As shown in Table 1, despite the reduction of the bearing surface by more than 2.5-fold, researchers estimate that the bearing force coefficient in the flight range will be more

¹ KBN/68/12823/IT1-B/U/08 pt. „New generation multifunctional two-seater motorglider”.

² NCBR PBS3/A6/24/2015 pt. „Hybrid propulsion using fuel cells of light aircraft”.

than twice as high. $C_{z\max}$, on the other hand, will be over 4 times higher due to the propellers placed on the wing leading edge. An accelerated airflow will flow around the upper surface of the airfoil much faster than in the case of a traditional aircraft design system, hence a significant increase in aerodynamic lift at the same value of energy put in the aircraft's propulsion.

The possibility of using distributed propulsion in the VTOL aircraft was described by the authors of [7]. They arranged the rotors in such a way that the vehicle could start vertically. Then, sequentially, the rotors together with the fixed wing would change the configuration for horizontal flight. Such a layout of the propulsion can bring measurable benefits in the form of more efficient energy distribution on board. An equally important element is the use of rotors to control the direction of flight of the aircraft, which reduce the number of complex elements of the aircraft control.

A number of studies, particularly represented by [21, 22], raised the idea of distributed propulsion for aircraft intended to replace traditional long-range passenger aircraft. There were demonstrated advantages of such a system, such as a 15% reduction in fuel consumption and a significant reduction of harmful compounds emitted into the atmosphere (NO_x and CO by 25%). There were described all-electric and hybrid jet systems. The hybrid power of the aircraft's engines uses energy generated by a traditional turbine engine coupled to an alternator. Depending on the concept, this engine can only be used to generate electricity, such as APU (Auxiliary Power Unit), or it can generate extra thrust. Studies [19, 21, 22] also show the possibilities of using hybrid or distributed propulsions in passenger aircraft. Propulsions of this type would be based on a large fan motor providing part of the thrust, the remaining part would be generated by electrically driven fans or by distributed propulsion. Analyses are carried out regarding energy flow, fuel consumption and range compared to currently used flying vehicles. The significant impact of the new approach on reducing emissions of pollutants present in the exhausts is indicated.

Based on the research work analysed, it can be concluded that the use of hybrid or distributed propulsion can bring measurable benefits in the form of reduced energy or fuel consumption. However, such analyses would require experimental verification (CFD tests, energy flow modelling, determination of electricity consumption by fans – going into megawatts) and bench tests of propulsion system components. This could bring a broader view on the considered problems of air-propulsion development.

The application of distributed propulsion can significantly improve the performance of the aircraft. In [20], the authors presented a proposal for the use of distributed propulsion for a hybrid glider based on a hydrogen fuel cell. Calculations showed that it is possible to reduce hydrogen consumption by 3 kg, which will increase flight duration by 26.5%.

Based on the analysed research from various scientific centres, it can be concluded that conducting further focused research on pro-ecological solutions is justified and is not a temporary fashion but it falls under the '3E' paradigm.

3. Conclusions

Electric propulsions constitute a very interesting solution from the point of view of the attained aircraft performance in various flight conditions and the attained ecological properties. The characteristic of electric motors allows for more beneficial use of the propeller characteristics – it is easier to maintain the propeller within optimal parameters in terms of its efficiency during flight. In addition, the electric motor generates a lower level of vibration compared to the piston engine. This seemingly ideal propulsion also has its weaknesses. There remains a problem related to the range limited by the capacity of heavy batteries that do not provide a sufficient level of energy density to ensure the satisfactory range of the aircraft. For the same aircraft, the energy density in the hydrocarbon fuel (for the combustion propulsion variant built on the airframe) is two orders of magnitude higher than the one stored in batteries. In addition, the mass of the batteries reduces the payload of the aircraft and also reduces the range due to the aircraft's performance during the flight.

The hybrid propulsion is a transition phase before developing batteries with the appropriate energy density or efficient (lighter) fuel cells. However, it has a significant drawback, which is the complexity of the structure and the increase in the aircraft's take-off mass. There are also problems with ensuring the electromagnetic compatibility of complex high-energy systems making a fuel cell-based propulsion system. In the case of hybrid propulsion with a low degree of hybridization, there is a reduction in fuel consumption and exhaust as well as noise emissions, but the electric motor supports the internal combustion engine only at take-off or climb. An internal combustion engine is used during the cruise. Because of this and the flight characteristics of the aircraft (take-off and climb are relatively short stages of the flight), such systems seem to be not completely accurate for usage in aviation applications. The greater advantages of such a system could be seen in automotive applications where variability of rotational speed and engine load is often found, e.g. during city driving. For aviation applications, it seems advisable to use propulsions where the internal combustion engine drives the generator to recharge only the battery of the marching electric motor. This generator can be replaced by a fuel cell. Further work on hybrid and electric propulsion indicates that rather heavy and inefficient fuel cells will be the source of electricity for now, which will in time acquire sufficient features to ensure satisfactory aircraft performance.

Distributed propulsion can compensate for some of the disadvantages of electric propulsion by more efficiently managing energy on board, thereby ensuring greater range and duration of the flight. The same observation can also be made for hybrid propulsion, where the energy source is accumulators and a combustion generator or fuel cell. Previous studies carried out in various centres around the world as well as the authors' own research indicate that potential benefits of distributed propulsion should be sought in improving the aerodynamic parameters of the aircraft. Just selecting the propellers with a small diameter and the engines so that they run at their best efficiency parameters can result in lower energy consumption from its sources by

a few percent. Only the forced acceleration of the air stream over the wing and thus increasing the lift coefficient (up to 4 times!) can bring measurable benefits for planning the power unit work strategy to minimize energy consumption, thereby increasing the range and duration of the flight.

The presented study indicates further research perspectives on the development of future propulsion for aviation falling under the 3E paradigm. The projections for devel-

opment of distributed propulsion are promising. This type of propulsion can enable to increase efficiency and reduce fuel consumption, thereby reducing pollutants emissions in the exhausts and improving economic indicators. The development of this concept will be associated with a new approach to the design of flying vehicles as a transport system, and not a system of components with different functionalities.

Nomenclature

APU	Auxiliary Power Unit	Degree of hybridization: the ratio of the amount of energy stored in batteries to the total amount of energy accumulated on board the aircraft
ATM	Air Traffic Management	Distributed propulsion: the propulsion composed of a series of low-power thrust units located on the wing leading edge or on the fuselage
CAEP	Committee on Aviation Environmental Protection	Energy density: the ratio of the amount of energy accumulated in the energy source to its mass
CFD	Computational Fluid Dynamics	Flying wing: the structural system of an aircraft or glider without tail and not define a fuselage
CO	carbon monoxide	Hybrid propulsion: a system using more than one energy source (e.g. battery and hydrocarbon fuel) to propel an aircraft or wheeled vehicle
CO ₂	carbon dioxide	Wing area: the surface of the projection of the aircraft's airfoil on a horizontal plane, giving the lift force
C _z	lift coefficient	Wing loading: the ratio of the aircraft's mass (kg) to its wing area (m ²)
E _{Bat}	amount of energy stored in the battery	Wing span: distance between the wing ends of the aircraft
E _{Tot}	total amount of energy stored on board the aircraft	
H	degree of hybridization	
NO _x	nitrogen oxides	
ICAO	International Civil Aviation Organization	
NASA	National Aeronautics and Space Administration	
SESAR	Single European Sky ATM Research programme	
UAV	unmanned aerial vehicle	
ULD	unit load device	
VTOL	Vertical Take Off and Landing	
Aspect ratio: a measure of leaf slenderness expressed by the quotient of the flap length and its average geometrical chord		

Bibliography

- [1] AYAR, M., GULEREN, K.M., KARAKOC, T. Motor selection process with AHP on mini electric UAV. *International Symposium on Electric Aviation and Autonomous Systems* (ISEAS), 2018.
- [2] BREJLE, B., MARTINS, J. Electric, hybrid, and turboelectric fixed-wing aircraft: A review of concepts, models, and design approaches. *Progress in Aerospace Sciences*. 2019, **104**, 1-19. <https://doi.org/10.1016/j.paerosci.2018.06.004>
- [3] DE VRIES, R. Preliminary sizing of a hybrid-electric passenger aircraft featuring over-the-wing distributed-propulsion. *American Institute of Aeronautics and Astronautics*. <https://doi.org/10.2514/6.2019-1811>
- [4] DONATEO, T., SPEDICANTO, L. Fuel economy of hybrid electric flight. *Applied Energy*. 2017, **206**, 723-738.
- [5] FERMANN, Y. et al. Hybrid-electric motive power systems for commuter transport applications. *ICAS* 2016.
- [6] FILLIPPONE, A. *Fixed and rotary wing aircraft*. Butterworth-Heinemann 2006, USA.
- [7] FINGER, F.D. et al. A review of configuration design for distributed propulsion transitioning VTOL aircraft. *2017 Asia-Pacific International Symposium on Aerospace Technology* (APISAT2018).
- [8] FINGER, F.D. et al. On aircraft design under the consideration of hybrid-electric propulsion systems. *2018 Asia-Pacific International Symposium on Aerospace Technology* (APISAT2018).
- [9] FINGER, F.D., BRAUN, C. Case studies in initial sizing for hybrid-electric general aviation aircraft. *2018 AIAA/IEEE Electric Aircraft Technologies Symposium*. <https://doi.org/10.2514/6.2018-5005>
- [10] FINGER, F.D., BRAUN, C. Impact of engine failure constraints on the initial sizing of hybrid-electric GA aircraft. *AIAA Scitech 2019 Forum*, San Diego. <https://doi.org/10.2514/6.2019-1812>
- [11] FINGER, F.D., BRAUN, C., CEES, B. Impact of electric propulsion technology and mission requirements on the performance of VTOL UAVs. *CEAS Aeronautical Journal*. 2019, **10**, 827-843.
- [12] FINGER, F.D., CEES, B., BRAUN, C., Initial sizing methodology for hybrid-electric general aviation aircraft. *Journal of Aircraft*. 2019 (published online). <https://doi.org/10.2514/1.C035428>
- [13] GEISS, I., STROHMYAYER, A., et al. Optimized operation strategies for serial hybrid-electric aircraft aviation technology. *Integration, and Operations Conference 2018*. <https://doi.org/10.2514/6.2018-4230>
- [14] GOTTFEN, F., FLINGER, F.D., BRAUN, C. Empirical correlations for geometry build-up of fixed wing unmanned air. *2018 Asia-Pacific International Symposium on Aerospace Technology* (APISAT2018).
- [15] HOELZEN, J. et al. Conceptual design of operation strategies for hybrid electric aircraft. *Energies*. 2018, **11**(217). <https://doi.org/10.3390/en11010217>

- [16] HOELZEN, J. et al. Hybrid electric aircraft propulsion case study for skydiving mission. *Aerospace*. 2017, **4**(45). <https://doi.org/10.3390/aerospace4030045>
- [17] ISIKVEREN, A. The method of quadrant based algorithmic nomographs for hybrid/electric aircraft pre-design. *Journal of Aircraft*. 2017. <https://doi.org/10.2514/1.C034355>
- [18] KAI, N. et al. Electrical and electronic technologies in more-electric aircraft: a review. *IEEE Access*. 2019. <https://doi.org/10.1109/ACCESS.2019.2921622>
- [19] KIRNER, R. et al. An assessment of distributed propulsion: Part B – Advanced propulsion system architectures for blended wing body aircraft configurations. *Aerospace Science and Technology*. 2016, **50**, 212-219.
- [20] KUŹNIAR, M., ORKISZ, M. Analysis of the application of distributed propulsion to the AOS H2 motor glider. *Journal of Kones*. 2019, **26**(2), 85-92.
- [21] LIU, C., DOULGERIS, G., PANAGIOTIS, L. et al. Turboelectric distributed propulsion system modelling for hybrid-wing-body aircraft.
- [22] LIU, C., XIAYI, S. Method to explore the design space of a turbo-electric distributed propulsion system. *Journal Aerospace Engineering*. 2016. [https://doi.org/10.1061/\(ASCE\)AS.1943-5525.0000617](https://doi.org/10.1061/(ASCE)AS.1943-5525.0000617).
- [23] ŁUKASIK, B. Analysis of the possibility of using full-electric, hybrid and turbo-electric technologies for future aircraft propulsion systems, in terms of mission energy consumption, NO_x/CO₂ emission and noise reduction. *Doctoral Thesis*. Instytut Lotnictwa 2018.
- [24] PAWLAK, M., KUŹNIAR, M. Analysis of the wind dependent duration of the cruise phase on jet engine exhaust emissions. *Journal of Kones*. 2018, **25**(3), 371-376.
- [25] PAWLAK, M., MAJKA, A., KUŹNIAR, M. et al. Emission of selected exhaust compounds in jet engines of a jet aircraft in cruise phase. *Combustion Engines*. 2018, **173**(2), 67-72.
- [26] PAWLAK, M., KUŹNIAR, M. Determination of CO₂ emissions for selected flight parameters of a business jet aircraft. *Journal of Kones*. 2019, **26**(1), 85-92.
- [27] PAWLAK, M., KUŹNIAR, M. Problematyka emisji toksycznych składników spalin silników lotniczych. *Autobusy*. 2017, **12**, 338-344.
- [28] PAWLAK, M., MAJKA, A., KUŹNIAR, M. et al. Analysis of wind impact on emission of selected exhaust compounds in jet engines of a business jet aircraft in cruise phase. *Combustion Engines*. 2018, **173**(2), 55-60.
- [29] PAWLAK, M. *Metoda modelowania emisji związków szkodliwych w spalinach silników odrzutowych samolotów pasażerskich w warunkach przelotowych*. Uniwersytet Morski w Gdyni 2019.
- [30] RINGS, R., FLINGER, F.D. et al. Sizing studies of light aircraft with parallel hybrid propulsion systems. *2018 Asia-Pacific International Symposium on Aerospace Technology* (APISAT2018)
- [31] STOLL, A.M., BEVIRT, J., MOORE, M. et al. Drag reduction through distributed electric aviation technology. *Integration, and Operations Conference*. 2014
- [32] VRATNY, P., HORNUNG, M. Sizing considerations of an electric ducted fan for hybrid energy aircraft. *Transportation Research Procedia*. 2018. <https://doi.org/10.1016/j.trpro.2018.02.037>
- [33] <https://airbus.com/>
- [34] <https://emrax.com/>
- [35] <https://nasa.gov/>
- [36] <https://pipistrel-aircraft.com/>
- [37] <http://wankel-ag.de>

Prof. Marek Orkisz, DSc., DEng. – Faculty of Mechanical Engineering and Aeronautics, Rzeszow University of Technology.

e-mail: mareko@prz.edu.pl



Michał Kuźniar, MEng. – Faculty of Mechanical Engineering and Aeronautics, Rzeszow University of Technology.

e-mail: mkuzniar@prz.edu.pl



By-products from thermal processing of rubber waste as fuel for the internal combustion piston engine

The article presents results of investigation on the combustion of a mixture of pyrolysis oil from tires and regular fuel in the internal combustion reciprocating piston engine. The tested fuel consisted of: diesel fuel and pyrolysis oil at amount of 10% by volume. The tests were carried out on a single-cylinder naturally aspirated compression-ignition engine. The engine was equipped with a common rail fuel injection system and an electronic control unit that allowed changing injection timing. A comparative analysis of pressure-volume charts for the reference fuel, which was diesel fuel, and for a mixture of diesel with 10% addition of pyrolysis oil was carried out. Injector characteristics for the reference fuel and the mixture were determined. Engine efficiency for both fuels was also determined. Unrepeatability of the engine work cycles for the diesel fuel and the tested mixture was calculated. Finally, exhaust toxic emission was analyzed. It was found that the pyrolysis oil can be used as valuable additive to regular diesel fuel at amount up to 10%, however, toxic exhaust gases emission was increased.

Key words: pyrolysis oil, thermal conversion, biocrude, diesel engine, alternative fuels

1. Introduction

Thermal processing of organic matter is an alternative method of obtaining fuel for internal combustion piston engines. Pyrolysis is one of the methods of organic thermal processing. Pyrolysis is a process in which organic material is heated up to temperature of approximately 500°C in oxygen-free atmosphere. The composition and quantity of individual fractions of pyrolysis products depends on the following [5, 15]:

- physical-chemical properties of the input material,
- temperature,
- pyrolysis reactor type,
- process speed (heating up time, retention time).

During pyrolysis, organic material is converted into the following [12, 13]:

- the gas fraction, also called pyrolysis gas, which apart from methane, ethane, carbon monoxide and dioxide and water vapors also contains vapors of hydrocarbon compounds,
- solid fraction consisting of carbon, metals and other inert substances,
- liquid fraction called pyrolysis oil, that is formed after cooling the pyrolysis gas to ambient temperature. The composition of pyrolysis oil includes: condensed hydrocarbon compounds, tars, water, alcohols and organic acids. Raw pyrolytic oil is a dark-brown substance with a strong characteristic odor [2, 8].

Exemplary fractions produced from the pilot installation at the Częstochowa University of Technology are shown in Fig. 1. The pyrolysis installation is equipped with a screw feeder for moving the input material. Heating is carried out by electric heaters. The system is equipped with a controller to control the set point temperature and a frequency converter that allows changing the retention time of keeping the charge material in the heating zone. The largest share is a solid fraction, which contains significant amount of energy up to 90% in comparison to the input material. The gas

fraction constitutes approximately 30% and contains nearly 10% input energy of the material [10].

The most desirable product of pyrolysis is the oil fraction, which can be used as liquid fuel that can be origin for further processing to obtain various chemical compounds. The gas fraction is most often used for process itself. The solid fraction is managed as a final product – char or activated carbon [4, 11, 15].

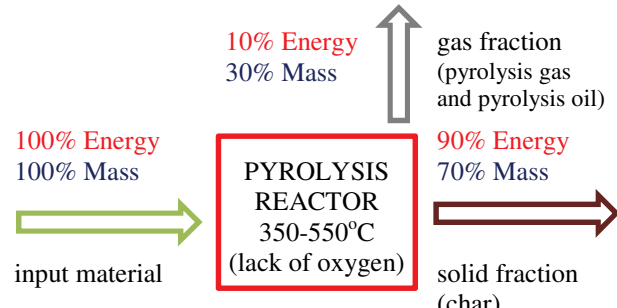


Fig. 1. Mass and energy distribution in pyrolysis process

Pyrolysis reactors have various construction. The most common installations are as follows: fixed bed reactor, fluidized bed reactor, screw conveyor reactors, rotary cone reactor, ablation reactor. Depending on the type of reactor, the worn out tires can load the reactor directly (fixed bed reactor) or require fragmentation (e.g. fluidized bed reactor). The pyrolysis process can be carried out with the addition of a catalyst, which aim is to remove unwanted compounds from the gas [7, 12].

As the input material for the pyrolysis process, various kinds of organic waste: from the food industry, waste from the agricultural industry, waste from the fish industry, waste from the wood industry, municipal waste, special purpose crops can be used. The problem of managing worn car tires has been growing in recent years. Tires do not degrade in the natural environment for up to 100 years.

They are a nuisance waste and have been classified as waste that should be professionally utilized [6, 9].

The amount of tires waste increases year by year. All rubber waste constitute about 80%. It is estimated that 1.5 billion tires are produced annually in the world. Until now, the main technology of tires recycling is to burn them in cement plants. Another option is to use them for the pyrolysis process [14].

The literature presents results of research on applying pyrolysis oil (PO) from tires as the additive to regular fuel (diesel fuel – DF) and also as a stand-alone fuel. For example, in [8] an analysis of engine operation was carried out on a mixture of diesel fuel mixed with biodiesel and pyrolysis oil from tires. The addition of individual components was as follows: 80% diesel fuel, 10% biodiesel and 10% pyrolysis oil from tires. As a result of the experiment, the authors found that the addition of this pyrolysis oil increases the engine torque and power. The addition of the pyrolysis oil reduces NO_x and CO emissions. According to the authors, the disadvantage of tire pyrolysis oil is the need to filter and desulphurize it before feeding it to the engine.

In article [11], the authors used tire pyrolysis oil as fuel to a 4-cylinder diesel engine. They concluded that the tire pyrolysis oil has a lower cetane rating but is still a promising alternative fuel. They observed that the engine can only work on pyrolysis oil without addition of improvers to get higher cetane number. The use of oil from the pyrolysis of tires allows to maintain the emission of toxic gas components at a level comparable to those where the engine is running on diesel fuel.

In [6] Authors used oil from tire pyrolysis as the additive to diesel fuel. The authors created mixtures with pyrolysis oil of 10%, 20% and 50% by volume. They concluded that the addition of 10% pyrolysis oil may occur as best alternative fuel due to satisfactory good engine performance and environmental aspects as well.

Based on the literature analysis, combustion tests of the mixture of diesel fuel and oil from pyrolysis of tires in a single-cylinder diesel engine were taken. Hence, the main target of the work was to investigate the pyrolysis oil as the additive at 10% to diesel fuel.

2. Description of the research stand

The test stand is shown in Fig. 2. It is the engine coupled with a generator connected to power grid. To measure electrical power three-phase electricity meter (1) was used. The three-phase asynchronous generator/motor (2), with a power of 15 kW at 400 V rated voltage is used first to start up the engine and then it works as a dynamometer. The asynchronous motor has two operating speeds: 1465 rpm and 975 rpm. A lower rotation speed of 975 rpm was applied to investigation.

The technical specifications of the compression ignition engine S320 (3) are shown in Table 1.

The engine underwent a number of modifications to be adapted to research. The most important change was modification of the cylinder head. It has additional mounting sockets needed to mount an additional injector and a pressure sensor. Currently, two common rail injectors and a piezoelectric pressure sensor are installed in the cylinder head. The second important change of the engine was re-

placement of the original evaporation based cooling system by an radiator cooler. The cooling system works at ambient pressure. The cooling system and all elements of test stand are shown in Fig. 3.

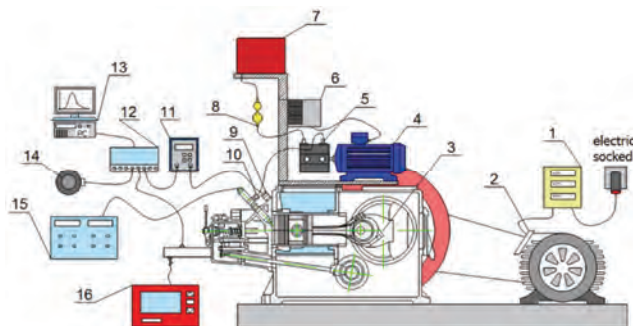


Fig. 2. Diagram of the test stand

Table 1. Technical data of the engine S320

Type of engine	Four-stroke
Fuel	Diesel Fuel
Number of cylinders	Single
Direct of cylinder	Horizontal
Number of valves	2
Cylinder bore	120 mm
Piston stroke	160 mm
Engine displacement	1810 cm ³
Compression ratio	17
Nominal power ⁽¹⁾	13.2 kW for 1500 RPM
Maximum torque ⁽¹⁾	93 Nm for 1300 RPM
Specific fuel consumption	234 g/kWh 172 g/HPh
Capacity lubrication system	10.5 dm ³
Oil consumption	4.1 g/kWh
Beginning of fuel delivery	variable
Injection pressure	to 200 MPa
Suction valve timing	Opening: 23 CA deg before TDC Closing: 40 CA deg after BDC
Exhaust valve timing	Opening: 46 CA deg before BDC Closing: 17 CA deg after TDC
Valve clearance for cold engine	suction 0.4 mm exhaust 0.4 mm
Oil pressure in the warm engine	150-300 kPa
Cooling	open water system
Engine weight	315 kg

(1) Parameters for temperature +15°C, pressure 100 kPa, relative humidity 60%

The original Andoria S320 engine fuel system was replaced by a modern common rail fuel injection system. The three-section twin-piston pump (5) is driven by an asynchronous engine (4) with a power of 2.2 kW. The injection pump contains three pressing sections arranged radially every 120°. The pump is equipped with a pressure regulator. The fuel injection pressure is controlled with a controller. During the tests, fuel is injected at a pressure of 100 MPa. The asynchronous motor (4) is powered by a frequency converter (6), which allows to control fuel flowrate. A fuel tank (7) is mounted next to the test stand. Fuel consumption is measured by the fuel flow meter (8). The fuel system is equipped with a fuel cooler and an additional preliminary, supporting low pressure a fuel pump. The

cooler is needed at the stand, because with long time continuous work of the engine the fuel temperature increases significantly. For fuel injection, the BOSCH 0445110076 (10) injector is used. An electronic system (15) is used to control the injector timing. The controller makes it possible to adjust the injection time with resolution of 10 μ s. In addition, it allows shifting start of injection. The electronic system reads pulses from the encoder which is installed on the camshaft (14). The encoder generates 360 pulses per revolution. As the encoder is installed on the camshaft, the change of injection start is at resolution of 2 deg crankshaft revolution. For measuring in-cylinder pressure the Kistler piezoelectric sensor type 6061B (9) is used. This sensor is mounted into the cylinder head. The sensor sensitivity is -25.8 pC/bar, measuring range up to 25 MPa. The signal from the piezoelectric sensor needs amplification, therefore another device in the measurement pathway is the charge amplifier (11). The signal after amplification is registered by the National Instrument measurement data acquisition card (12). The encoder signal (14) is used to determine p-V diagram in real time working conditions. SAWIR program by Dr M. Gruca (13) is used to register and process engine parameters in real time working conditions. The view of the program window with real-time charts is shown in Fig. 4.



Fig. 3. The test stand

The exhaust gas analyzer Radiotechnika model AI9600 (16) is used to measure the concentration of toxic exhaust compounds.

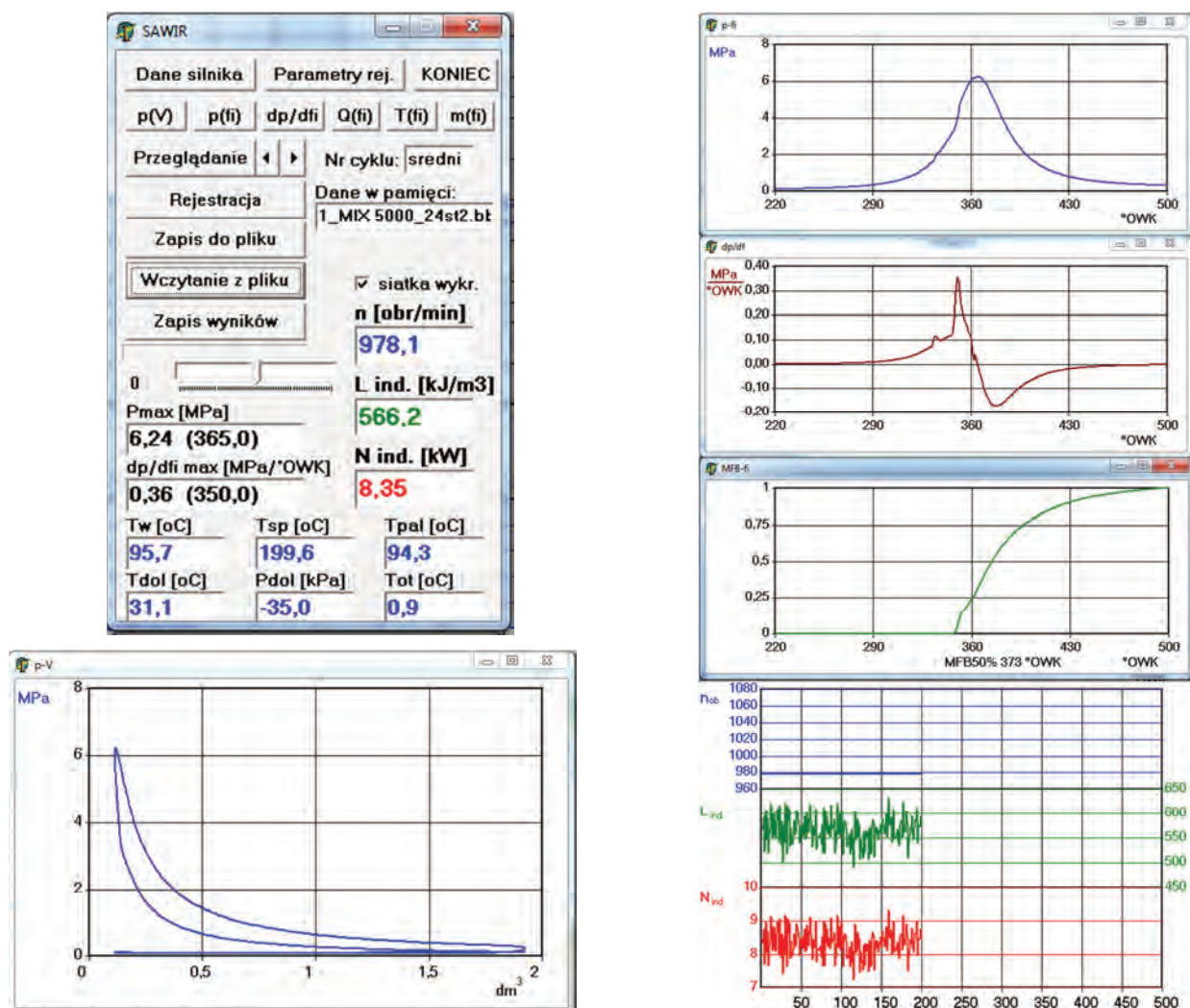


Fig. 4. View of the SAWIR program graphical interface and results

3. Methodology

Before tests, correct determination of TDC (top dead center) location was done. Next, several engine geometrical data were input to the software: crank radius, connecting rod length, piston diameter, compression ratio. The engine worked on reference fuel to reach operating temperature, i.e. 363 K. At the beginning, the injector characteristics for reference fuel and mixture of diesel fuel+10%PO were determined, the injection time was changed in the range of: 2–6 ms with resolution of 10 μ s. Fuel consumption time was measured from a 41 cm³ meter. Fuel consumption time was measured with accuracy of 0.01 s. Each test series consisted of 200 engine consecutive combustion events. During the experiment, the influence of the beginning of the fuel injection start on the p-v plots was also examined. At the same time, the concentrations of CO, NO_x, HC in the exhaust gas were measured. The tests were conducted for regular diesel fuel as the reference fuel and the mixture of diesel fuel and 10%PO. The proposed addition of 10% pyrolysis oil to diesel fuel resulted from the research conducted so far on fuels. During the study, the authors measured: the concentration of hazardous compounds in the exhaust gas using an exhaust gas analyzer that was connected to the exhaust gas outlet duct. During the fuel test, a fixed injection time of 5 ms was maintained.

4. Analysis of results

The time-pressure signals obtained from tests were used to determine the following: indicated mean effective pressure (IMEP), injector characteristics, thermal efficiency of the engine, toxic exhaust emissions.

The tests consisted of 2 stages. In the first stage, engine tests were carried out with reference fuel, i.e. diesel fuel. The fuel injection timing was changed in the range of 24–32 CA deg bTDC. The injection time was 5 ms at 100 MPa injection pressure. Start of injection was limited by diesel knock occurring at timings advanced over 32 CA deg bTDC. Graphs with exemplary in-cylinder pressure curves are shown in Fig. 5.

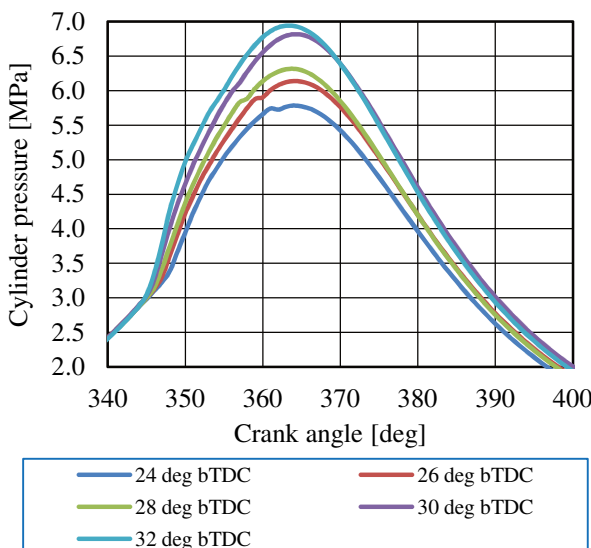


Fig. 5. Cylinder pressure vs. crank angle range 340–400 deg for a variable start of fuel injection, fuel: DF

In next stage of tests, as seen in Fig. 6, the fuel applied to tests was the mixture containing diesel fuel and oil from tire pyrolysis (PO) at 10% by volume. Amount of PO was limited to 10% only with risk of damaging the high pressure fuel pump. As previously, the fuel injection timing was changed in the range of 24–34 CA deg bTDC. The duration of injection was also 5 ms. The injection pressure was 100 MPa.

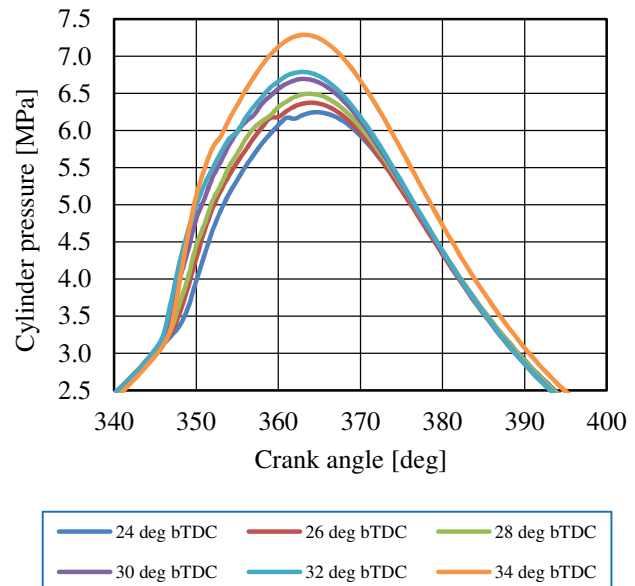


Fig. 6. Cylinder pressure vs. crank angle range 340–390 deg for a variable start of fuel injection, fuel: DF+10%PO

On the basis of the data obtained, a comparative analysis of the combustion pressure traces inside the engine cylinder was carried out maintaining fixed injection timings. Both in-cylinder pressure and pressure rise rates for reference fuel and mixture: DF+10%PO are presented in Figs 7 and 9.

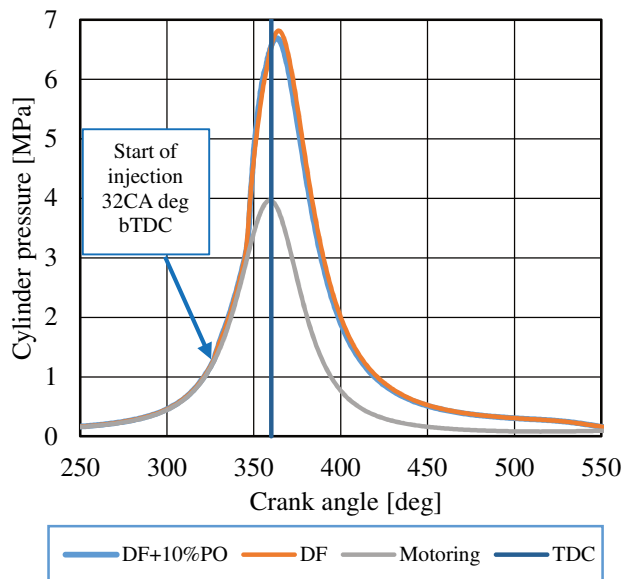


Fig. 7. Cylinder pressure vs. crank angle range 250–550 deg for a variable fuel

The graph (Fig. 7) shows a slight decrease in in-cylinder pressure after adding 10% PO. It affected lower combustion pressure and decrease in the indicated work (Lind the same as IMEP) and engine power. Pressure rise rate slightly increased with PO addition as shown in Fig. 8. The mean indicated work (IMEP) from 200 measurements was 578 kJ/m³. The unrepeatability of the engine's cycles was 4.18%. In the case of an engine fueled with a mixture of diesel fuel and PO, the mean indicated work is 530 kJ/m³ (decrease by 8.3%) and the engine work cycles unrepeatability unremarkably increased to 4.93%.

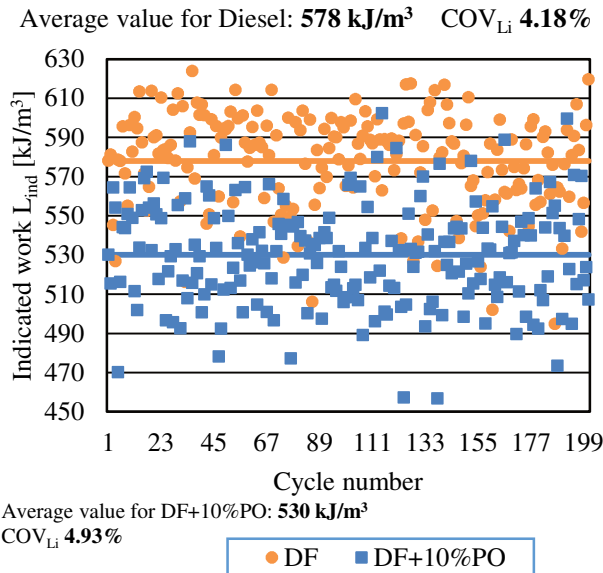


Fig. 8. Unrepeatability of the engine work for reference fuel and for research fuel

Figure 9 shows the rate of pressure rise. It can be seen that in the initial phase there is a faster pressure increase for DF+10%PO than for reference fuel (DF). Visible peaks, deviations from mileage caused by the start and end of fuel injection.

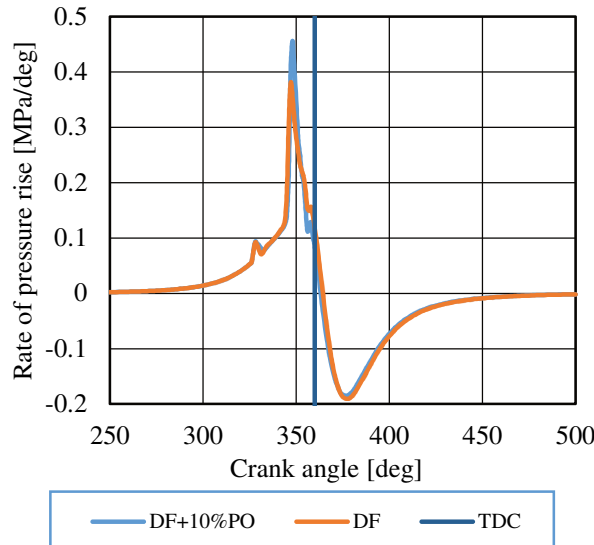


Fig. 9. Rate of pressure rise vs. crank angle

Figure 10 shows the pressure increase due to fuel combustion in the engine cylinder. The pressure plots present positive pressure over the pressure from motored events. The ignition timing in the studied case was 17 CA deg. The injection time was 5 ms, i.e. fuel injection in crank angle was 29.25 deg bTDC. Fuel injection ended approximately 1 CA deg bTDC.

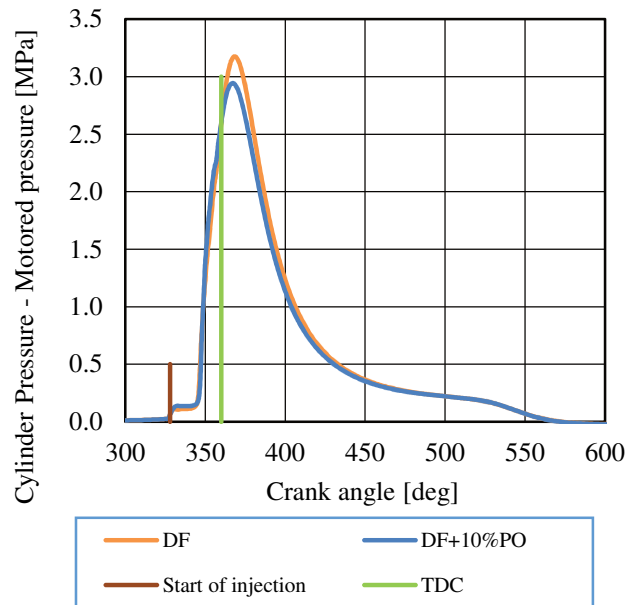


Fig. 10. Combustion pressure increase

The injector characteristics were determined for the reference fuel (DF) and for the tested mixture: DF+10%PO. The results are shown in Fig. 11.

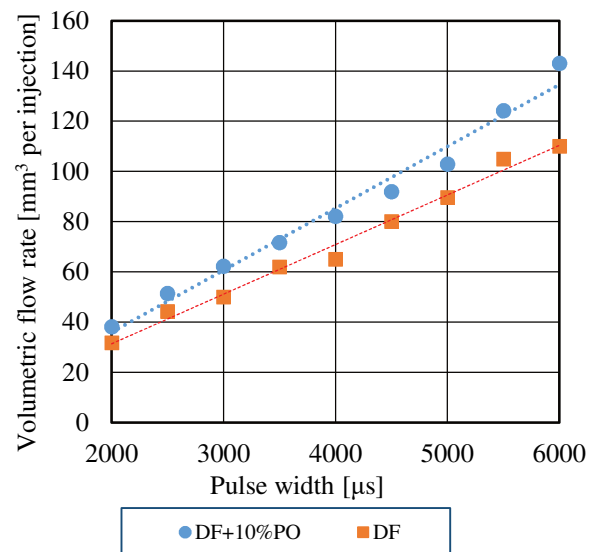


Fig. 11. Characteristic curves of the injection rate for both fuel

From the injector characteristics it can be seen that the addition of 10%PO increases volumetric flow. Based on the measurement of the amount of fuel burned in a given time

and indicated work, the engine efficiency could be calculated according to the equation:

$$\eta_T = \frac{L_i}{Q_F} \quad (1)$$

where: L_i – indicated work per cycle [kJ], Q_F – fuel energy in a dose injected to the engine cylinder [kJ].

Table 2. Net heating value of fuels used [1, 3]

	DF	PO	DF+10%PO
Net heating value [J/mg]	42.5	39	42.15
Density [g/cm ³]	0.82	0.95	0.833
Net heating value [J/mm ³]	34.85	37.05	35.07

The results of the indicated efficiency for the tested fuels with various injection timings are shown in Fig. 12. The efficiency of the engine slightly decreased while supplying the engine with DF+10%PO mixture. The engine achieved its highest efficiency for the most advanced fuel injection timing (32 CA deg bTDC). The efficiency was over 36%. The efficiency decreased with delayed fuel injection. The lowest calculated efficiency was 26% at injection timing of 24 CA deg bTDC.

In addition, in Table 3, the IMEP as average from 200 combustion events is presented. For diesel fuel IMEP reaches the highest value for 30 CA deg bTDC. For DF+10%PO the highest IMEP value is for start of injection timing 32 CA deg bTDC.

Table 3. Average IMEP for reference fuel and Diesel Fuel+10%PO

Start of injection timing [CA deg bTDC]	IMEP Fuel DF [kPa]	IMEP Fuel DF+10%PO [kPa]
24	462	449
26	514	522
28	507	501
30	578	530
32	552	546

The lowest IMEP achieved for the retarded fuel injection i.e. 24 CA deg bTDC.

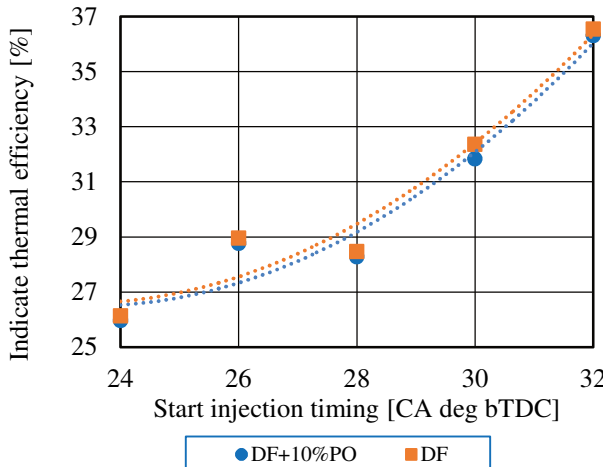


Fig. 12. Indicated thermal efficiency curves

The concentration of toxic exhaust compounds was also measured during the tests. The results of the CO concentration in exhaust gases are shown in Fig. 13.

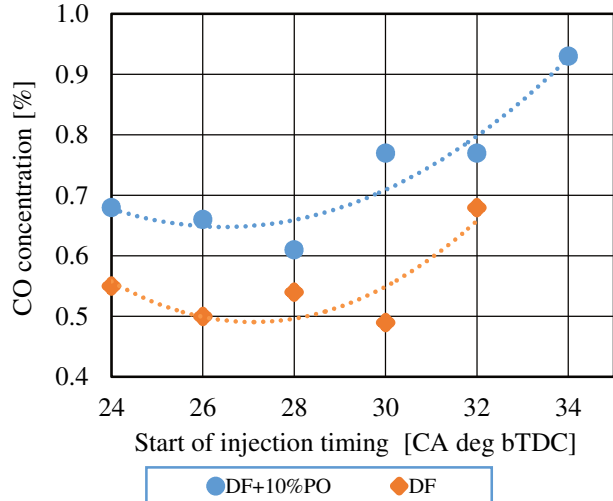


Fig. 13. CO concentration in exhaust gases

The CO concentration increased significantly after adding 10%PO. The minimum CO was observed at 28 CA deg. Retarding or advancing the injection increased the CO content in the exhaust gas. It probably was caused by heavy hydrocarbons in the pyrolysis oil that required longer time for breaking up chemical bonds and complete combustion that caused combustion process of PO slowed, that resulted in slowing the overall combustion.

The NO_x content is shown in Fig. 14. Regardless the fuel fed, the earlier the fuel injection into the cylinder, the higher the NO_x content in the exhaust gas. For all cases, the NO_x concentration was higher when the engine was fueled with DF+10%PO. Higher NO_x emission is difficult for explanation when both CO and unburnt HC also increased. The NO_x emission probably was caused by locally higher temperatures that promoted thermal mechanism for NO_x formation.

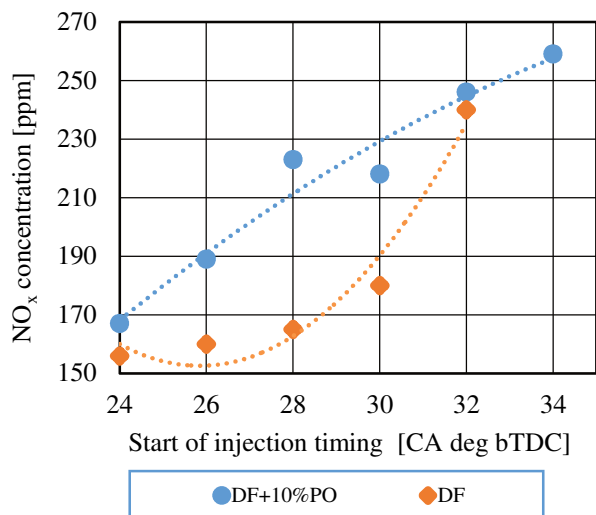


Fig. 14. NO_x concentration in flue gases

The toxic unburnt hydrocarbons (HC) in exhaust gases is shown in Fig. 15. The HC was also significantly higher in the case of engine operation on the mixture: DF+10%PO rather than on reference fuel (DF). The reason was probably the same as for CO, so presence of heavy hydrocarbons in the pyrolysis oil taken for investigation.

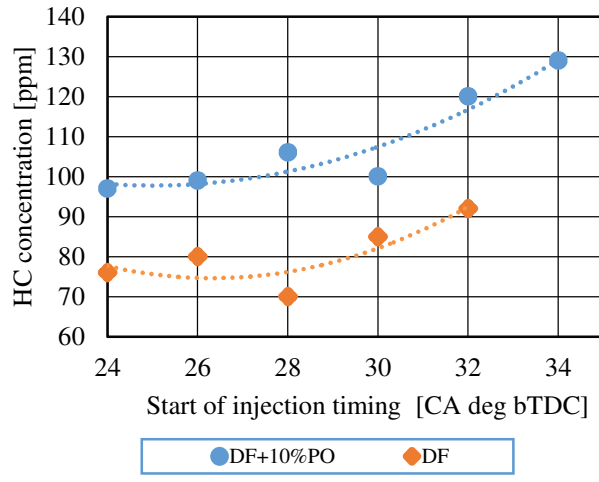


Fig. 15. HC concentration in exhaust gases

5. Conclusion

Utilization of liquid products from the thermal treatment of waste rubber (car tires) through combusting them in the IC engine is one of the methods that might be less harmful to the natural environment.

Oil from tire pyrolysis (PO) can be mixed with diesel fuel (DF) at amount of 10% by volume and used to power diesel engines.

As observed, addition of this pyrolysis oil (PO) causes decrease in-cylinder combustion peak pressure, that causes decrease in the mean indicated work (IMEP) and the engine power as well as its efficiency.

After adding PO the unrepeatability of consecutive engine work cycles increased slightly.

PO added to DF causes increase in injector flowrate by 15–25%.

The addition of pyrolysis oil from tires to diesel fuel causes increase in toxic engine exhaust emissions: carbon monoxide, nitrogen oxides and unburnt hydrocarbons.

Acknowledgements

European Union's Horizon 2020 research and innovation programme under grant agreement No 691232 – Knocky – H2020-MSCA-RISE-2015/H2020-MSCA-RISE-2015 and the research was additionally co-financed by Polish Ministry of Science within the frame of science support funds for international co-funded projects in 2016–2019.

Nomenclature

BDC	bottom dead center
bTDC	before top dead center
CA	crank angle
CI	compression ignition
CO	carbon monoxide
COV	coefficient of variation
DF	diesel fuel
HC	unburnt hydrocarbons

HPh	horse power-hour
IMEP	indicated mean effective pressure
Li	indicated work
NO _x	nitrogen oxides
PO	pyrolysis oil
QF	fuel injected energy
RPM	revolutions per minute
TDC	top dead center

Bibliography

- [1] AMBROSEWICZ-WALACIK, M., TAŃSKA, M., WALACIK, M. et al. Production of fuel blends from diesel oil and waste products. *Combustion Engines*. 2017, **171**(4), 255–258. <https://doi.org/10.19206/CE-2017-443>
- [2] ANCHIETA COSTA, G., GONÇALVES DOS SANTOS, R. Fractionation of tire pyrolysis oil into a light fuel fraction by steam distillation. *Fuel*. 2019, **241**, 558–563. <https://doi.org/10.1016/j.fuel.2018.12.075>
- [3] BOGARRA-MACIAS, M., OMID DOUSTDAR, O., FAYA, M., A. et al. Performance of a drop-in biofuel emulsion on a single-cylinder research diesel engine. *Combustion Engines*. 2016, **166**(3), 9–16. <https://doi.org/10.19206/CE-2016-324>
- [4] CHERBANSKI, R., WRÓBLEWSKI, K., MOLGA, E. Badanie procesu pirolizy zużytych opon samochodowych w reaktorze laboratoryjnym. *Inżynieria i aparatura chemiczna*. 2016, **1**, 016–017.
- [5] GRABOWSKI, Ł., WOŁOSIEWICZ, M., SAS, S. et al. Odzysk energii z odpadów pochodzących ze stacji demontażu pojazdów przy wykorzystaniu pirolizy niskotemperaturowej. *Logistyka*. 2015, **4**, 8896–8901.
- [6] HURDOGAN, E., OZALP, C., KARA, O. et al. Experimental investigation on performance and emission characteristics of waste tire pyrolysis oil-diesel blends in a diesel engine. *International Journal of Hydrogen Energy*. 2017, **42**, 23373–23378. <https://doi.org/10.1016/j.ijhydene.2016.12.126>
- [7] JAWORSKI, T. Reaktory do pirolizy odpadów i biomasy. *Pieczę przemysłowe & kotły*. 2017, **1**, 18–24.
- [8] KOC, A.B., ABDULLAH, M. Performance of a 4-cylinder diesel engine running on tire oil–biodiesel–diesel blend. *Fuel Processing Technology*. 2014, **118**, 264–269. <https://doi.org/10.1016/j.fuproc.2013.09.013>
- [9] LAM, S.S., MAHARI, W.A.W., OK, Y.S. et al. Microwave vacuum pyrolysis of waste plastic and used cooking oil for simultaneous waste reduction and sustainable energy conversion: Recovery of cleaner liquid fuel and techno-economic analysis. *Renewable and Sustainable Energy Reviews*. 2019, **115**, 1–13. <https://doi.org/10.1016/j.rser.2019.109359>

- [10] SZWAJA, S., GRAB-ROGALIŃSKI, K., CHWIST, M. Pyrolysis oil combustion in the CI engine. *Combustion Engines*. 2019, **179**(4), 126-131.
<https://doi.org/10.19206/CE-2019-420>
- [11] VIHAR, R., BAŠKOVIC, U.Z., SELJAK, T. et al. Combustion and emission formation phenomena of tire pyrolysis oil in a common rail Diesel engine. *Energy Conversion and Management*. 2017, **149**, 706-721.
- [12] WNUKOWSKI, M. Methods used in tar removal from biomass gasification gas – a review. *Archives of Waste Management and Environmental Protection*. 2016, **18**(2), 17-34.
- [13] WOŁOSIEWICZ-GŁĄB, M., GRABOWSKI, Ł. Możliwości oraz perspektywy wykorzystania oleju popirolitycznego w transporcie. *Logistyka*. 2014, **4**, 5054-5060.
- [14] WRZESIŃSKA, B., KRZYWDA, R., WĄSOWSKI, T. et al. Badania ciekłych produktów pirolizy zużytych opon samochodowych. *CHEMIK*. 2016, **70**(10), 611-615.
- [15] ŻMUDA, W., BUDZYŃ, S., TORA, B. Badania chromatograficzne produktów pirolizy granulatu ze zużytych opon. *Górnictwo i GEOFIZYKA*. 2006, **30**(3/1), 375-386.

Mariusz Chwist, MSc. – PhD student, Faculty of Mechanical Engineering and Computer Science at Czestochowa University of Technology.

e-mail: chwist@imc.pcz.pl



Michał Pyrc, DEng. – Faculty of Mechanical Engineering and Computer Science at Czestochowa University of Technology.

e-mail: mpyrc@imc.pcz.czest.pl



Michał Gruca, DEng. – Faculty of Mechanical Engineering and Computer Science at Czestochowa University of Technology.

e-mail: gruca@imc.pcz.czest.pl



Magdalena Szwaja, MSc. – PhD student, Faculty of Mechanical Engineering and Computer Science at Czestochowa University of Technology.

e-mail: mszwaja@imc.pcz.pl



The analysis of vibrations in the vehicle with naturally aspirated and turbocharged gasoline engine

In this paper, the author presents a study of vibrations in a passenger vehicle and the possible influence on driver's body in the process of natural operation. The author describes the dependence of engine size and additional equipment as the possible primary source of the vibration variations and their further propagation in the entire vehicle structure. The analysis was performed on the passenger cars with naturally aspirated and turbocharged gasoline engines. The aim of this study was to verify the level of vibrations in the vehicle structure with these particular engines, especially influence of downsized power unit, during various state of engine operation. The second goal was to examine the vibrations in the specified location related to driver's body. The measuring method used piezoelectric accelerometers, which were attached to the designated locations in the vehicle and were able to detect variations of the acceleration. The signals were collected as characteristics in the time domain. In order to achieve frequency domain for spectral analyses, the author applied the Fast Fourier Transform (FFT).

Key words: *vehicle, vibration, engine, downsizing, fast Fourier transform, accelerometry*

1. Introduction

Nowadays, the most challenging task for every car manufacturer is to fulfill environment regulations imposed by governments and among others, the European Union. Restricted requirements for toxic products emission trigger additional actions which every car company has to take into consideration from the beginning of the new project for a new vehicle release [1, 2].

The problem with the current approach to emission regulations is that they focus strongly on the one aspect of harmful emission from engine combustion and its impact on the environment, while not covering the others enough.

One of those aspect is the vibrations which are the inseparable characteristic for every running light and heavy machinery. The measured type and level of vibrations can display technical condition much easier, faster and more precisely than the traditional disassembly inspection.

Vibrations have significant impact on two major aspects. The first one is a degradation of the machine, which can lead to malfunction and eventually serious failure [3]. The second one is the potential harmful effects on the human body, which can cause discomfort during the operation or even the vibrational disease [4].

The existing tests before every car production launch show, that besides the Euro NCAP crush tests, there is no sufficient research about essential effects on people in the car while everyday operation, excluding unexpected and rare events, such as road accidents.

The review of recent exemplary studies [5-8] describe the test methodologies in this subject, yet they do not cover this issue entirely. They most often focus on one aspect during the tests, neglecting the state and technical description of the car. They also do not have specified various measurement locations for sensors related to people in the vehicle, especially the driver.

There is an apparent lack of advanced researches into vibrations which affect human's body during operation of passenger vehicles. The author would like to broaden the view for this subject and fill in the gap on this significant matter.

This paper presents the introduction of author's approach for vehicle testing in regard to vibrations occurring in the car structure during the driving, which could have vital influence on driver's body.

The author considers these studies as essential in regard to vibroacoustic measurements for passenger cars and a development of methodology comparing to current researches. Moreover, the author indicates the importance of verification for the new generation of small, high power engines equipped with high-speed turbochargers. This validation should evaluate whether those engines have possible harmful effects on vehicle users.

The purpose of this study is to verify the utility of this measuring method and furthermore, the author would like to examine vibroacoustic emission in different cars, distinctive in various categories, such as year of manufacture, engine size and auxiliary equipment.

This could lead to important correlations between indicated variables and displays potentially dangerous factors for users.

2. Measurements

2.1. Investigated objects

The examinations were performed on the two similar cars from different model generations. The first one is Seat Leon 1.6 and the second one is Seat Leon 3 1.4 TSI. The gasoline engines had comparable power and torque. The Seat Leon 3 was equipped with turbocharger. The smaller engine belongs to recent trend of engine design in the car industry, where engine capacity is decreased while at the same time the power is maintained at the same level by addition of auxiliary

Table 1. Cars specification [4, 5]

	Seat Leon 1 1.6	Seat Leon 3 1.4 TSI
YoM	2004	2018
Mileage [m]	208 000	73 000
Power [HP]	105	125
Torque [Nm]	148	200
Auxiliary	-	Turbocharger

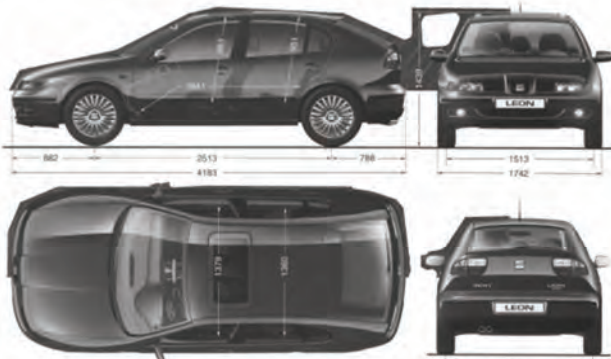


Fig. 1. Seat Leon 1 body overview [6]



Fig. 2. Seat Leon 3 body overview [7]

2.2. Measurement system

For the purpose of this research, there was chosen the non-invasive measurement method using piezoelectric accelerometers. It utilizes the piezoelectric effect, which is occurrence of the electric potential on the surface of the piezoelectric material, which is caused by the material deformation, alongside with the applied force [8].

During the mechanical vibrations the kinetic energy of the material surface is converted into potential energy and vice versa [9]. The force which causes the surface displacement effects on attached sensor. Inside the sensor, the mentioned crystal is exposed to inertia, which allows obtain certain acceleration of vibrating object surface [10].

The measuring system consisted of the PCB Piezotronics single axis sensors, model 352C04 (Table 2).

The input module was National Instruments 4-Channel Dynamic Signal Acquisition Module, model NI-9234 (Table 3).

Table 2. PCB Piezotronics Accelerometer 352C04 specification [11]

PCB Piezotronics Accelerometer 352C04	
Sensitivity	10 mV/g ($\pm 10\%$)
Measurement Range	± 500 g pk
Frequency Range	0.5 to 10000 Hz ($\pm 5\%$)
Broadband Resolution	0.0005 g rms

Table 3. National Instruments Module NI-9234 specification [12]

National Instruments Module NI-9234	
Signal Ranges	± 5 V
Input Impedance	305 k Ω
Frequency Range	51.2 kHz
Accuracy	± 50 ppm, $\pm 0.006\%$, 0.3 mV
Frequency Range	0.5 to 10000 Hz ($\pm 5\%$)
Broadband Resolution	0.0005 g rms

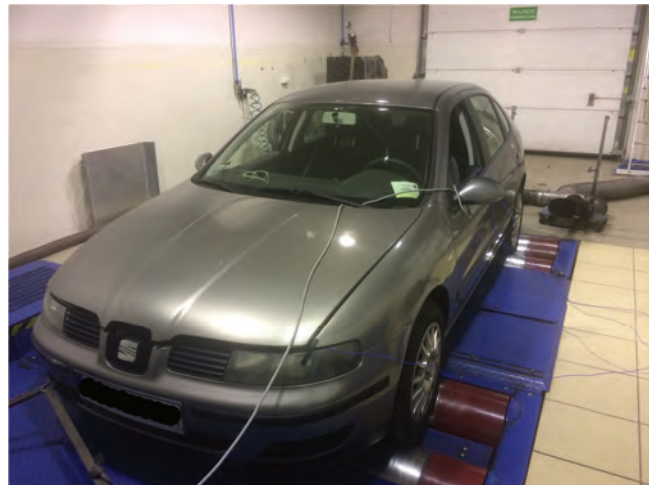


Fig. 3. Test bench for vibration measurements



Fig. 4. Functional diagram for accelerometric measurements: 1 – vehicle, 2 – accelerometer, 3 – vibration signal input module, 4 – computer

2.3. Measurement methodology

The examination was performed on the dyno MAHA LPS 3000 [18]. The vehicle was prepared for examination as it is shown in Fig. 3 and connected with measuring equipment (Fig. 4). The ambient temperature was set to the room temperature. The cars were technically fit and pre-running before measurements to obtain the proper working oil temperature.

The ISO 2631-1:1997 [19] describes evaluation of human exposure to whole body vibration as well as the Polish equivalent standard PN-EN 14253:2005 [20]. Both of them present the subject in general manner, not focusing on particular cases.

Another Polish standard PN-91/S-04100 [21] describes methodology and evaluation of vibrations at the workplace in vehicles. This requirement presents more specific approach for vibration measurements, however the author did not consider this one as covering the whole subject entirely.

For that reason, the author decided to develop original approach for vibration measurements, which would extend and supplement current standards.

The existing studies [22] proves that vertical direction of measurements contains significantly lower frequency range of signal, which is the most important regarding the influence on human body.

The author selected two measurement points: on the engine mount and on the steering wheel. The locations were related to driver's body parts exposed for vibrations in his seated position in the car. The sensors were positioned vertically, along the gravitational force vector direction.

There were specified particular states for every run, in which the cars were being measured. The velocities (30 km/h, 50 km/h, 90 km/h) were chosen as the most popular, operational speeds which the vehicles are frequently driven.

For every speed, the signals were collected on two selected gears. (Table 4 and 5).

The methodology for conducted research is designed to be comparative, therefore all measurement errors are considered as systematic and not taken into result calculations.

Table 4. Car cases specification – Leon 1

	Seat Leon 1	30 km/h	50 km/h	90 km/h
2 gear [rev/min]	2180	–	–	–
3 gear [rev/min]	1530	2550	–	–
4 gear [rev/min]	–	1920	3420	–
5 gear [rev/min]	–	–	2820	–

Table 5. Car cases specification – Leon 3

	Seat Leon 3	30 km/h	50 km/h	90 km/h
2 gear [rev/min]	1980	–	–	–
3 gear [rev/min]	1310	2170	–	–
4 gear [rev/min]	–	1650	2960	–
5 gear [rev/min]	–	–	2370	–

2.4. Signal processing

The character of signals received from engine as a primary source of vibrations is considered as stationary. The stochastic processes are stationary when the arithmetic mean, variance and autocorrelation do not change in time. The signals were transformed with the Fast Fourier Transform (FFT), which is a very effective tool for processing this type of signals [23].

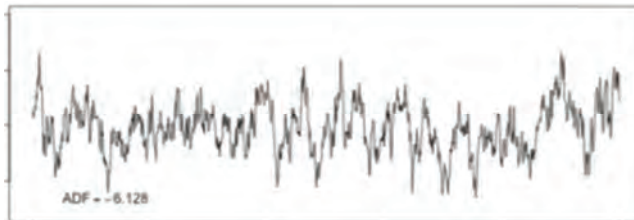


Fig. 5. The stationary signal [24]

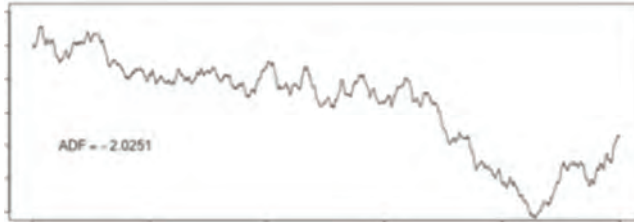


Fig. 6. The non-stationary signal [24]

3. Results

The vibration signals were registered as plots of a voltage in time domain. The postprocessing based on FFT in order to obtain spectra in a frequency domain. The waveforms recorded for the 2 seconds were taken for the analysis. The sampling frequency equated 2048 Hz.

Vibration signals were recognized as the stationary type, which supported the statement, that the engines have stationary characteristics of running. Such sampling frequency allowed to receive large amount of measurement samples and it was sufficient to perform the FFT for receiving the spectra for further analysis [13].

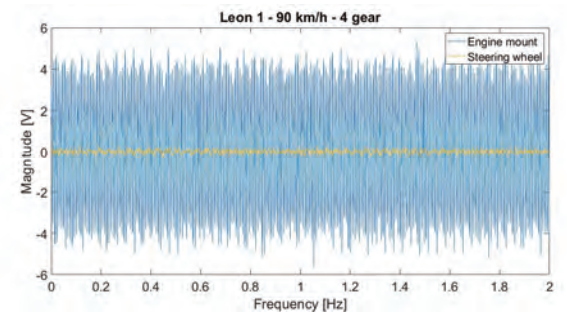


Fig. 7. Time course of the two sensors in the Leon 1

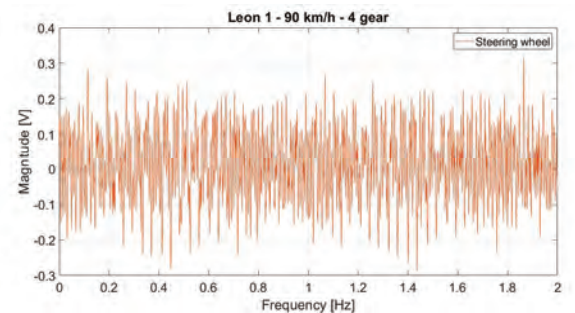


Fig. 8. Time course of the steering wheel sensor in the Leon 1

As it can be seen in the diagram above (Fig. 7), the signal from the engine mount in the Leon 1 has significantly larger amplitude in compare to the other. The same can be observed in the Leon 3 (Fig. 9). It can be understood as the engine is one of the main source of the vibrations in the car and the another location for the sensor is damped.

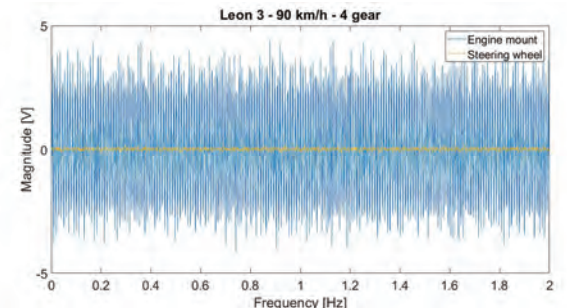


Fig. 9. Time course of the two sensors in the Leon 3

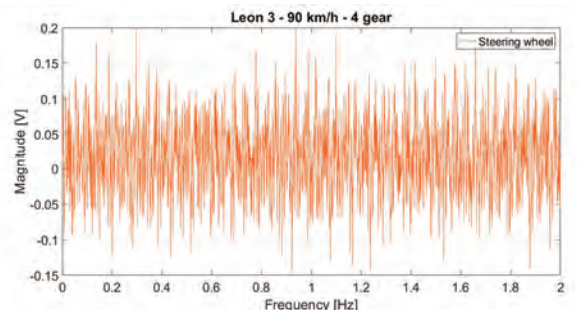


Fig. 10. Time course of the steering wheel sensor in the Leon 3

The location on steering wheel is the one of the places, where the constant contact between the driver and the vehicle is.

The spectra for both cars were compared in order to distinguish the differences between the vehicles and the influence of downsized engine on vibration frequencies.



Fig. 11. Spectrum of the engine mount sensor in the Leon 1

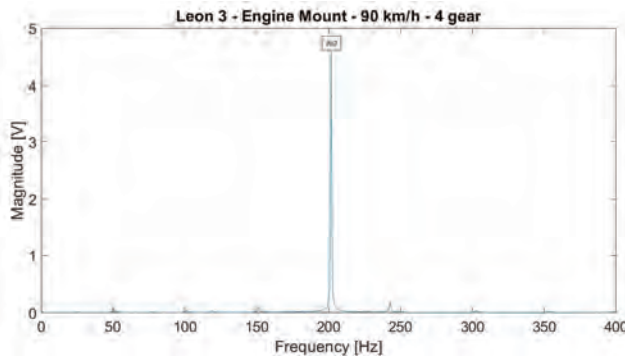


Fig. 12. Spectrum of the engine mount sensor in the Leon 3

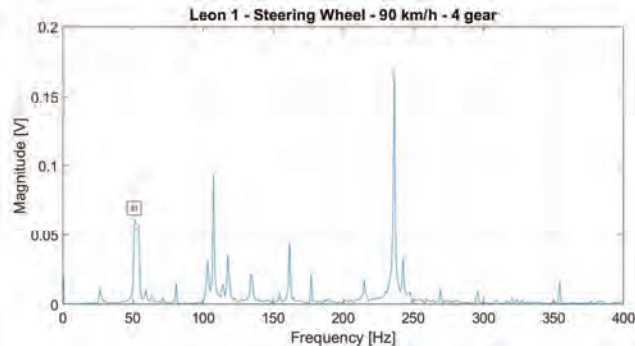


Fig. 13. Spectrum of the steering wheel sensor in the Leon 1

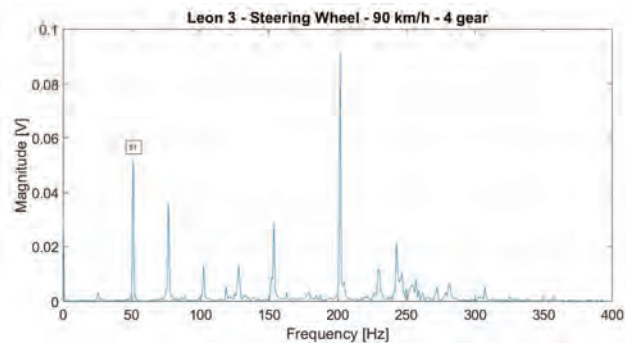


Fig. 14. Spectrum of the steering wheel sensor in the Leon 3

In the diagrams above (Fig. 11-14) it can be seen the examples of spectra for engine mount and steering wheel for both cars. The author focused on comparing only the dominant harmonics of the original signal. The complete results for these two locations for every case of the measurements are presented below (Table 6 and 7).

Table 6. Frequencies for the engine mount

	Engine mount					
	30 km/h		50 km/h		90 km/h	
Gear	2	3	3	4	4	5
Leon 1 [Hz]	147	106	175	132	237	194
Leon 3 [Hz]	137	89	148	112	202	161

Table 7. Frequencies for the steering wheel

	Steering wheel					
	30 km/h		50 km/h		90 km/h	
Gear	2	3	3	4	4	5
Leon 1 [hz]	53	54	60	60	51	54
Leon 3 [hz]	8	8	43	43	51	51

4. Conclusions

This introduction study shows, that accelerometry is a valid methodology for author's approach on vibrations measurements in the passenger vehicles.

The measurements of vibrations generated by the engine display, that waveform signals have stationary characteristic, therefore the Fast Fourier Transform is legitimate method for measurements and provides meaningful results.

The amplitude in time domain of the engine mount signal, as it is the primary source of vibrations for this study, is much higher than the location on the steering wheel, which shows the damping effect.

The results for the engine location for both cars show that the frequencies are higher with the increase of velocity. The higher gear of each speed decreases the frequency. The turbocharged engine has lower frequencies than naturally aspirated one in all cases of velocity and gear combination.

The results for the steering wheel location in the car with turbocharged engine show, that frequencies for two velocities are lower than in the another one and for one velocity are equal. The change of gear in this case does not have any impact for frequency value.

This study shows that the engine manufactured in the downsized technology, equipped with turbochargers, can have more negative or harmful effects on the driver, due to existence of lower frequencies than the car with naturally aspirated engine.

Currently available information about vibrations influence on human body show, that lower frequencies are the most dangerous for people, however the exact limits are not officially established and can vary depending on each person.

The author would like to continue studies and development of this methodology with higher number of vehicles and additional measurement locations verifying the observed tendency on the larger research sample.

The author acknowledges the huge necessity for further studies of possibly harmful effects of low frequencies occurring in the passenger vehicles.

Nomenclature

TSI	Turbo Stratified Injection
YoM	Year of Manufacture
FFT	Fast Fourier Transform

HP	Horse Power
Euro NCAP	European New Car Assessment Programme

Bibliography

- [1] Commission Regulation (EC) No 692/2008 of 18 July 2008 implementing and amending Regulation (EC) No 715/2007 of the European Parliament and of the Council on type-approval of motor vehicles with respect to emissions from light passenger and commercial vehicles (Euro 5 and Euro 6) and on access to vehicle repair and maintenance information.
- [2] Regulation (EU) 2019/631 of the European Parliament and of the Council of 17 April 2019 setting CO₂ emission performance standards for new passenger cars and for new light commercial vehicles, and repealing Regulations (EC) No. 443/2009 and (EU) No 510/2011.
- [3] SCHEFFER, C., GIRDHAR, P. Practical machinery vibration analysis and predictive maintenance (Practical Professional). *Newnes*. 2004.
- [4] WORLD HEALTH ORGANIZATION. Occupational exposure to vibration from handheld tools. *UMEA Universitet*.
- [5] BURDZIK, R., KONIECZNY, L. Vibration issues in passenger car. *Transport Problems*. 2014, **9**(3), 83-90.
- [6] BURDZIK, R., KONIECZNY, L. Application of vibroacoustic methods for monitoring and control of comfort and safety of passenger cars. *Solid State Phenomena*. 2014, **210**, 20-25.
- [7] KUMARESH, S.A., ALADDIN, M.F. A study of vibration transmission on seated person in passenger vehicle. *AIP Conference Proceedings*. 2019, **2137**(1).
- [8] NAHAVI, H., FOULADI, M.H., NOR, M.J.M. Evaluation of whole-body vibration and ride comfort in a passenger car. *International Journal of Acoustic and Vibration*. 2009, **14**(3).
- [9] <https://www.autocentrum.pl/dane-techniczne/seat/leon/i/hatchback/silnik-benzynowy-1.6-105km-2000-2004/>
- [10] <https://www.autocentrum.pl/dane-techniczne/seat/leon/iii/hatchback-facelifting/silnik-benzynowy-1.4-tsi-125km-2016-2018/>
- [11] https://www.the-blueprints.com/blueprints/cars/seat/985/view/seat_leon/
- [12] <https://m.autocentrum.pl/ac-file/car-blueprint/578cd964582c7db4438baba3/szkic-techniczny-seat-leon-iii-cupra-sc.jpg>
- [13] CADY, W.G. Piezoelectricity: volume one and two: an introduction to the theory and applications of electromechanical phenomena in crystals. *Dover Publications*. 2018.
- [14] DE SILVA, C. Vibrations Fundamentals and Practice. *CRC Press*, NY 2000.
- [15] GIERGIEL, J. Mechanical vibrations (in Polish). *University Scientific-Educational Publishers*, Cracow 2000.
- [16] <https://www.pcb.com/products?m=352C04>
- [17] https://www.ni.com/pdf/manuals/374238a_02.pdf
- [18] Hamownia podwoziowa do kontroli mocy MAHA LPS 300 dla samochodów osobowych, Instrukcja obsługi.
- [19] ISO 2631-1:1997 Mechanical vibration and shock – Evaluation of human exposure to whole-body vibration – Part 1: general requirements.
- [20] PN-EN 14253:2005 Drgania mechaniczne. Pomiar i obliczanie zawodowej ekspozycji na drgania o ogólnym działaniu na organizm człowieka dla potrzeb ochrony zdrowia. Wytyczne praktyczne.
- [21] PN-91/S-04100 Drgania. Metody badań i oceny drgań mechanicznych na stanowiskach pracy w pojazdach.
- [22] ŁAZARZ, B., MADEJ, H., CZECH, P. Fotel kierowcy jako element układu tłumienia drgań. *Transport*. 2009, **65**, Zeszyty Naukowe Politechniki Śląskiej.
- [23] BRIGHAM, E. Fast Fourier Transform and its applications, *Pearson*, 1988.
- [24] pl.wikipedia.org/wiki/Plik:Stationarycomparison.png

Łukasz Łoza, MEng. – Faculty of Mechanical Engineering, Wrocław University of Science and Technology.

e-mail: lukasz.loza@pwr.edu.pl



Cold start emissions from a gasoline engine in RDE tests at different ambient temperatures

The implementation of the 3rd package of the RDE test procedure has extended the test method by considering emissions from a cold start period into the total exhaust emissions from a vehicle. The article presents the research results of exhaust emissions of a vehicle equipped with a gasoline engine. The tests were carried out at two different ambient temperatures, in line with the requirements of the RDE test procedure for passenger cars, meeting the Euro 6d-Temp emissions standard. The obtained results were analyzed, i.e. there were compared the engine and vehicle operating parameters and the values of road exhaust emissions during the cold start at two different ambient temperatures. The summary presents the shares of the cold start phase for each exhaust emission compound in the urban part of the test and the entire RDE test, depending on the ambient temperature (8°C and 25°C).

Key words: *cold start, RDE test, exhaust emissions, ambient temperature, gasoline engine*

1. Introduction

Road transport is still considered the most important source of air pollution. Scientific research [16] indicates that the emission of harmful exhaust compounds has a negative impact not only on air quality but also on human health. This phenomenon is particularly visible in urban agglomerations. One of the European Union's tasks, set off for the coming years, is to continue and even intensify work on improving air quality. The European Commission's assumption is to achieve climate neutrality. However, to gain this, the level of air pollution should first be gradually reduced. To this end, among other, increasingly restrictive legal acts concerning vehicle exhaust emissions are introduced [2-6]. Meeting these requirements is not easy, so it is necessary to use more and more advanced exhaust after-treatment systems.

In recent years, many research papers on cold start emissions have been published (i.a. [13, 17, 19, 24, 30]). The need to take into account emissions from the cold start phase has been noticed not only in Europe but also worldwide. The authors of the articles [18, 26] pointed out the importance of the cold start issue as well as the necessity of further improvement of exhaust after-treatment systems. Whereas, the authors of the publications [8, 10, 11] suggested that NO_x emission should be an issue addressed in subsequent updates of EU regulations. According to the authors of the publication [8], the NO_x emissions from vehicles, equipped with a gasoline engine, are increasingly higher and consequently, particularly important in the context of urban air quality. The authors also pay attention to the value of the ambient temperature at which the RDE test is performed.

The authors of the articles [31, 33] came to the same conclusions. They determined the impact of different ambient temperatures (-7°C and 23°C) on the emission results of vehicles equipped with compression and spark-ignition engines. The aim of the test was to verify the results according to Euro 6 emissions standard and check if the exhaust emissions in the WLTC test increase during the cold season in comparison to higher ambient temperatures [7, 8]. The authors of this article noticed the need to develop a new and independent procedure allowing verification of the emissions level at low ambient temperatures.

2. RDE test conditions

Although the RDE test is performed under real traffic conditions, it is highly formalized. The requirements concern not only the vehicle conditioning for the test but also the provision of research conditions [1, 12, 14, 20-23]. According to [27, 28], this is necessary for the proper performance of the test and further analysis of the results obtained. The main requirements to be met during the test are shown in Fig. 1. Due to the vehicle speed, the test route is divided into three parts: urban, rural and motorway conditions. The test drive is carried out continuously, but there are a few exceptions [9]. The rural drive section can be interrupted by short periods of urban driving if urban areas are on the route. Driving on the motorway can interrupt short driving periods in urban or rural areas. The duration of the test is within the acceptable range, i.e. between 90 min and 120 min.

Requirements	Urban	Rural	Motorway
Vehicle speed	0–60 km/h	60–90 km/h	> 90 km/h
Distance share	29–44 %	23–43 %	23–43 %
Min distance	16 km	16 km	16 km
Average speed	15–40 km/h	–	–
Total stop time	6–30 %	–	–
Individual stops	≤ 300 s	–	–
V > 100 km/h	–	–	–
V > 145 km/h	–	–	≥ 5 min < 3%*

Total test duration: 90–120 min
Start/end test elevation difference: ≤ 100 m
* Max speed of 145 km/h may be exceeded by: 15 km/h for < 3% of the motorway time duration

Fig. 1. The RDE test requirements [25-28]

Package 3 [27] of the RDE test procedure has introduced primarily the inclusion of cold-start period emissions in the entire RDE test. The definition of cold start is as follows – the period from the first start of a combustion engine until the point when the combustion engine has run cumulative for 5 min. The cold start period ends once the coolant temperature has reached 70°C for the first time but

no later than after 5 min from the initial engine start. The main requirements for a cold start are listed in Fig. 2.

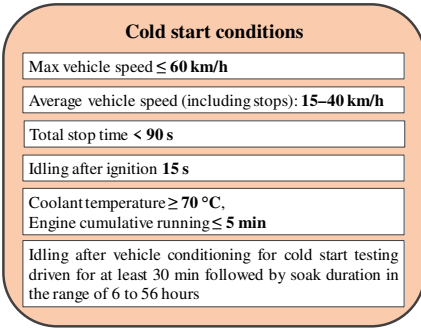


Fig. 2. Cold start requirements [32]

The 4th [28] package of the RDE test procedure modified the calculation of total exhaust emissions but also specified the exhaust emissions obtained in the urban part (compared to total emissions in the test). This article aims to determine the shares of specific exhaust compounds during the cold start phase and in the entire test, depending on the ambient temperature (8°C and 25°C).

3. Research methodology

3.1. Research object

One of the popular midsize passenger car class was used for testing. The vehicle was equipped with a gasoline engine that met the Euro 6d-Temp emissions norm. The exhaust after-treatment system consists of a 3-way catalytic converter and a particulate filter. Details of the vehicle used are shown in Table 1.

Table 1. Characteristics of the passenger car used in testing

Curb weight	1450 kg
Engine type	turbocharged gasoline engine with direct injection
Displacement volume	1.6 dm^3
Maximum power	130 kW
Emission standards	Euro 6d-Temp
The after-treatment system	three-way catalytic converter with a particulate filter

3.2. Test route and exhaust emission measurements

The test route has been designated in accordance with RDE requirements and divided into 3 sections; urban, rural and motorway (Fig. 3). The driving distances, shares of the individual portion of the test have been chosen so that they meet the requirements described in [26].

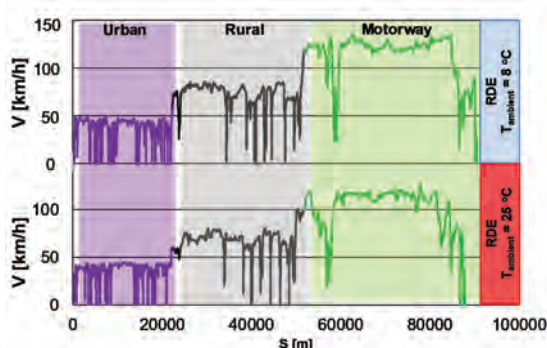


Fig. 3. Vehicle speed profiles in both RDE test drives

The authors carried out two test drives on the same research route in the city of Poznan and its surroundings by the same driver. Measurements were conducted in two different ambient temperatures (8°C and 25°C). For measuring the concentration of exhaust compounds, a PEMS apparatus was used. Besides, the GPS signal was recorded at a frequency of 1 Hz during testing. The research equipment used was compliant with the European Union requirements concerning the measurement of harmful exhaust compounds from passenger cars under real driving conditions.

4. The analysis of recorded parameters

4.1. Engine operating parameters of the vehicle

The first stage of the analysis was to validate the performance of road tests with the requirements of the RDE test procedure. All parameters were verified by appropriate procedures and no deviations from the required values were found. However, in the case of this article the most important was to check the validity of the cold start emission parameters and the boundary conditions (these parameters were discussed in the next point).

Therefore, the analysis of vehicle speed during the cold start period has been made. It is required to start driving for a maximum of 15 seconds after starting the engine (Fig. 4). This condition was met in both cases and at the same time a similar character of the vehicle speed profiles in the first 300 s of the RDE test is shown. Slightly higher values of the maximum vehicle speed were recorded for the lower ambient temperature.

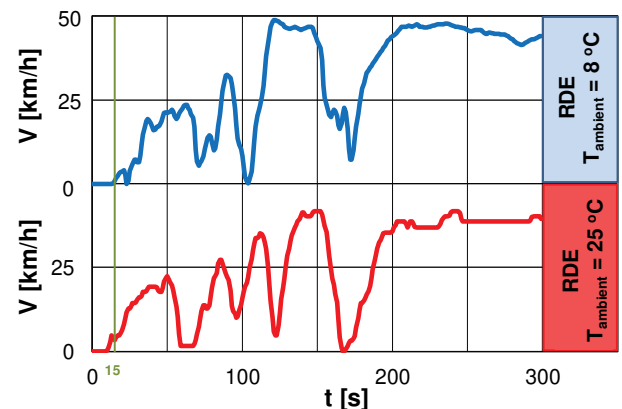


Fig. 4. Vehicle speed during the cold start phase at different ambient temperatures

The comparison of the coolant temperature in both cases also shown that the requirements of the RDE test procedure have been met, i.e. it did not exceed the value of 70°C . For the cold start at the ambient temperature of 25°C , 300 s from the engine start, the coolant temperature achieved a value of 69°C . For the ambient temperature of 8°C , the coolant temperature was only 57°C . Firstly, the initial coolant temperature difference of 17°C but after 300 s (since the engine was started) it decreased to 12°C . Therefore, a greater coolant temperature gradient was found for lower ambient temperature (Fig. 5).

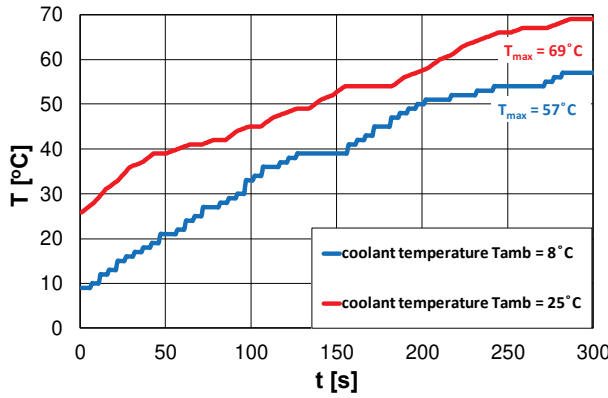


Fig. 5. The coolant temperature during the cold start phase at different ambient temperatures

A similar character of the changes was also observed during the analysis of exhaust temperature, measured at the end of the vehicle exhaust system. The difference for the measurement time ($t = 0$ s), amounting to about 12°C , is compensated already after about 100 s, where the exhaust temperature is around 30°C . The further profile of exhaust temperature is very similar to each other, and the differences occurring in the period up to 300 s are very small (Fig. 6).

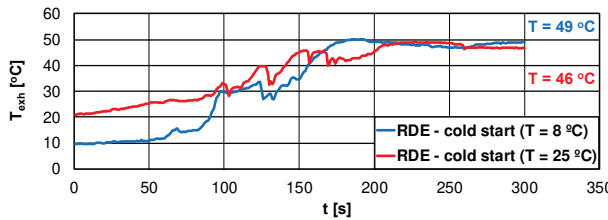


Fig. 6. The exhaust temperature during the cold start phase at different ambient temperatures

4.2. Ecological parameters

The recorded profile of emission intensity changes in the cold start period ($t = 0$ –300 s) for two different ambient temperatures (8°C and 25°C) are shown in Figs. 7–10.

The carbon monoxide mass is almost 3 times higher at the ambient temperature of 8°C (3.47 g) in comparison to the value of 25°C (1.21 g). The average value of the emission intensity is 0.011 g/s (at the ambient temperature of 8°C) and 0.004 g/s (at 25°C). For the cold start at the ambient temperature of 25°C , the highest value of emissions intensity is 0.09 g/s. While for the temperature of 8°C this value is twice higher (Fig. 7).

The analysis of carbon dioxide emission intensity shows that during the cold start and warming the engine, the mass of this compound is about 16% higher at the ambient temperature of 8°C (687 g) than at 25°C (592 g). The average value of the emission intensity is 2.19 g/s and 1.89 g/s, respectively. The fluctuations between the results of test drives were caused by the changes in the dynamic motion conditions. However, the average value of this parameter is not affected by the ambient temperature at which the cold engine started (Fig. 8).

The analysis of nitrogen oxides emission intensity shows that for this exhaust compound the relations are completely different than for the previous compounds. For

the higher ambient temperature (25°C) the main increase of nitrogen oxides intensity (up to 0.005 g/s) is observed at the first 50 seconds after the engine started. During the cold start phase, the mass of this compound is equal to 0.400 g and the average value of the emission intensity is 0.0293 g/s. In the case of lower ambient temperature (8°C), the intensity of nitrogen oxides is about 11% higher than at 25°C . For the value of 8°C , the highest values of emission intensity are reached at the first 100 s and then they are being reduced (Fig. 9).

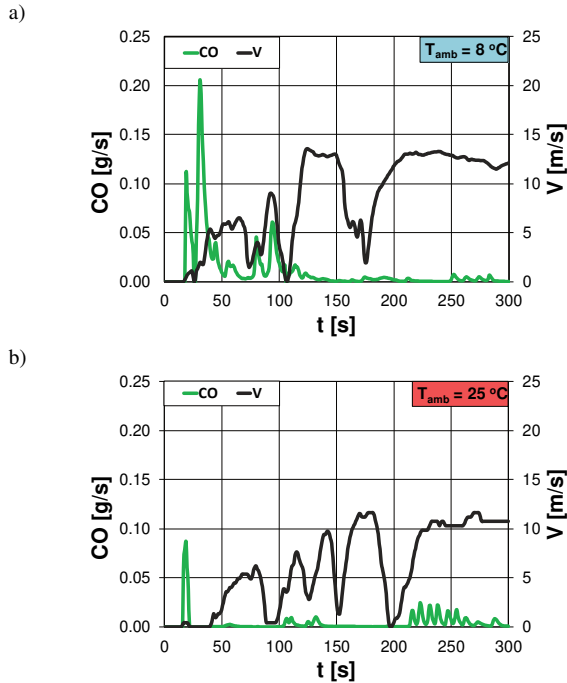


Fig. 7. Emission intensity of carbon monoxide and vehicle speed during cold start at ambient temperature of 8°C (a) and 25°C (b)

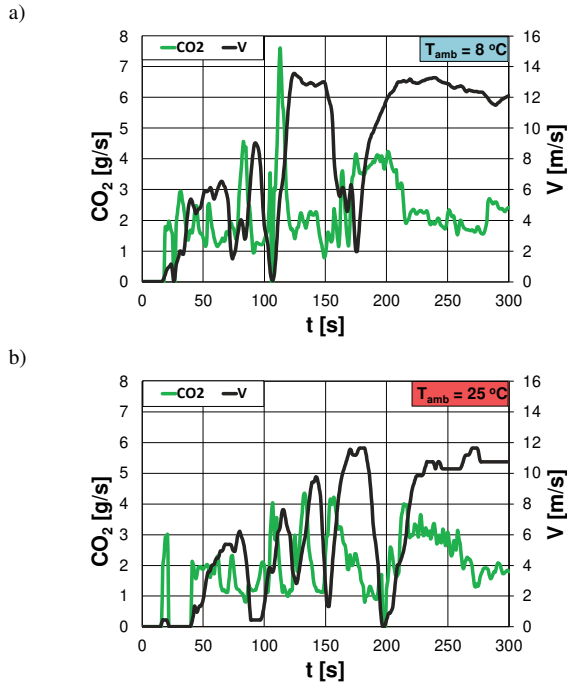


Fig. 8. Emission intensity of carbon monoxide and vehicle speed during cold start at ambient temperature of 8°C (a) and 25°C (b)

Regarding the number of particulates at the ambient temperature of 25°C, there is a peak (up to 1.45E+09) in the first 40 s after the engine started. At the ambient temperature of 8°C, this peak occurs earlier ($t = 30$ s) and reaches 1.20E+10 (Fig. 10). The particles number, in the period of 300 s from starting, increased by almost 4 times during the reduction of temperature value from 25°C to 8°C (7.5E+10 and 2.8E+11). The research results of emission intensity (Fig. 7) were used to determine the road emissions (converting the mass per unit of the road) during the cold start phase (lasting 300 s).

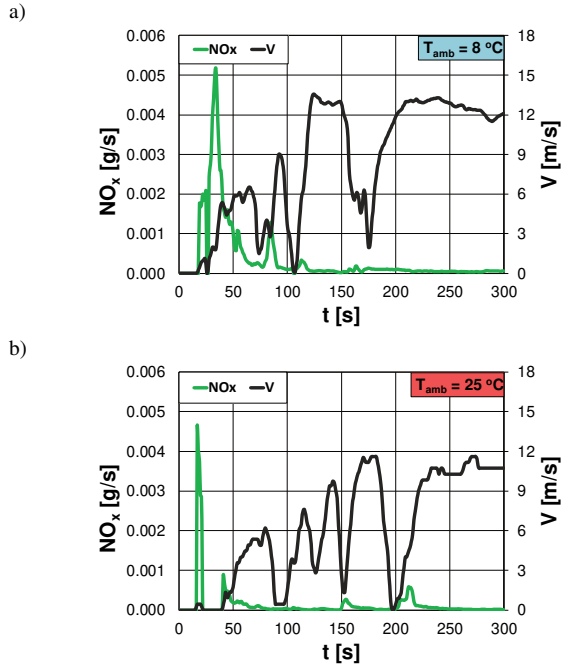


Fig. 9. Emission intensity of nitrogen oxides and vehicle speed during cold start at ambient temperature of 8°C (a) and 25°C (b)

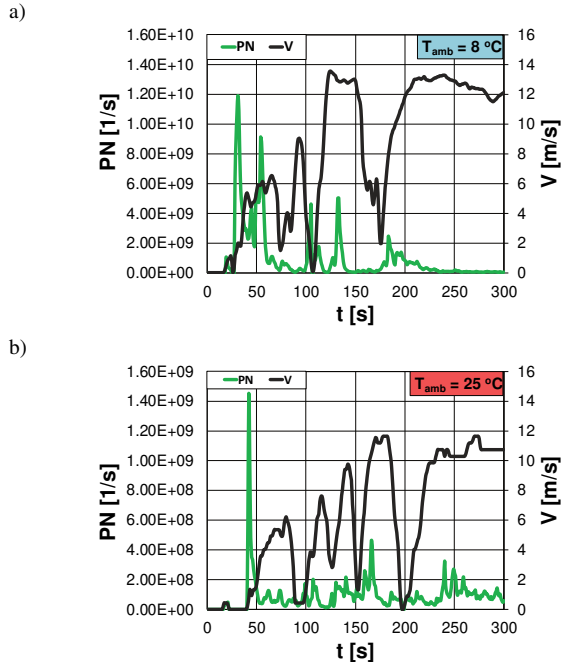


Fig. 10. Emission intensity of particle numbers and vehicle speed during cold start at ambient temperature of 8°C (a) and 25°C (b)

The reduction of the ambient temperature (from 25°C to 8°C) during the cold start (in the considered period of 300 s) results in (Fig. 11):

- an increase by 68% of CO road emissions,
- an increase by 15% of CO_2 road emissions,
- a decrease by 50% of NO_x road emissions,
- an increase by 47% of PN road emissions.

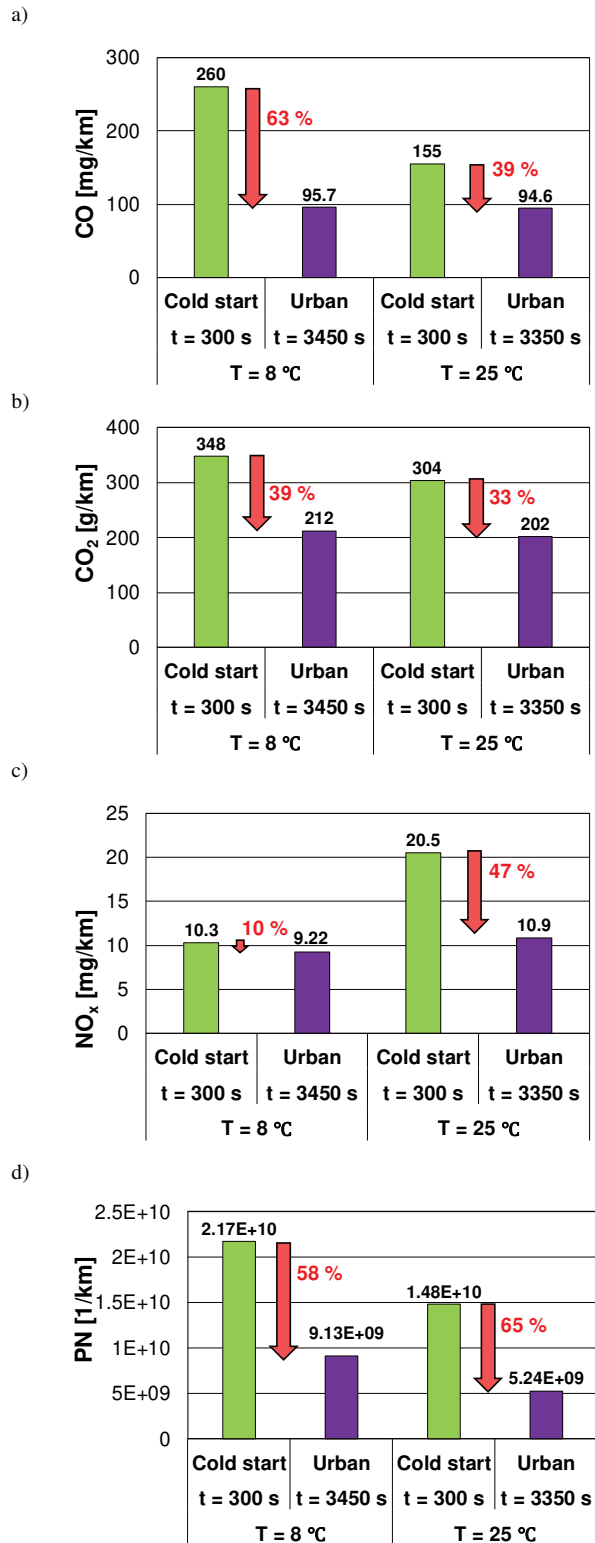


Fig. 11. Road emissions of CO (a), CO_2 (b), NO_x (c), PN (d) at two different ambient temperatures

Comparing the cold start phase for different ambient temperatures in the urban part of the RDE test and in the entire RDE test are shown in Fig. 12 and 13. For the value of ambient temperature equal to 8°C, the results are as follows:

1. The share of CO emissions during the cold start (300 s) in relation to the urban part of RDE test is 26.0%; and in the relation to the entire RDE test it increases to 10.8%.
2. The share of CO₂ emissions during the cold start (300 s) in relation to the urban part of the RDE test is 11.6%; and in the relation to the entire RDE test it decreases to 3.40%.
3. The share of NO_x emission during the cold start (300 s) in relation to the urban part of RDE test is 10.6%; and in the relation to the entire RDE test it decreases to 2.92%.
4. The share of PN emissions during the cold start (300 s) in relation to the urban part of RDE test is 22.7%; and in the relation to the entire RDE test it decreases to 0.05%.

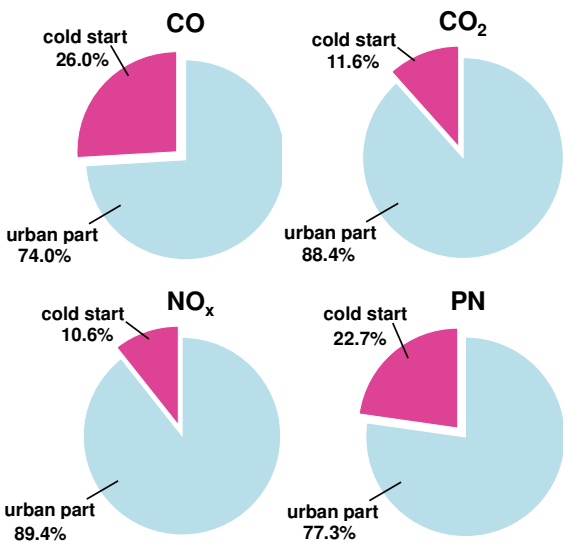


Fig. 12. Share of CO, CO₂, NO_x and PN emissions in urban section during cold start at 8°C

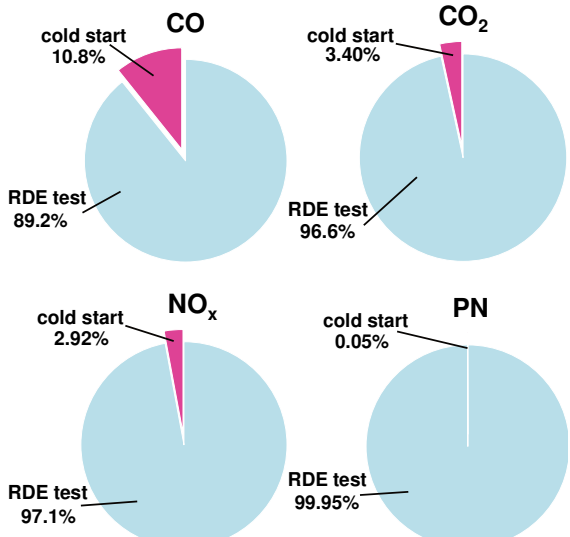


Fig. 13. Share of CO, CO₂, NO_x and PN road emissions in the entire RDE test during cold start at 8°C

In the case of the ambient temperature equals to 25°C the results are as follows (Fig. 14 and 15):

1. The share of CO emissions during the cold start (300 s) in relation to the urban part of RDE test is 10.7%; and in the relation to the entire RDE test it decreases to 4.63%.
2. The share of CO₂ emissions during the cold start (300 s) in relation to the urban part of the RDE test is 9.80%; and in the relation to the entire RDE test it decreases to 3.40%.
3. The share of NO_x emission during the cold start (300 s) in relation to the urban part of RDE test is 12.3%; and in the relation to the entire RDE test it decreases to 3.42%.
4. The share of PN emissions during the cold start (300 s) in relation to the urban part of RDE test is 18.4%; and in the relation to the entire RDE test it decreases to 0.05%.

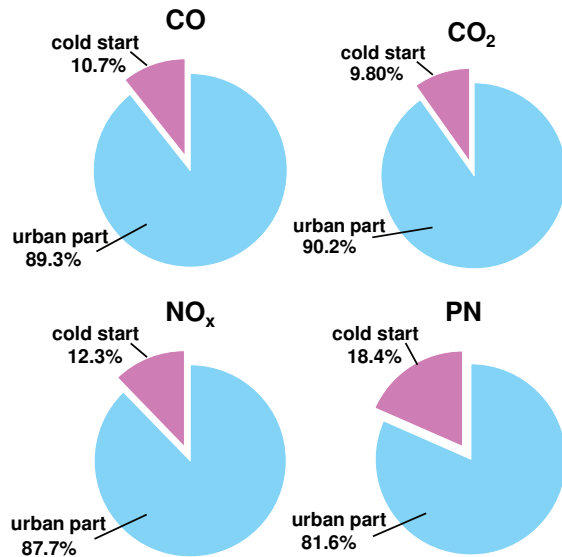


Fig. 14. Share of CO, CO₂, NO_x and PN emissions in urban section during cold start at 25°C

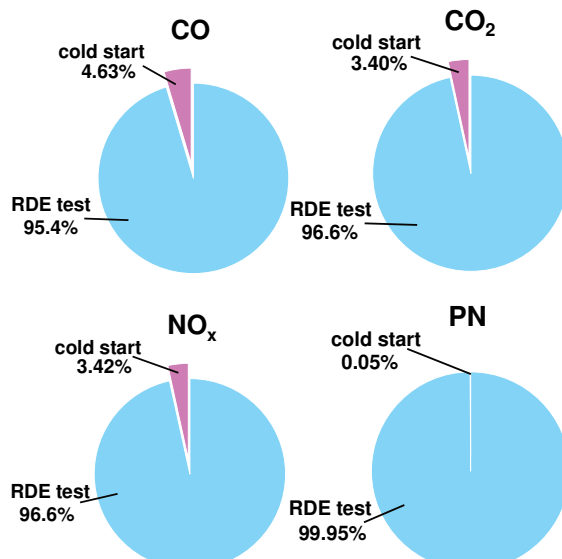


Fig. 15. Share of CO, CO₂, NO_x and PN road emissions in the entire RDE test during cold start at 25°C

5. Summary and conclusions

The RDE test procedure is still being developed and improved. Package 3 extended this road emission test by taking into account the emissions from cold start phase to the total value of exhaust emissions.

The article presents and discuss the research results on the impact of ambient temperature (8°C and 25°C) during the cold start phase of the gasoline engine in emission road tests. The measurements were carried out in compliance with the latest legislative procedures applicable to passenger cars. After the analysis of the engine operating parameters, there were defined its ecological parameters (emission intensity and road emissions) in the cold start period ($t = 300$ s). Finally, there were determined the shares of CO, CO₂, NO_x and PN emissions in urban part and in the entire RDE test; during the cold start at 8°C and 25°C (Table 2).

The reduction of the ambient temperature (from 25°C to 8°C) during the cold start (in the considered period of

300 s) results in an increase of all exhaust compounds, except NO_x. The share of this compound is greater at the higher ambient temperature. This trend is caused by the combustion process in the engine and the formation of nitrogen oxides. Another reason is warming of exhaust after-treatment system. It is necessary to modify and improve exhaust after-treatment systems so that they fulfil their function at a lower operating temperature.

Table 2. Characteristics of the passenger car used in testing

	T _{amb} = 8°C		T _{amb} = 25°C	
	Share in the urban part	Share in the RDE test	Share in the urban part	Share in the RDE test
CO	26.0%	10.8%	10.7%	4.63%
CO ₂	11.6%	3.40%	9.80%	3.40%
NO _x	10.6%	2.92%	12.3%	3.42%
PN	22.7%	0.05%	18.4%	0.05%

Acknowledgements

This study was funded by Projects 05/52/DSPB/1278.

Nomenclature

CO	carbon monoxide
CO ₂	carbon dioxide
GPS	Global Positioning Signal
NO _x	nitrogen oxides

PEMS	Portable Emissions Measurement System
PN	particle number
RDE	Real Driving Emissions
WLTC	Worldwide Harmonized Light Vehicles Test Cycle

Bibliography

- [1] CHEN, Y., BORKEN-KLEEFELD, J. Real-driving emissions from cars and light commercial vehicles – Results from 13 years remote sensing at Zurich/CH. *Atmospheric Environment*. 2014, **88**, 157-164.
<https://doi.org/10.1016/j.atmosenv.2014.01.040>
- [2] Commission Regulation (EU) 2014 No 133/2014 of 31 January 2014 amending, for the purposes of adapting to technical progress as regards emission limits, Directive 2007/46/EC of the European Parliament and of the Council, Regulation (EC) No 595/2009 of the European Parliament and of the Council and Commission Regulation (EU) No 582/2011.
- [3] Commission Regulation (EU) 2014 No 136/2014 of 11 February 2014 amending Directive 2007/46/EC of the European Parliament and of the Council, Commission Regulation (EC) No 692/2008 as regards emissions from light passenger and commercial vehicles (Euro 5 and Euro 6) and Commission Regulation (EU) No 582/2011 as regards emissions from heavy duty vehicles (Euro VI).
- [4] Commission Regulation (EU) 2014 No 627/2014 of 12 June 2014 amending Regulation (EU) No 582/2011 for the purposes of adapting it to technical progress as regards particulate matter monitoring by the on-board diagnostic system.
- [5] Commission Regulation (EU) 2016 No 2016/1718 of 20 September 2016 amending Regulation (EU) No 582/2011 with respect to emissions from heavy-duty vehicles as regards the provisions on testing by means of portable emission measurement systems (PEMS) and the procedure for the testing of the durability of replacement pollution control devices.
- [6] Commission Regulation (EU) 2017 No 2017/1347 of 13 July 2017 correcting Directive 2007/46/EC of the European Parliament and of the Council, Commission Regulation (EU) No 582/2011 and Commission Regulation (EU) 2017/1151 supplementing Regulation (EC) No 715/2007 of the European Parliament and of the Council on type-approval of motor vehicles with respect to emissions from light passenger and commercial vehicles (Euro 5 and Euro 6) and on access to vehicle repair and maintenance information, amending Directive 2007/46/EC of the European Parliament and of the Council, Commission Regulation (EC) No 692/2008 and Commission Regulation (EU) No 1230/2012 and repealing Regulation (EC) No 692/2008.
- [7] DAHAM, B., LI, H., ANDREWS, G. et al. Comparison of real world emissions in urban driving for Euro 1-4 vehicles using a PEMS. *SAE Technical Paper* 2009-01-0941. 2009. <https://doi.org/10.4271/2009-01-0941>
- [8] DIMARATOS, A., TOUMASATOS, Z., DOULGERIS, S. et al. Assessment of CO₂ and NO_x emissions of one diesel and one bi-fuel gasoline/CNG Euro 6 vehicles during real-world driving and laboratory testing. *Frontiers in Mechanical Engineering*. 2019, **3**. <https://doi.org/10.3389/fmech.2019.00062>
- [9] DONATEO, T., GIOVINAZZI, M. Some repeatability and reproducibility issues in real driving emission tests. *SAE Technical Paper* 2018-01-5020. 2018. <https://doi.org/10.4271/2018-01-5020>
- [10] FARIA, M., VARELLA, R., DUARTE, G. et al. Engine cold start analysis using naturalistic driving data: City level impacts on local pollutants emissions and energy consumption. *Science of The Total Environment*. 2018, **630**, 544-559. <https://doi.org/10.1016/j.scitotenv.2018.02.232>
- [11] FRANCO, V., ZACHAROPOULOU, T., HAMMER, J. et al. Evaluation of exhaust emissions from three diesel-hybrid cars and simulation of after-treatment systems for ultralow real-world NO_x emissions. *Environmental Science & Technology*. 2016, **50**, 13151-13159. <https://doi.org/10.1021/acs.est.6b03585>
- [12] GALLUS, J., KIRCHNER, U., VOGT, R. et al. Impact of driving style and road grade on gaseous exhaust emissions

- of passenger vehicles measured by a portable emission measurement system (PEMS). *Transportation Research Part D: Transport and Environment*. 2017, **52**, 215-226. <https://doi.org/10.1016/j.trd.2017.03.011>
- [13] GIS, M. Assessment of exhaust emissions from vehicles in real traffic conditions. *IOP Conference Series: Earth and Environmental Science*. 2019, **214**, 012035. <https://doi.org/10.1088/1755-1315/214/1/012035>
- [14] HOOFTMAN, N. A review of the European passenger car regulations – real driving emissions vs local air quality. *Renewable and Sustainable Energy Reviews*. 2018, **86**, 1-21. <https://doi.org/10.1016/j.rser.2018.01.012>
- [15] JOHNSON, T., JOSHI, A. Review of vehicle engine efficiency and emissions. *SAE International Journal of Engines*. 2018, **11**(6), 1307-1330. <https://doi.org/10.2307/26649163>
- [16] KRZESZOWIAK, J., STEFANOW, D., PAWLAS, K. The impact of particulate matter (PM) and nitric oxides (NO_x) on human health and an analysis of selected sources accounting for their emission in Poland. *Medycyna Środowiskowa-Environmental Medicine*. 2016, **19**(3), 7-15. <https://doi.org/10.19243/2016301>
- [17] LAIRENLAKPAM, R., JAIN, A., GUPTA, P. et al. Effect of Real world driving and different drive modes on vehicle emissions and fuel consumption. *SAE Technical Paper* 2018-01-5017. 2018. <https://doi.org/10.4271/2018-01-5017>
- [18] LEMAN, A.M., RAHMAN, F., JAJULI, A. et al. Emission treatment towards cold start and back pressure in internal combustion engine against performance of catalytic converter: A review. *MATEC Web of Conferences*. 2017, **87**, 02021. <https://doi.org/10.1051/matecconf/20178702021>
- [19] MCCAFFERY, C., ZHU, H., LI, C. et al. On-road gaseous and particulate emissions from GDI vehicles with and without gasoline particulate filters (GPFs) using portable emissions measurement systems (PEMS). *Science of the Total Environment*. 2020, **710**, 136366. <https://doi.org/10.1016/j.scitotenv.2019.136366>
- [20] MERKISZ, J., PIELECHA, J., GIS, W. Comparison of vehicle emission factors in NEDC cycle and road test. *Proceedings of The Ninth Asia-Pacific International Symposium on Combustion and Energy Utilization*. 2008, 477-482.
- [21] MERKISZ, J., PIELECHA, J., GIS W. On-road testing and characterization of the exhaust emissions of light-duty vehicles. *Sustainable Development and Planning*. 2009, **1-2**(120), 439-449.
- [22] MERKISZ, J., PIELECHA, J., RADZIMIRSKI, S. New trends in emission control in the European Union. *Springer Tracts on Transportation and Traffic*. 2014, **4**, 67-90. <https://doi.org/10.1007/978-3-319-02705-0>
- [23] NOWAK, M., PIELECHA, J. Comparison of exhaust emission on the basis of Real Driving Emissions measurements and simulation. *MATEC Web of Conferences*. 2017, **118**, 00026. <https://doi.org/10.1051/matecconf/20171180026>
- [24] PRATI, M., MECCARIELLO, G., DELLA RAGIONE, L. et al. Real driving emissions of a light-duty vehicle in Na-
- ples. Influence of Road Grade. *SAE Technical Paper* 2015-24-2509. 2015. <https://doi.org/10.4271/2015-24-2509>
- [25] RDE Act 1 2016 Commission Regulation (EU) 2016/427 of 10 March 2016 amending Regulation (EC) No 692/2008 as regards emissions from light passenger and commercial vehicles (Euro 6).
- [26] RDE Act 2 2016 Commission Regulation (EU) 2016/646 of 20 April 2016 amending Regulation (EC) No 692/2008 as regards emissions from light passenger and commercial vehicles (Euro 6).
- [27] RDE Act 3 2017 Commission Regulation (EU) 2017/1154 of 7 June 2017 amending Regulation (EU) 2017/1151 supplementing Regulation (EC) No 715/2007 of the European Parliament and of the Council on type-approval of motor vehicles with respect to emissions from light passenger and commercial vehicles (Euro 5 and Euro 6) and on access to vehicle repair and maintenance information, amending Directive 2007/46/EC of the European Parliament and of the Council, Commission Regulation (EC) No 692/2008 and Commission Regulation (EU) No 1230/2012 and repealing Regulation (EC) No 692/2008 and Directive 2007/46/EC of the European Parliament and of the Council as regards real-driving emissions from light passenger and commercial vehicles (Euro 6).
- [28] RDE Act 4 2018 Commission Regulation (EU) 2018/1832 of 5 November 2018 amending Directive 2007/46/EC of the European Parliament and of the Council, Commission Regulation (EC) No 692/2008 and Commission Regulation (EU) 2017/1151 for the purpose of improving the emission type approval tests and procedures for light passenger and commercial vehicles, including those for in-service conformity and real-driving emissions and introducing devices for monitoring the consumption of fuel and electric energy.
- [29] SUAREZ-BERTOA, R., ASTORGA, C. Impact of cold temperature on Euro 6 passenger car emissions. *Environmental Pollution*. 2018, **234**, 318-329. <https://doi.org/10.1016/j.envpol.2017.10.096>
- [30] SUAREZ-BERTOA, R., VALVERDE, V., CLAIROTTTE, M. et al. On-road emissions of passenger cars beyond the boundary conditions of the Real-Driving Emissions Test. *Environmental Research*. 2019, **176**. <https://doi.org/10.1016/j.envres.2019.108572>
- [31] VARELLA, R., DUARTE, G., BAPTISTA, P. et al. Analysis of the influence of outdoor temperature in vehicle cold-start operation following EU real driving emission test procedure. *SAE International Journal of Commercial Vehicles*. 2017, **10**(2), 596-697. <https://doi.org/10.4271/2017-24-0140>
- [32] VARELLA, R., DUARTE, G., BAPTISTA, P. et al. Comparison of data analysis methods for European Real Driving Emissions Regulation. *SAE Technical Paper* 2017-01-0997. 2017. <https://doi.org/10.4271/2017-01-0997>
- [33] WILLIAMS, R., ANDERSSON, J., HAMJE, H. et al. Impact of demanding low temperature urban operation on the real driving emissions performance of three European diesel passenger cars. *SAE Technical Paper* 2018-01-1819. 2018. <https://doi.org/10.4271/2018-01-1819>

Karolina Kurtyka, MEng. – Faculty of Civil and Transport Engineering, Poznan University of Technology.

e-mail: karolina.t.kurtyka@doctorate.put.poznan.pl



Prof. Jacek Pielecha, DSc., DEng. – Faculty of Civil and Transport Engineering, Poznan University of Technology.

e-mail: jacek.pielecha@put.poznan.pl



Numerical investigation of lambda-value prechamber ignition in heavy duty natural gas engine

Turbulent Jet Ignition systems are mainly dedicated to the combustion of lean mixtures of natural gas in heavy duty engines. The use of such a system in combination with lean mixtures leads to an increase in its overall efficiency. The article presents simulation analyzes of the impact of the air excess coefficient occurring in prechamber on the combustion process: combustion indicators and emission indicators. Tests on a single-cylinder engine with a displacement of about 4 dm³ at medium mixture (IMEP = 1.0 MPa) were carried out using the AVL Fire software. It was found that the incineration of global lean mixtures ($\lambda = 2$) is effective when initiating this process (in the prechamber) with a charge of a stoichiometric composition. A strong relationship was found between the thermodynamic indicators in both prechamber and main chamber and the air excess coefficient initiating combustion.

Key words: *Turbulent Jet Ignition, combustion thermodynamics, combustion process indicators, numerical simulation*

1. Introduction

Turbulent Jet Ignition (TJI) systems are mainly used in engines running on lean mixtures. The solutions of the TJI system analyzed by Attard [3, 4] obtained an indicated thermal efficiency of 42% when burning lean mixtures. They find use mainly in large heavy duty (HD) engines [15]. Solutions for TJI systems were presented by Alvarez et al. [1]. He pointed to the possibility of increasing the range of lean mixtures to $\lambda = 2.5$, however, while using hydrogen as fuel for the prechamber (PC); petrol was fed to the main chamber (MC).

However, research on their possible applications in engines with small displacement is noted increasingly more often [4, 12, 17]. Road tests in the Real Driving Emissions (RDE) test were presented by Roso et al. [18] with the use of an engine with the PCIS (Pre Chamber Ignition System) with an air excess coefficient equal to $\lambda = 1.4$. Similar scientific papers with the use of internal combustion engines with the TJI system in hybrid drives and Range Extender (REX) were also published by Sens et al. [19].

Most TJI solutions use the stoichiometric compound value in the prechamber [5]. The latest solution is the so-called Dual Mode TJI (DM-TJI) – a system based on controlling the amount of recirculated exhaust gas in the prechamber [2]. The use of an additional valve supplying air to the prechamber allows for the proportion of recirculated exhaust gas to be increased to 40%.

In the research conducted by da Costa et al. [9] on the AVL 5496 engine (0.454 dm³) different values of the air excess coefficient in the prechamber ($\lambda = 1.0\text{--}1.6$) were used, however the same values were used in the main chamber. The maximum combustion indicator values were obtained for λ in the range of 1.3–1.4.

Korb et al. used the large global air excess coefficient [13] in simulations and experimental research. It was found that turbulence in the prechamber and use of the Miller cycle during the air intake have great significance in the combustion process.

TJI systems are made with passive prechambers (without fuel supply). However, the latest research confirms that depending on their design, it is possible to burn lean mixtures up to the value of $\lambda = 1.6$ [16] or $\lambda = 1.8$ [6].

A literature review reveals that research on ultra-lean mixtures is the subject of high research interest, however, no information can be found on the impact of the air excess coefficient value in the prechamber on combustion process indicators.

2. Research aim

The aim of the research was to determine the best values of the air excess coefficient in the prechamber in the vicinity of $\lambda = 1$ leading to favorable thermodynamic and ecological impact for the combustion of ultra-lean mixtures ($\lambda = 2$).

Research was focused on obtaining both one- and two-dimensional information on the global and local combustion process indicators.

The article seeks to answer the question of what the value of the air excess ratio during the start of the combustion process should be, in order to obtain the best thermodynamic indicators of the combustion process.

3. Method

3.1. Research object

The most widespread use of TJI combustion system can be found in HD engines. For this reason, an object similar in construction parameters to the supercharged GS6R2-PTK [14] engine from Mitsubishi was selected for analysis. It is an engine for Power Generation and Cogeneration applications. The maximum power output among the engine family (GS16R2-PTK – 16 cylinder engine) is 1.5 MW at 1500 rpm. The engine is powered with lean natural gas mixtures and operates in the Miller cycle (Table 1).

Table 1. Characteristics of the GS16R2-PTK engine [14]

Parameter	Unit	Value
Type	–	4-cycle, intercooled
Aspiration	–	turbocharged
Number of cylinders	–	6
Bore × stroke	mm	170 × 180
Displacement	dm ³	24.52
Combustion system	–	prechamber, spark ignited
Fuel	–	natural gas
Continuous power rating output (50 Hz 1500 rpm)	kW	363

In accordance with the above parameters, combustion system consisting of a prechamber with 7 holes ($\phi = 1.8$ mm and $l = 3.9$ mm) arranged symmetrically connected to the main chamber and having dimensions as shown in Fig. 1 was adopted for combustion tests. The combustion chamber is an original design modeled in the analyzed natural gas engine (which is the result of the lack of access to the original solution).

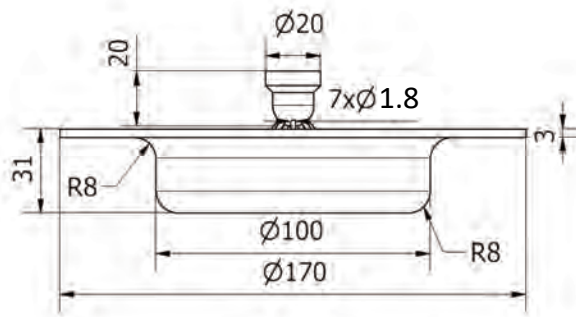


Fig. 1. Model of the engine combustion chamber powered by natural gas used for testing

The volume of one cylinder (V_{cyl}) was 4.085 dm^3 . Based on the adopted dimensions of the combustion chamber its volume was determined – $V_{CH} = 298.08 \text{ cm}^3$. The figure indicates the volume of the preliminary chamber – $V_{PC} = 11.86 \text{ cm}^3$. For these adopted values, the volume of the prechamber equals 3.98% of the combustion chamber volume. The compression ratio of such a model combustion system is $\epsilon = 14.79$.

3.2. Simulation method

The combustion process was based on the ECFM-3Z (Extended Coherent Flame Model-three Zone) [8]. This model is used in GDI engines with a large proportion of recirculated exhaust gas [10], as well as in gas-fueled engines [11].

The ECFM model is derived from the classic combustion model based on CFM flame density (Coherent Flame Model). The main assumption is that the fresh mixture does not contain recirculated flue gas. Due to the heterogeneity of the air-fuel mixture composition in the ECFM model, the so-called fuel and oxygen traces were introduced for more accurate local calculations of the intake gas composition. The gas enthalpy equation was defined in a similar way, enabling accurate assessment of temperature. As a consequence, it is possible to assess the local laminar flame speed [10, 11].

According to the division of the ECFM-3Z zone (Fig. 2), each calculation cell is divided into three mixing zones: mixed fuel zone (letter F), zone containing fuel mixture, air and EGR (letter M) and unmixed air zone + EGR (letter A).

In the ECFM model, we solve a transport equation for the average quantities of chemical species of O₂, N₂, CO₂, CO, H₂, H₂O, O, H, N, and OH. This equation is classically denoted as:

$$\frac{\partial \bar{\rho} \bar{y}_x}{\partial t} + \frac{\partial \bar{\rho} \bar{u}_i \bar{y}_x}{\partial x_i} - \frac{\partial}{\partial x_i} \left(\left(\frac{\mu}{S_c} + \frac{\mu_t}{S_{c_t}} \right) \frac{\partial \bar{y}_x}{\partial x_i} \right) = \bar{\omega}_x \quad (1)$$

where $\bar{\omega}_x$ is the combustion source term and \bar{y}_x is the averaged mass fraction of species α .

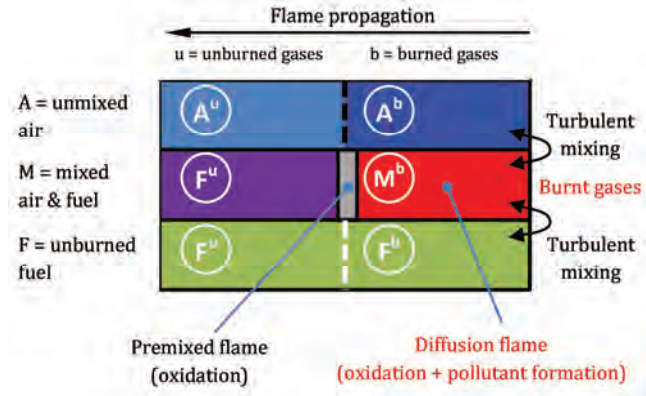


Fig. 2. Schematic of the ECFM-3Z model computational cell [7]

The fuel is divided in two parts: the fuel present in the fresh gases \bar{y}_{Fu}^u , and the fuel present in the burnt gases \bar{y}_{Fu}^b :

$$\bar{y}_{Fu}^u = \frac{\bar{m}_{Fu}^u}{\bar{m}} = \frac{\bar{m}_{Fu}^u/V}{\bar{m}/V} = \frac{\bar{\rho}_{Fu}^u}{\bar{\rho}} \quad (2)$$

and

$$\bar{y}_{Fu}^b = \frac{\bar{m}_{Fu}^b}{\bar{m}} = \frac{\bar{m}_{Fu}^b/V}{\bar{m}/V} = \frac{\bar{\rho}_{Fu}^b}{\bar{\rho}} \quad (3)$$

where $\bar{y}_{Fu} = \bar{y}_{Fu}^u + \bar{y}_{Fu}^b$ is the mean fuel mass fraction in the computational cell. \bar{m}_{Fu}^u (or \bar{m}_{Fu}^b) is the mass of the fuel contained in the fresh gases (resp. burnt gases). A transport equation is used to compute \bar{y}_{Fu}^u :

$$\frac{\partial \bar{\rho} \bar{y}_{Fu}^u}{\partial t} + \frac{\partial \bar{\rho} \bar{u}_i \bar{y}_{Fu}^u}{\partial x_i} - \frac{\partial}{\partial x_i} \left(\left(\frac{\mu}{S_c} + \frac{\mu_t}{S_{c_t}} \right) \frac{\partial \bar{y}_{Fu}^u}{\partial x_i} \right) = \bar{\rho} \tilde{S}_{Fu}^u + \bar{\omega}_{Fu}^u \quad (4)$$

where \tilde{S}_{Fu}^u is the source term quantifying the fuel evaporation in fresh gases. $\bar{\omega}_{Fu}^u$ is a source term taking auto-ignition, premixed flame and mixing between mixed unburned and mixed burnt areas into account.

3.3. Simulation conditions

The analysis of the air excess ratio impact in the prechamber on the combustion process was carried out at engine speed of $n = 1500 \text{ rpm}$ at an average load (IMEP = 1.08 MPa).

The fuel dose fed into the cylinder is divided in such a way that a lean homogeneous mixture with λ value close to 2 is supplied to the main chamber. A different dose of fuel q_{o_PC} is supplied to the prechamber in such a way that the sum of both fuel doses is constant ($\lambda_{ALL} = \text{const}$):

$$\lambda_{ALL} = \frac{m_{air}}{(q_{o_MC} + q_{o_PC}) \cdot 17.2} \quad (5)$$

The test conditions were set in such a way that the total fuel dose generated an air excess coefficient value of 2. This means that increasing the prechamber dose should lead to an increase the air excess ratio in the MC. Table 2 summarizes the initial simulation values.

Table 2. Simulation test conditions (initial condition)

Parameter	Unit	Value					
λ_{ALL}	–	2					
P _{air}	MPa	0.2					
q _{o_MC}	mg	222.0	221.8	221.6	221.3	221.1	220.8
λ_{MC}	–	2.023	2.027	2.030	2.036	2.039	2.045
q _{o_PC}	mg	1.3	1.5	1.7	2.0	2.2	2.5
$\lambda_{\text{ign_PC}}$	–	1.102	1.038	0.984	0.919	0.882	0.835
IVC	deg	500 deg (Miller cycle)					
Temperature		350 K					
TKE		20 m ² /s ²					
Turb. length scale		0.003 m					
Turb. diss. rate		4899 m ² /s ³					
Combustion model		Coherent Flame Model; ECFM-3Z					
Emission model		Extended Zeldovich (NO), kinetic model (Soot)					

In the conducted research, the most interesting aspect were the conditions present in the pre-chamber. The compression stroke (early closing of the intake valve) and the combustion stroke were modeled. For this reason, modeling of valve movement as well as inlet and outlet channels was not performed.

Due to the above, the boundary conditions are limited only to the main combustion chamber and the prechamber (Table 3).

Table 3. Boundary conditions

Parameter	Unit	Value
Head	T [K]	550
Liner	T [K]	475
Piston	T [K]	525
Prechamber	T [K]	575

3.4. Method

Research on thermodynamic processes was carried out using the AVL FIRE 2019 R2 software. The combustion chamber model was made as a polymesh mesh with a variable number of cells (min: 32805; max: 80057). The computational grid was compacted around the prechamber, assuming a minimum cell length of 0.5 mm (Fig. 3a). The optimization of the computational domain was not carried out, however, it was compacted for the prechamber. The mesh was generated using the Flame Engine Plus module of the AVL FIRE program. A visualization of the combustion chamber used for the analysis is shown in Fig. 3b.

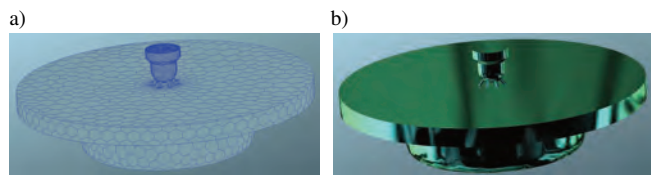


Fig. 3. Combustion chamber: a) mesh with compaction of the prechamber, b) shape of the combustion chamber

4. Analysis of thermodynamic quantities of the combustion process

4.1. Ignition conditions in the PC

The analysis of ignition conditions in the prechamber begun by determining the value of $\lambda_{\text{PC,ign}}$ after assuming a few determined values of the fuel dose fed to the pre-

chamber – q_{o_PC}. The values of $\lambda_{\text{PC,ign}}$ were determined on this basis in accordance with Fig. 4.

In this research, AVL FIRE was used to adopt a methodology in which engine TDC during combustion is reached at 720 deg on the crankshaft. Although it is a 360 deg shift, it does not change the engine operating conditions.

Prechamber gas injection was performed ($\alpha_{\text{inj,PC}} = 510 - 540 \text{ CA}$) in the early phase after closing the intake valve (IVC = 500 deg). The ignition of the mixture in the pre-chamber was set at 695 deg CA.

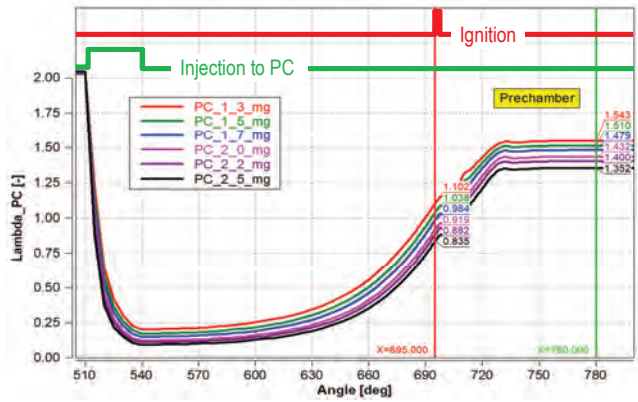


Fig. 4. Prechamber fuel dose values and the determined λ values during ignition in the prechamber

The mean value of the air excess coefficient in the combustion chamber is reduced proportionally to the increasing fuel dose value q_{o_PC}. When the combustion process begins the λ value is not constant – it increases as a result of mass flow from the main chamber to the prechamber. The changes in $\lambda_{\text{PC,ign}}$ were determined based on the selection of the q_{o_PC} value. These trends are shown in Fig. 5. It can be seen that the adopted strategies for changing the air excess coefficient for (global) combustion of lean mixtures maintained it around $\lambda = 1$.

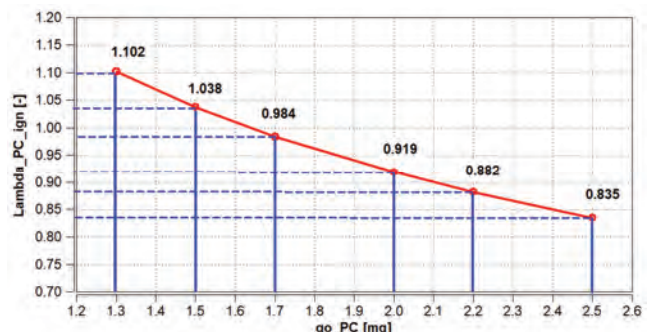


Fig. 5. The adopted initial dose values for prechamber and the corresponding values of the air excess coefficient during ignition

Gas injection at high doses in the early phase of the piston movement was found to cause the flow of this mixture to the main chamber (Fig. 6 – 2.5 mg). During the compression stroke, this tendency is not observed only at the smallest values of the dose fed into the cylinder. In the vicinity of the ignition angle in prechamber there is still no homogeneous combustible mixture. However, with q_o values in the range of

1.3 to 1.7, the quality of the mixture most closely resembles homogeneous. The symmetry of the openings connecting the PC and MC causes the charge from the main chamber to reach the center of the prechamber. The use of the k-zeta-f model results in a rich mixture being formed in the vicinity of the prechamber walls.

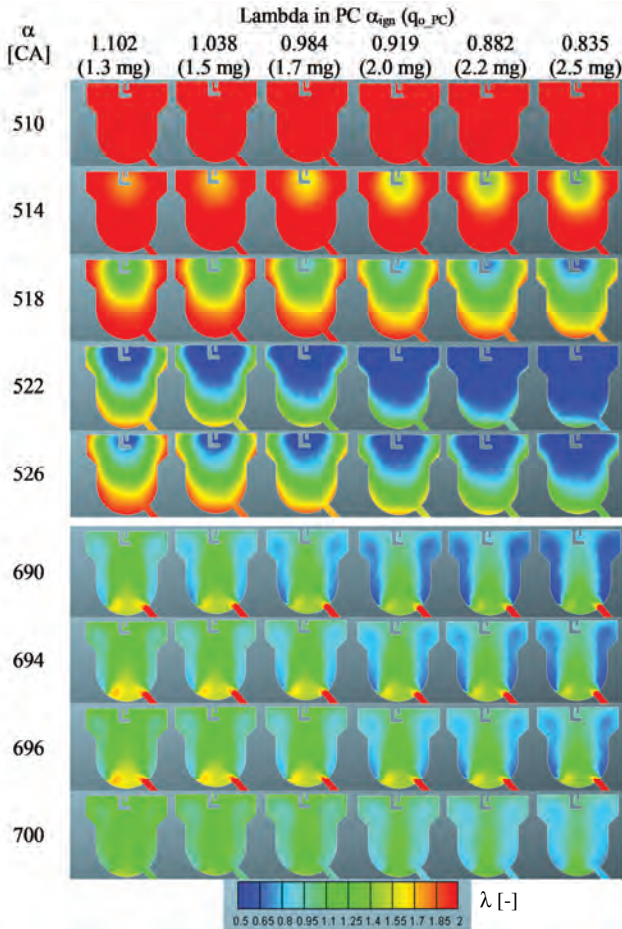


Fig. 6. Air excess ratio in prechamber for different fuel dose values q_{o_pc}

Different values of λ_{PC} resulted in a different combustion process in the prechamber. Mean λ values close to the value of 1 mean that the maximum value of the combustion pressure in the prechamber is the lowest (Fig. 7). The highest values of combustion pressure occurred when the fuel

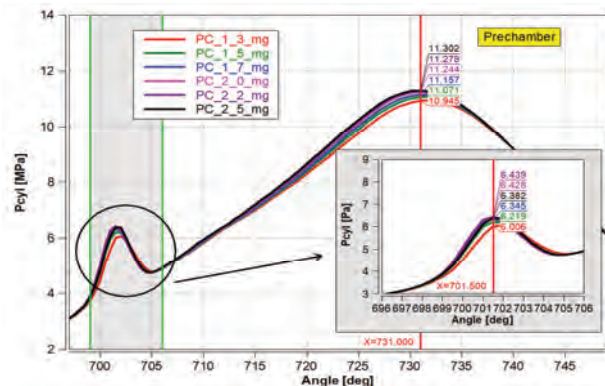


Fig. 7. Combustion pressure characteristic in the prechamber

was burned at the value of $\lambda_{PC} = 0.88\text{--}0.92$. This means that a mixture that is richer than stoichiometric was more favorable here, which was manifested in the rapid build-up of pressure in the prechamber, but also its rapid termination.

4.2. Inter-chamber flows

Confirmation of the limited combustion process at $\lambda_{PC} = 1.102$ ($q_{o_pc} = 1.3$ mg) is the analysis of inter-chamber flows. At this air excess coefficient value, the flow to the MC is also the smallest (Fig. 8 – PC_1_3_mg). At an angle of 725 and beyond, the flows were the same.

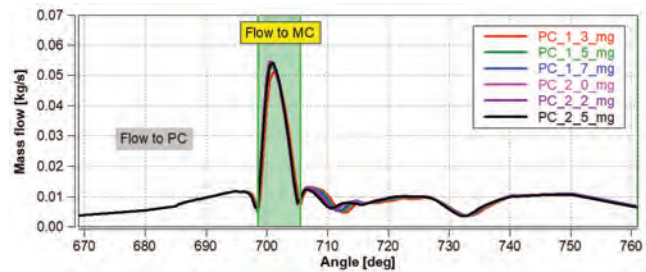


Fig. 8. Inter-chamber flows

The pressure changes in the prechamber during the start of the combustion process were reflected in the obtained maximum pressure values in the PC (around 730 CA). Combustion at $\lambda = 1.102$ ($q_{o_pc} = 1.3$ mg) also resulted in the lowest maximum pressure in the prechamber. Small doses of fuel fed to the prechamber burn with the smallest maximum values occurring in the prechamber.

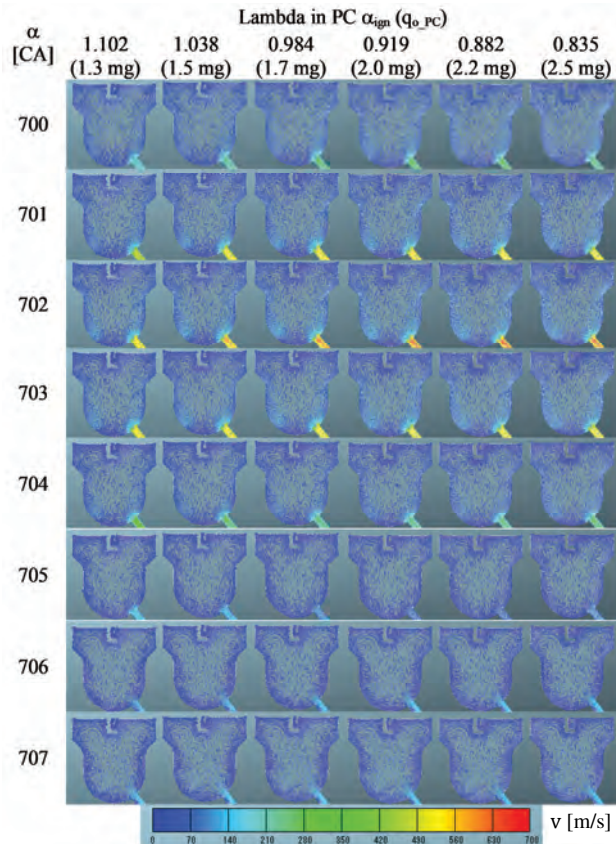


Fig. 9. Impact of the fuel dose fed to the prechamber on the fuel flow rate value between the prechamber and the main chamber

Spatial analysis of inter-chamber flows (Fig. 9) indicates the existence of the highest flow speeds at $\lambda = 0.919$ and at an angle of 702 deg. A comparison with Fig. 8 indicates the point of maximum flow. The flow velocity at this angle was about 600 m/s, however only in the middle of the flow channel. At lower flow rates, the speed is lower, around 150–200 m/s.

The conditions of inter-chamber flows indicate the existence of an air excess coefficient with a value slightly less than stoichiometric (by about 10%), which resulted in the combustion process being qualitatively best.

4.3. Flame development and temperature changes in the prechamber

The analysis of further combustion process indicators concerns flame development and the related temperature changes. Despite the different combustion process conditions (resulting from different lambda values in the PC), the flame front changes were quite similar (Fig. 10). This means that changes in the λ_{PC} value by about 10–15% from the stoichiometric value did not significantly affect the changes in the flame front.

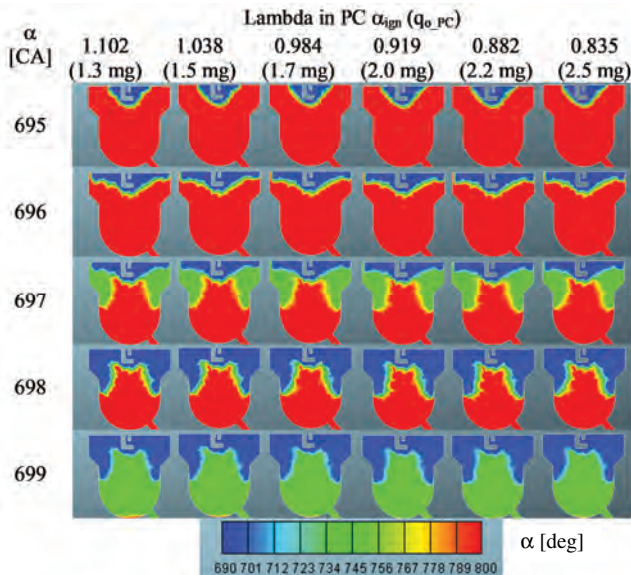


Fig. 10. Flame development (blue area) in the prechamber at different fuel dose values q_o_{PC}

Although the flame development in the prechamber had a similar character for all test cases, the temperature changes were significant (Fig. 11). Similar ignition delay values resulted from the temperature changes. Rapid temperature rise in the prechamber (at 698 deg. CA) had the same character, but the following aspects of the process were different. Small doses administered to the prechamber (λ close to 1) resulted in the lowest temperature values being observed. For the adopted q_o_{PC} values, the temperature changes were about 5%. The temperature characteristic in the prechamber caused the occurrence of a second maximum in the vicinity of the TDC. Here the differences were clearer and amounted to about 7% – but the nature of the changes was still the same as before. Large q_o_{PC} fuel doses resulted in the formation of the highest temperature values in the prechamber.

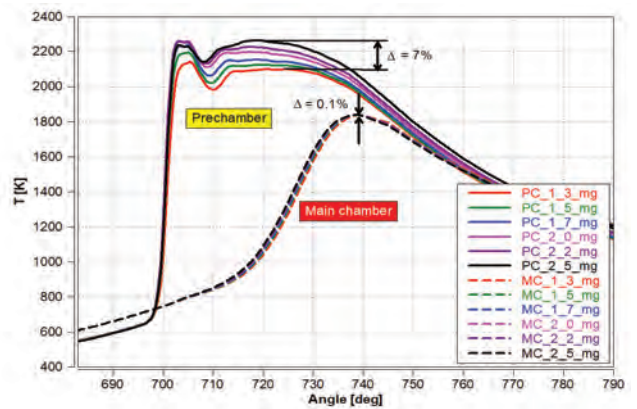


Fig. 11. Combustion temperature changes in the prechamber and in the main chamber

Division of the computational grid into selections allowed an independent determination of the average temperature values in the main chamber. The temperature changes in this part of the cylinder were practically the same (changes in T_{max} were about 0.1%). Maximum values observed in the main chamber were about 350–400 K smaller than in the prechamber. Temperature increase in the main chamber was shifted by about 20 deg CA in relation to the temperature increase in the prechamber.

Analysis of the temperature distribution in the prechamber indicates that the largest temperature values occur around the cylinder walls (Fig. 12). This mirrors the deve-

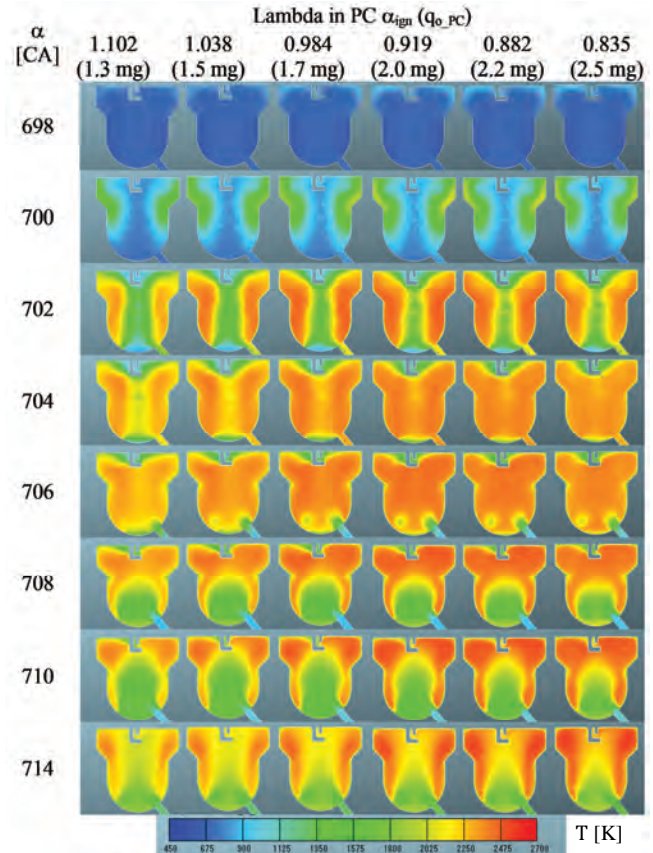


Fig. 12. Temperature changes in the prechamber at different fuel dose values q_o_{PC}

lopment of the flame front (Fig. 10). Figure 12 shows that only in a small angular range (about 704 CA) a burning mixture with the largest temperature range (up to 2500 K) flows through the cross sections connecting the two chambers.

4.4. Heat release in combustion chambers

The heat release rate is determined by the speed of burning the fuel dose mainly in the prechamber. The maximum release rate values increase with the increasing prechamber fuel dose values (Fig. 13). This maximum was reached at $q_{o_PC} = 2.2$ mg. This means that the maximum increase in q_{o_PC} dose did not lead to an increase in the rate of heat release. Differences between extreme q_{o_PC} values lead to 18% HRR changes. Maximum HR changes were smaller but also significant. They amounted to 9% (the lowest at low doses of q_{o_PC}).

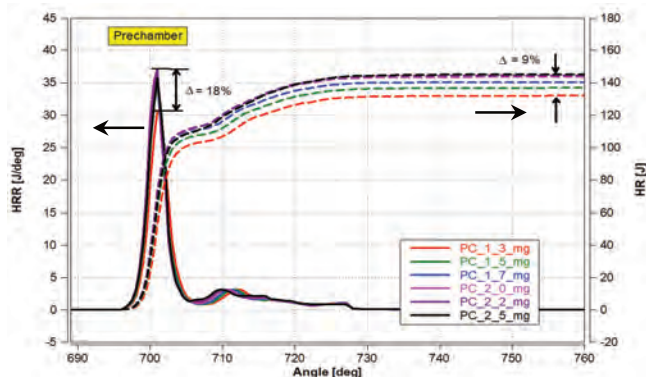


Fig. 13. Changes in HRR and HR in prechamber at different fuel dose values q_{o_PC}

The analysis of HRR and HR in the main chamber indicated no significant differences in the character of changes in these quantities (Fig. 14). The maximum combustion rate values differed by 0.6%, while the maximum values of heat released by only 1%. Combustion efficiency was defined as:

$$\eta_c = \frac{HR_{mx}}{(q_{o_PC} + q_{o_MC}) \cdot LHV} \quad (6)$$

where HR_{mx} is the maximum of heat release and LHV is the Lower Heating Value of fuel (50 MJ/kg).

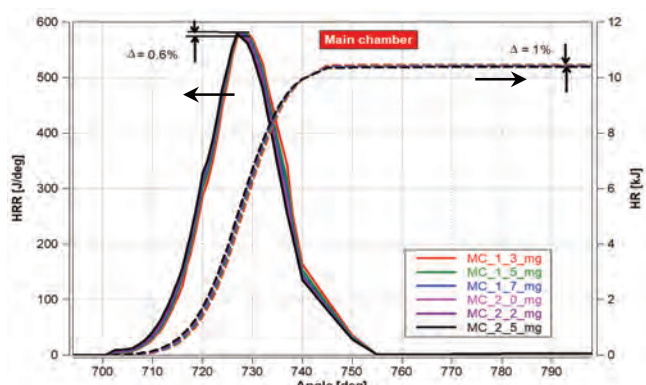


Fig. 14. HRR and HR changes in the main chamber at different fuel dose values q_{o_PC}

Using the data in Table 2, the above combustion efficiency was determined for the sum of the fuel doses fed to the prechamber and to the main chamber. At the smallest doses of q_{o_PC} the combustion efficiency was 93.63%, at the highest doses – 92.88%. This means that as the air excess coefficient in the prechamber increases, the combustion efficiency increases as well (but less significantly).

4.5. Combustion process emission values

The exhaust emissions evaluation was limited to nitrogen oxides and soot. Both of these values were presented in relation to their mass fraction. The mass fraction of NO in the prechamber at the start of combustion was the highest for a dose close to stoichiometric (Fig. 15). This tendency changes in the following combustion period. A large initial dose produced large amounts of NO, which tended to decrease as q_{o_PC} decreased. The obtained different final NO concentrations reach over 50%.

Soot production behaved differently. With increasing q_{o_PC} its quantity increased – it reached its maximum at $q_{o_PC} = 2.5$ mg. The soot amount is then 50% greater than for the minimum dose of q_{o_PC} . The advantage of such a combustion system is that the soot concentration, although it appears early in the combustion process, also drops sharply (it burns off) – after TDC its value is only below 5% of the maximum value (Fig. 15).

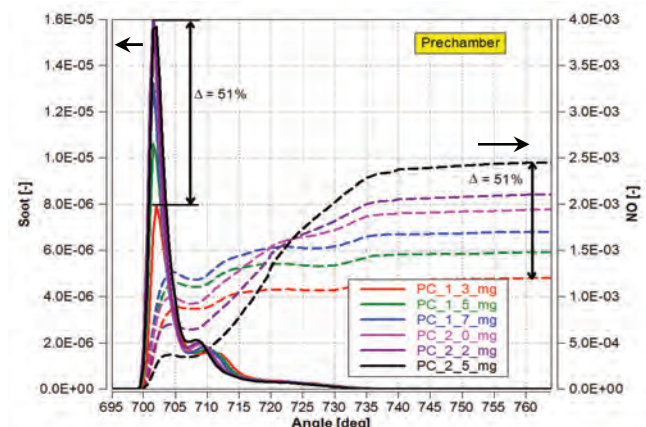


Fig. 15. Changes in NO and soot mass fractions in the prechamber at different fuel dose values q_{o_PC}

The confirmation of the above trends is the spatial analysis of the nitrogen oxides distribution in the prechamber. The highest NO concentration occurred at λ close to 1 (Fig. 16) in the initial period of the combustion process. At angles after TDC, the NO concentration was significant when burning large fuel doses in the PC. This indicates a long burning period and persistence of large temperature values in this volume. Maximum NO values occurred locally at large q_{o_PC} fuel doses around TDC.

The emissions analysis in the main chamber indicated its similarities regardless of the amount of fuel in the prechamber. This situation applies primarily to soot (change in the maximum value to 4%) – Fig. 17. With respect to NO, the changes mainly concern the final part of the process (at an angle above 730 CA).

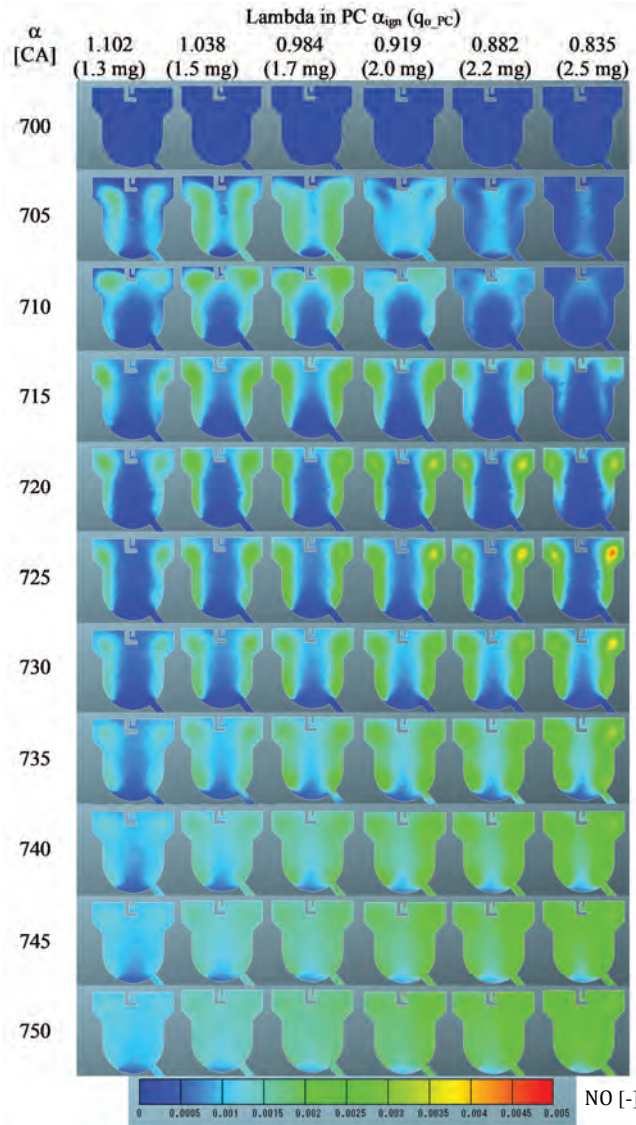


Fig. 16. Impact of the fuel dose fed to the prechamber on the resulting NO mass fraction

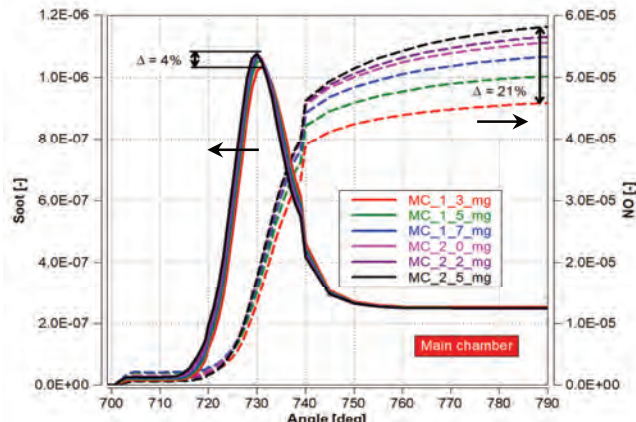


Fig. 17. Changes in NO and soot mass fraction in the main chamber at different fuel dose values q_{o_PC}

The soot concentration is proportional to the fuel dose q_{o_PC} . Soot is formed mainly at the walls of the combustion chamber (even though the fuel is natural gas) – Fig. 18.

When analyzing the formation of NO and soot, it should be stated that soot is formed earlier (insufficient oxidation) in the combustion process than NO. Soot particles appear already at 710 CA, while NO – only at 705 CA (for large fuel doses q_{o_PC}). Similar to the mean values (Fig. 15), spatial analysis indicates the dissipation of soot concentration around 705–709 CA. The differences in NO concentration in the prechamber (Fig. 15) and the main chamber (Fig. 17) were mainly due to the air excess ratio. In the prechamber this value is close to one, while in the main chamber – the mixture is much leaner. Lower combustion temperature in the initial phase of the process in the main chamber (Fig. 11) also results in lower values of NO formed in this chamber.

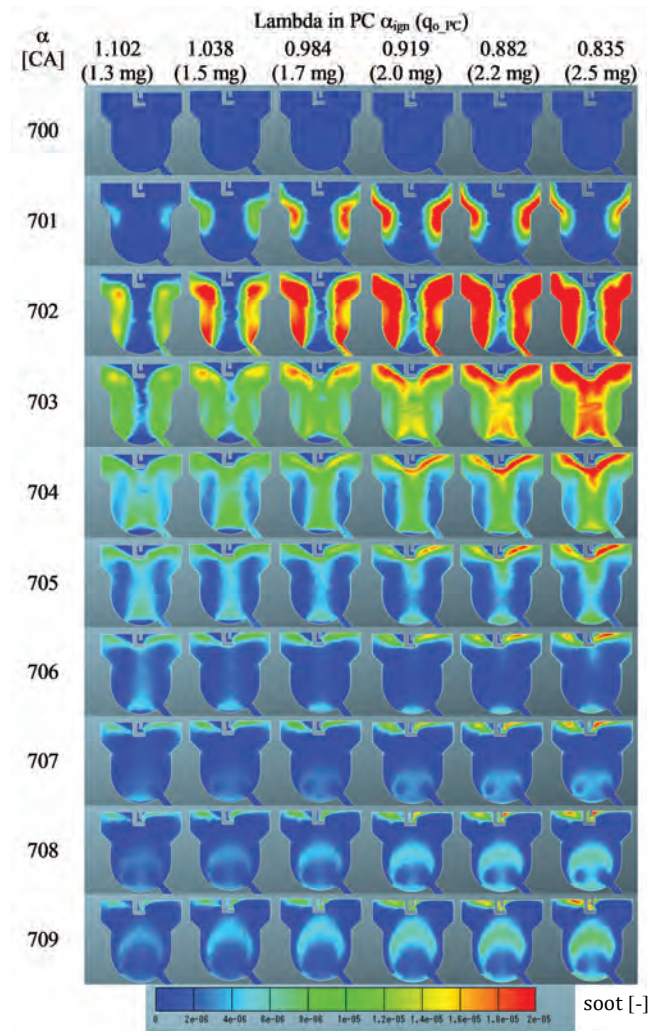


Fig. 18. Influence of the fuel dose fed to the prechamber on the resulting soot mass fraction

5. Conclusions

Analysis of thermodynamic processes, in relation to changes in the air excess coefficient value in the prechamber, during the combustion of lean mixtures in HD engines resulted in the following conclusions:

- in relations to combustion process indicators (Fig. 19):
 - maximum value of combustion pressure in prechamber during ignition occurs for rich mixtures ($\lambda \approx 0.9$);

- the P_{mx} pressure in the main chamber increases with the decreasing lambda in prechamber (increasing q_{o_PC}); the combustion pressure values in both chambers were similar;
- the heat release rate in the prechamber reached its maximum during combustion of stoichiometric mixtures in PC; HR_{mx} is highest at small λ_{PC} (large fuel doses q_{o_PC});
- slight changes, however, were noted in the main chamber: with increasing λ_{PC} the HR_{mx} also increases;
- the maximum combustion temperature in the PC occurred while burning rich mixtures in it; maximum air excess coefficient values in the MC were around $\lambda = 1$;

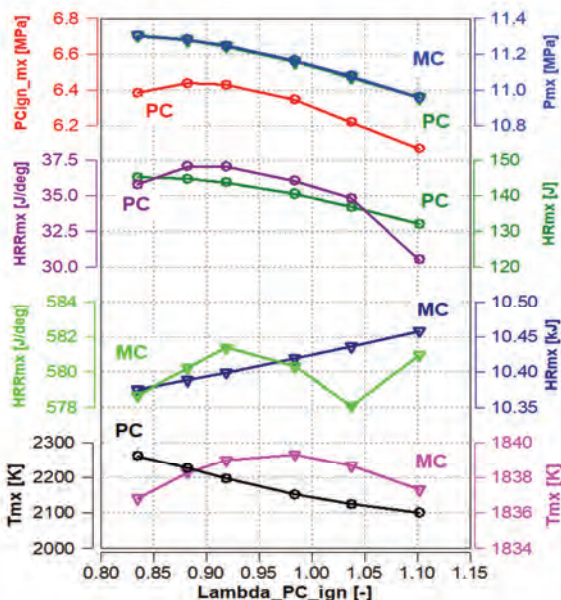


Fig. 19. Changes in combustion process indicators at different air excess ratio at PC_{ign}

Nomenclature

DM	Dual Mode
ECFM	Extended Coherent Flame Model
HD	heavy duty
HR	heat release
HRR	heat release rate
IMEP	indicating mean effective pressure
IVC	intake valve closed
LHV	Lower Heating Value
MC	main chamber
NO	nitric oxygen
P	pressure
PC	prechamber
PCIS	Pre Chamber Ignition System
q_o	fuel dose
T	temperature
TDC	top dead center

– in relations to exhaust emission indicators (Fig. 20):

- maximum mass fraction values in the prechamber occurred when burning rich mixtures; this parameter has a similar characteristic the main chamber; the level of exhaust emissions in the PC is 2 orders higher than in the MC;
- maximum soot values also occurred when burning rich mixtures in both PC and MC; the soot level in the PC was an order of magnitude higher than in the MC.

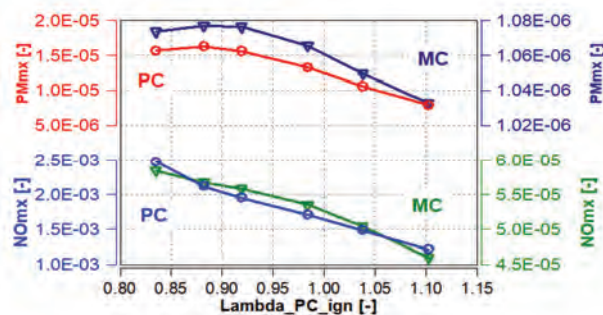


Fig. 19. Changes in NO and soot mass fractions at different air excess ratio at PC_{ign}

Analysis of the thermodynamic and emission indicators in the tests carried out while feeding the gas engine with a lean mixture at $\lambda = 2$ indicates that the most advantageous solution is to use the air excess coefficient value $\lambda = 0.9 - 1.0$ in the prechamber. For such a solution, the highest thermodynamic indicators of the combustion process were obtained (even though the minimum exhaust emission values were obtained at $\lambda \sim 1.1$).

Acknowledgements

This work has been done under AVL University Partnership Program.

TJI	Turbulent Jet Ignition
V	volume
indexes	
ALL	overall air excess ratio
CH	chamber
cyl	cylinder
ign	ignition
mx	maximum
mn	minimum
n	engine speed
α	crank angle
λ	air excess coefficient
ϵ	compression ratio

Bibliography

- [1] ALVAREZ, C.E.C., COUTO, G.E., ROSO, V.R. et al. A review of prechamber ignition systems as lean combustion technology for SI engines. *Applied Thermal Engineering*. 2018, **128**, 107-120.
<https://doi.org/10.1016/j.applthermaleng.2017.08.118>
- [2] ATIS, C., CHOWDHURY, S., AYELE, Y. et al. Ultra-lean and high EGR operation of Dual Mode, Turbulent Jet Ignition (DM-TJI) engine with active pre-chamber scavenging. *SAE Technical Paper* 2020-01-1117. 2020.
<https://doi.org/10.4271/2020-01-1117>
- [3] ATTARD, W.P., FRASER, N., PARSONS, P. et al. A Turbulent Jet Ignition pre-chamber combustion system for large fuel economy improvements in a modern vehicle powertrain. *SAE Technical Paper* 2010-01-1457. 2010.
<https://doi.org/10.4271/2010-01-1457>
- [4] ATTARD, W.P., PARSONS, P. A normally aspirated spark initiated combustion system capable of high load, high efficiency and near zero NO_x emissions in a modern vehicle powertrain. *SAE Technical Paper* 2010-01-2196. 2010.
<https://doi.org/10.4271/2010-01-2196>
- [5] BUNCE, M., BLAXILL, H. Methodology for combustion analysis of a spark ignition engine incorporating a pre-chamber combustor. *SAE Technical Paper* 2014-01-2603. 2014. <https://doi.org/10.4271/2014-01-2603>
- [6] CHINNATHAMBI, P., BUNCE, M., CRUFF, L. RANS based multidimensional modeling of an ultra-lean burn pre-chamber combustion system with auxiliary liquid gasoline injection. *SAE Technical Paper* 2015-01-0386. 2015. <https://doi.org/10.4271/2015-01-0386>
- [7] COLIN, O., BENKENIDA, A. The 3-Zones Extended Coherent Flame Model (ECFM3Z) for computing premixed/diffusion combustion. *Oil&Gas Science and Technology – Rev. IFP*. 2004, **59**(6), 593-609.
<https://doi.org/10.2516/ogst:2004043>
- [8] COLIN, O., BENKENIDA, A., ANGELBERGER, C. A 3D modeling of mixing, ignition and combustion phenomena in highly stratified gasoline engines. *Oil&Gas Science and Technology – Rev. IFP*. 2003, **58**(1), 47-62.
<https://doi.org/10.2516/ogst:2003004>
- [9] DA COSTA, R.B.R., TEIXEIRA, A.F., FILHO, F.A.R. et al. Development of a homogeneous charge pre-chamber torch ignition system for an SI engine fuelled with hydrous ethanol. *Applied Thermal Engineering*. 2019, **152**, 261-274.
<https://doi.org/10.1016/j.applthermaleng.2019.02.090>
- [10] GARG, M., RAVIKRISHNA, R.V. In-cylinder flow and combustion modeling of a CNG-fuelled stratified charge engine. *Applied Thermal Engineering*. 2019, **149**, 425-438. <https://doi.org/10.1016/j.applthermaleng.2018.12.036>
- [11] GIANETTI, G., SFORZA, L., LUCCHINI, T. et al. CFD modeling of combustion of a natural gas light-duty engine. *Energy Procedia*. 2018, **148**, 954-961.
<https://doi.org/10.1016/j.egypro.2018.08.067>
- [12] HUA, J., ZHOU, L., GAO, Q. et al. Effects on cycle-to-cycle variations and knocking combustion of Turbulent Jet Ignition (TJI) with a small volume pre-chamber. *SAE Technical Paper* 2020-01-1119. 2020.
<https://doi.org/10.4271/2020-01-1119>
- [13] KORB, B., KUPPA, K., NGUYEN, H.D. et al. Experimental and numerical investigations of charge motion and combustion in lean-burn natural gas engines. *Combustion and Flame*. 2020, **212**, 309-322.
<https://doi.org/10.1016/j.combustflame.2019.11.005>
- [14] Mitsubishi Turbocharger and Engine Europe B.V. Gas engine GS16R2-PTK.
<https://www.mtee.eu/news/403/introducing-new-gs16r2-ptk>
- [15] NEUMANN, S., BIENWALD, M., HERDIN, G. Pre-chamber pressure-based management of gas engines. *MTZ Industry*. 2016, **6**, 58-63. <https://doi.org/10.1007/s40353-016-0011-9>
- [16] NOVELLA, R., PASTOR, J., GOMEZ-SORIANO, J. et al. Experimental and numerical analysis of passive pre-chamber ignition with EGR and air dilution for future generation passenger car engines. *SAE Technical Paper* 2020-01-0238. 2020. <https://doi.org/10.4271/2020-01-0238>
- [17] PIELECHA, I., BUESCHKE, W., SKOWRON, M. et al. Prechamber optimal selection for a two stage turbulent jet ignition type combustion system in CNG-fuelled engine. *Combustion Engines*. 2019, **176**(1), 16-26.
<https://doi.org/10.19206/CE-2019-103>
- [18] ROSO, V.R., SANTOS, N.D.S., VALLE, R.M. et al. Evaluation of a stratified prechamber ignition concept for vehicular applications in real world and standardized driving cycles. *Applied Energy*. 2019, **254**, 113691.
<https://doi.org/10.1016/j.apenergy.2019.113691>
- [19] SENS, M., BINDER, E. Pre-chamber ignition as a key technology for future powertrain fleets. *MTZ Worldwide*. 2019, **80**, 44-51. <https://doi.org/10.1007/s38313-018-0150-1>

Prof. Ireneusz Pielecha, DSc., DEng. – Faculty of Civil and Transport Engineering, Poznan University of Technology.

e-mail: ireneusz.pielecha@put.poznan.pl



Evaluation of adequacy of a model of a marine diesel engine based upon empirical research

The article presents a mathematical model of a marine diesel engine developed for the needs of the research on the innovative method of evaluating technical condition of a marine engine. Basic assumptions of the method under development have also been included. The main focus has been directed on the evaluation of adequacy of a mathematical model of a marine diesel engine proposed in this article. In addition, measures of adequacy for the needs of the conducted research have also been presented. Finally, the article shows results from the conducted research followed by conclusions.

Key words: marine diesel engine, diagnostics, modelling

1. Introduction

Evaluation of technical condition of marine diesel engines driving electric power generators constitutes a vital issue in their operation. Certain number of marine diesel engines is operated following their technical condition strategy. These are mostly the engines of a high diagnostic susceptibility (provided by their manufacturers with indicator valves) [9] intended for the ships' propulsion. A separate group of these engines are used as auxiliary engines intended for driving synchronous electric power generators. These engines usually represent a low diagnostic susceptibility (they are not equipped with indicator valves). Such engines are operated following the strategy of the so-called hourly resources (a definite amount of time of reliable operation). The strategy provides periodical replacement of the engine component parts regardless of their actual technical condition. This implies necessity to put the engine out of service and often to replace elements still fit for use. High cost of maintenance to be performed and considerable amounts of labour raise necessity to seek non-invasive, parametric evaluation methods of technical condition of the said engines. One of the most popular methods is assessing the technical condition of engines is their indication [10, 11, 14]. Another popular methods is assessment of the technical condition of engines based on acceleration measurements are particularly popular [2, 3, 6, 20]. Optical studies using endoscopes to assess the surface condition of engine working spaces are also popular. Another method is the evaluation of technical condition of a marine diesel engine based on measurements of pressure in the exhaust outlet ducts [5, 8, 15]. One of them is a method developed for evaluation of technical condition of an engine used for driving synchronous electric power generators based on measurements of its phase-to-phase voltage.

The article presents a part of conducted research included an assessment of the adequacy of the developed mathematical model. The tests were conducted on an engine with high diagnostic susceptibility (SULZER type 6AL20/24 laboratory engine). They included an active experiment for the engine and model both. The tests were carried out for full range of rotational speeds of the engine crankshaft and torque load. In addition, tests were carried out for the full and partial condition of the engine (one of the engine cylin-

ders was shut down). The research included measures of adequacy parameters measurable on a real object as well as those obtainable as a result of solving model equations. Additionally, a measure of adequacy was proposed taking into account the similarity of the indicator charts.

2. Assumptions regarding the developed method

This method is based upon the assumption that technical condition of a marine diesel engine driving a synchronous electric power generator produce direct impact on the shape of waveforms of the phase-to-phase voltage of the generator. During the tests it was observed that technical condition of an engine and its load with a torque (the course of the working process inside the cylinders) have a direct impact on fluctuations of the rotational speed of its crankshaft during its working process [1, 16]. The fluctuations of the rotational speed of the engine crankshaft and those of the generator impeller (in case of a generating set driven by an diesel engine) are practically of the same nature. They modify the shapes of the waveform of the phase-to-phase voltage of the generator.

The course of the working process of an engine depends mainly on its technical condition and on its loading with a torque. This translates into the indicated pressure (Fig. 1) and by the same into the torque generated by the engine (Fig. 2). The shape of the waveform of the rotational speed of the engine crankshaft as a function of time depends on the torque and on the moments of inertia of the components of the engine performing reciprocating motion, rotating motion and a complex (both reciprocating and rotating) motion. As the inertia moments of the engine components are constant, the course of the angular velocity depends on the torque of the crankshaft (indicated pressure) (Fig. 3).

The forces generating the load of the engine with a torque cause the occurrence of pseudo-periodical deformations [4] of the shape of the torque waveform and variations of the rotational speed of the crankshaft as a function of the duration time equal to the multiplicity of the basic harmonic wave (resulting from the rotational motion of the crankshaft) and of the half-number of the engine cylinders (in case of a four-stroke engine). On the other hand, the forces generated by the disturbances of the waveform of the working process in one of the engine cylinders have a peri-

od equal to a half of the basic harmonic wave resulting from the rotational motion of the engine crankshaft (in case of a four-stroke engine).

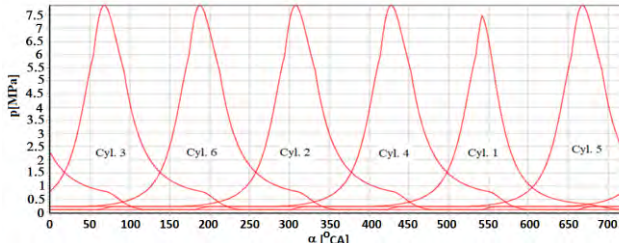


Fig. 1. The waveform of the indicated pressure in the engine cylinders as a function of the rotation angle of the crankshaft (cylinder no. 1 is supplied with an amount of fuel reduced by 80%)

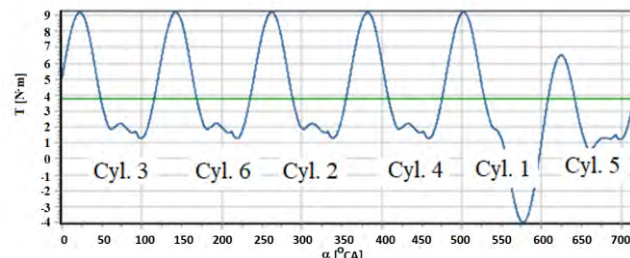


Fig. 2. The waveform of the torque of the engine crankshaft as a function of the rotation angle of the crankshaft (cylinder no. 1 is supplied with an amount of fuel reduced by 80%)

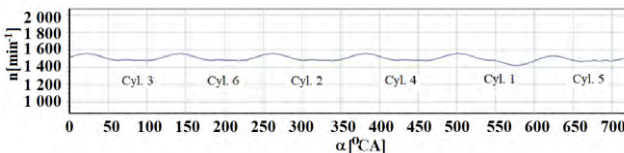


Fig. 3. The waveform of the rotational speed of the engine crankshaft as a function of the rotation angle of the crankshaft (cylinder no. 1 is supplied with an amount of fuel reduced by 80%)

3. Program of the conduct of the research

Work on the development of a new method of technical condition evaluation of a marine auxiliary diesel engine were preceded by the development of a research program [5, 7, 16, 19]. Usually such programs are presented in a form of an algorithm (Fig. 4). It includes all main stages of the conducted research. It has been decided that the research problem presented in this article will be solved [16] in two basic stages. The first stage covers the development of models of a diesel engine, i.e. physical and mathematical models accompanied by a computer program (to solve equations of the mathematical model). This stage ends with an evaluation of the adequacy of the mathematical model, carried out on the basis of the model and empirical tests. The second stage begins once the mathematical model of the engine has been found adequate. This stage includes extension of the developed model of the engine with a model of a synchronous type generator. This stage ends with the evaluation of adequacy of the mathematical model of an diesel-electric generator set based both upon the model and empirical examinations.

Division into two stages applied in our research is a result of the restricted possibilities we have had in con-

ducing the research in case of auxiliary engines (representing restricted diagnostic susceptibility). Evaluation of adequacy of a model based upon the empirical tests would be extremely complex, if impossible at all. Therefore decision has been made to evaluate adequacy of the engine model (first stage) by applying empirical research to be conducted on an engine of a high diagnostic susceptibility (a laboratory test engine SULZER, type 6AL20/24). At the second stage it has been decided that a comparative analysis of measures describing the waveforms of the phase-to-phase voltages of the generator will be sufficient for the evaluation of adequacy of a model of the diesel-electric generator set (both for model and empirical examinations) [16].

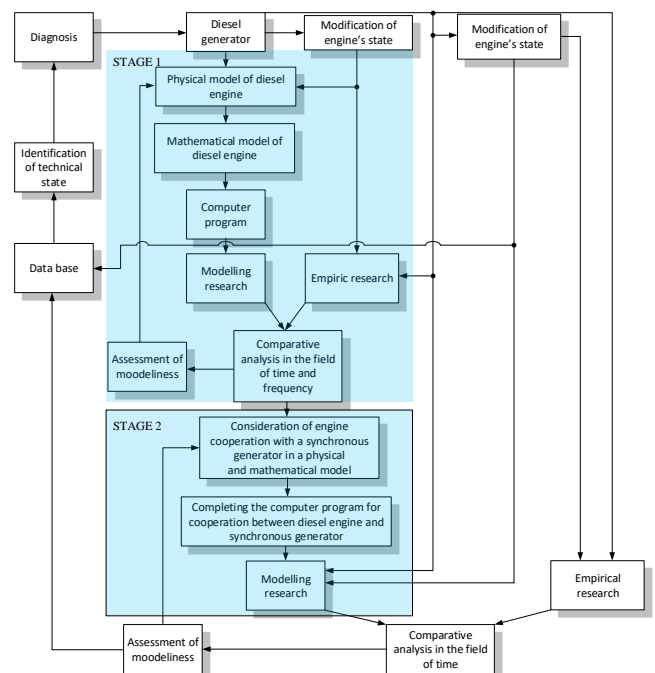


Fig. 4. Program of the research

4. Mathematical model

Following the program of the research presented in Fig. 4 (stage one) both physical model [17], and mathematical model [18] accompanied by a computer program have been developed. The physical and mathematical models allowed to conduct model tests for practically any of the four-stroke marine diesel engine. Such model allows to conduct the research on an engine representing both full and partial technical operational fitness. Solution of the equations of the mathematical model results in getting the waveforms of the following parameters (as the function of time or rotation angle of the crankshaft):

- stroke path, velocity and acceleration of a piston,
- volume of the combustion chamber,
- pitch of the inlet and outlet valves,
- cross-section areas of the inlet and outlet valves,
- velocity of the flow of the medium through the inlet and outlet valves,
- flow rate of the medium mass into and out of the engine cylinders,
- pressure, temperature, and medium mass inside the cylinders,

- gas induced force moment,
- crankshaft revolution speed.

In addition, the following operational parameters of the engine are calculated:

- air excess factor,
- power indicated for any particular cylinder of the engine,
- fuel mass flow,
- heat flow stream carried off outside (together with exhaust gas) and to the cooling water.

The mathematical model provides possibility to conduct research on the following conditions of partial technical fitness for use:

- change in the fuel rate supplied to each one cylinder of the engine,
- change in the cross-section for any inlet and outlet valves,
- change in the fuel injection advance angle for any cylinder,
- leakage in the piston-piston rings-cylinder system for any piston,
- change in the cross-section area of the openings in the discharge jet of any injector,
- change in supercharging pressure,
- change in the resistance of the exhaust outlet duct.

When modelling the defects of the engine, consideration was directed to the impact of the speed governor operation that modifies fuel rates supplied to any of the cylinders of the engine in order to maintain the revolution rate of the crankshaft constant (i.e. constant power indicated of the engine).

5. The plan of the experiment

According to the adopted research methodology, the experiment was conducted following three main stages: the planning of the experiment, its performance followed by evaluation of the obtained results [13]. In case of evaluating of adequacy of the mathematical model it was decided to conduct both empirical and model research according to the same plan. According to the research realization program (Fig. 4) the analysis of the results allows to conclude whether the proposed model is adequate to the degree assumed by the researcher. In case of an insufficient adequacy of the model in relation to the adopted research program decision is made to return to the modelling stage by changing the level of the applied simplifications. The plan of the experiment was developed for an engine operated in a static condition (a static plan was adopted) [13]. It was decided to adopt a determined plan (the values of the input parameters were selected at the very early stage of the plan development on the basis of a logical analysis of the structure and operational conditions of the object of the research. In our research it was assumed that the input parameters were the crankshaft revolution speed and torque. These parameters were converted into the indicated engine power. The tests were conducted following a selective plan (limited number of input parameters that allow possibility to determine the functions of the object under the test).

Empirical tests were carried out on the SULZER engine type 6AL20/24, installed on a laboratory work-stand at the

Polish Naval Academy. It is a four-stroke Diesel engine, six-cylinder, in line type, supercharged by means of a turbocharger. The reason for such selection was its high diagnostic susceptibility (engine provided with indicator valves) and a unique system for measuring and recording its power parameters (the latter developed at the Polish Naval Academy). The applied measuring system allows measurement and registration of a number of engine operating parameters. The following were used in the research:

- Indicated pressure measured with the MA 2005 instrument (KISTLER 7613B transmitter) with a measuring range from 0 to 25 MPa and a resolution of 12 bit. The measurement error did not exceed 0.5%.
- Hourly fuel consumption measured by a weighing system, the measurement error did not exceed 1%.
- Excess air ratio meeting the requirements of MAR-POL Annex VI convention.
- Indicated power was calculated on indicated pressure.

It was decided that the tests would be carried out for the following engine crankshaft rotational speeds: 400, 500, 600, 700 and 750 rpm. However, the engine's torque load will be as follows: idle, 2.2, 2.96, 3.7, 4.2 and 5.12 kNm. The scope of measurements was limited by characteristics of marine diesel engine cooperated with fixed propeller.

In case of tests conducted on a defective engine (one cylinder out of service) it was decided to restrict the number of measuring points (in relation to the fully fit engine). This results from the fact that in case of the defective engine it was impossible to apply the load torque within the entire range of its propeller propulsion characteristics. Such a conclusion results from the initial empirical tests and tests carried on the model.

6. Measures of adequacy of the mathematical model

Based upon an analysis of the parameters resulting from the solution of equations of the mathematical model and from empirical tests (initial tests) it was decided that the measures of adequacy will be the following engine operational parameters:

- air excess factor (it was assumed that its relative value should not differ by more than by 20%),
- fuel mass stream (relative difference should not exceed 10%),
- maximum rate of the indicated pressure (not more than by 5%).

In addition, measure "K" was developed for the needs of evaluating adequacy of the model that characterizes, in an objective manner, differences between the indicated pressure curves being a function of the rotation angle of the crankshaft.

The value ranges of adequacy measures were selected on the basis of preliminary studies (model and empirical). These studies concerned the assessment of the impact of modeled engine damage on the shape of the crankshaft angular velocity as a function of the crankshaft angle [16]. It has been observed that the introduced damages (concerning all engine cylinders) acceptable for the researcher (allowing for unambiguous identification of damages based on

the developed method) cause changes in the adequacy of examined measures in the range.

In case of empirical tests it was observed that the indicated pressure curves as a function of the rotation angle of the crankshaft fundamentally differ from any particular cylinder of one engine (difference between the maximum rates of the indicated pressure for a particular cylinder of the engine differ from one another even by 10%). Therefore for the needs of developing measure "K" it was decided to establish an averaged curve of the indicated pressure (as the function of revolution angle of the crankshaft) for all cylinders of the said engine (this was found to be representative for the engine). The curves of the indicated pressure as the function of the revolution angle of the engine crankshaft (an averaged curve) and the curve obtained as a result of solving the equations of the mathematical model are shown in the Graph 5. Then, the curve of the surface area under the curves of the indicated pressure was determined as the functions of the crankshaft revolution angle based upon the equation (1), what is shown in Fig. 6:

$$S_1(\alpha) = \int_0^{720} p_{SC\text{model}}(\alpha) d\alpha$$

$$\text{and } S_2(\alpha) = \int_0^{720} p_{SC\text{measure}}(\alpha) d\alpha \quad (1)$$

where: $S_1(\alpha)$ – Surface area grow under the averaged curve of the indicated pressure as the function of crankshaft revolution angle for the real object, $S_2(\alpha)$ – Surface area under the curve of the indicated pressure as the function of the crankshaft revolution angle for the model.

The value of the "S" parameter is an increment as a function of the crankshaft rotation angle (in Fig. 5). This approach specify its value for each crankshaft's angle of rotation (it is the so-called integral course). The value of the adequacy measure "K" was calculated using the following formula:

$$K(\alpha) = 1 - \frac{S_1(\alpha)}{S_2(\alpha)} \quad (2)$$

The "K" parameter calculated on the basis of the " S_1 " and " S_2 " integral waveforms also it is a function of the engine crankshaft rotation. Therefore, its value changes during the engine's operating cycle. Presenting this parameter as a function of the angle of rotation allows for comparison of the shape of the indicated pressure waveforms obtained as a result of model and empirical tests for each angle of rotation of the crankshaft. The curve for parameter "K" is shown in the Fig. 7.

It was found that high values of the "K" measure in the range from 0° CA up to the angle of the injector opening are not significant from the point of view of the research. This is due to the fact that in this range the value of the indicated pressure is low, due to which its impact on the torque values (angular velocity fluctuations) is small. The high values of the "K" measure in this respect are a consequence of the method used to calculate the "K" parameter as the relative value of the difference between " S_1 " and " S_2 ". For low values of indicated pressure, even a small discrepancy (quantity) causes significant values of the "K" parameter. From the point of view of the conducted re-

search, it is important to "similarity" waveforms in terms of the crankshaft rotation angle corresponding to the highest value of indicated pressure. The range from the injector opening angle to the outlet valve opening angle was considered to be the most important. The values of the injected pressure are then the largest and therefore have the greatest impact on the torque values.

It was assumed that the reference level will be the rate of the "K" index calculated for the angle of the injection starting point. The deviations from such rate by more than 10 prove an insufficient adequacy of the model.

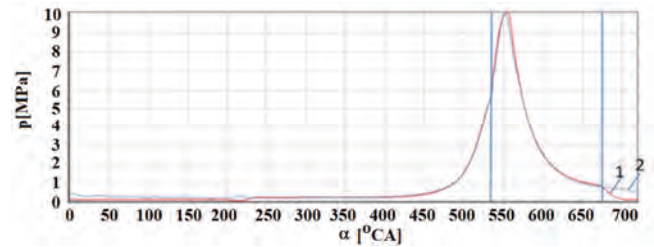


Fig. 5. Curves of the medium pressure: 1 – obtained from the model, 2 – measured as the function of the crankshaft revolution angle

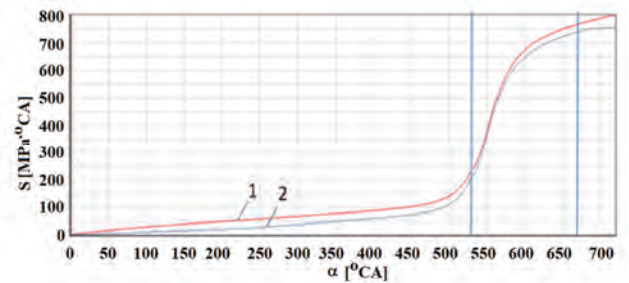


Fig. 6. Integral curves of the medium pressure: 1 – obtained from the model, 2 – measured as the function of the crankshaft revolution angle

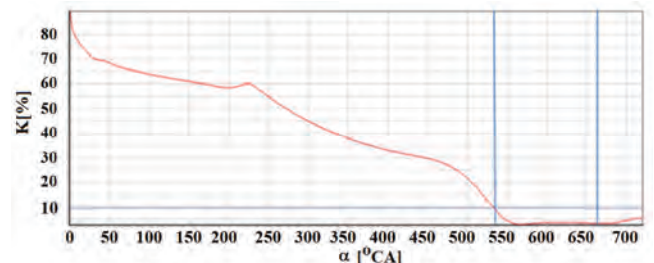


Fig. 7. The curve of the "K" parameter as the function of the crankshaft revolution angle

7. Analysis of the test results

Following the presented research plan for the engine fit for use empirical and model tests were carried out. Their results were presented in publications of the authors [7, 16, 17]. The adequacy measure values calculated for both the fit for use and defective engine are shown in Tables 1 and 2. The yellow colour indicates measures exceeding the assumed values.

In the case of tests conducted for engines in a state of partial technical fitness, the use of the "K" adequacy measure was resigned. This is due to the method used to determine the indicated pressure course for the real engine. It was assumed in the research that the indicated pressure

course used to calculate the "S" parameter is averaged for all engine cylinders (synchronous averaging). This approach was specified by the fact that there were significant discrepancies in the indicated pressure course for individual engine cylinders (the combustion pressure difference between engine cylinders sometimes reaches up to 10%). These discrepancies result from:

- the adjustment of the engine pump for its nominal operating conditions,
- simultaneous measurement of the indicated pressure on all engine cylinders,
- wave phenomena occurring in the indicator valve channels.

In the case of a damaged engine (cylinder out of operation), calculating the average indicated pressure course would lead to significant errors.

In case of tests carried out on the damaged engine the number of adequacy measures has been reduced by measure "K". This results from the fact that when developing the probability measure for the indicated pressure waveform an averaged rate of indicated pressure has been applied and that has been obtained from all cylinders of the marine engine. In case of the damaged engine application of such measure is not justified [16].

Table 1. The adequacy measure rates adopted for the engine of full technical state

Measurement Number	5.12	p_{SCmax} [%] G_{er} [%] λ_r [%] K [-]			2.19 6.05 0.00 2.17
	4.2	p_{SCmax} [%] G_{er} [%] λ_r [%] K [-]		0.20 8.08 2.06 4.64	0.19 7.66 3.09 3.80
	3.7	p_{SCmax} [%] G_{er} [%] λ_r [%] K [-]		0.72 4.96 7.69 8.16	0.54 3.32 2.70 4.76
	2.96	p_{SCmax} [%] G_{er} [%] λ_r [%] K [-]	4.32 0.29 0.55 4.14	4.14 1.99 8.00 8.90	2.07 4.18 2.44 4.27
	2.2	p_{SCmax} [%] G_{er} [%] λ_r [%] K [-]	4.73 3.76 1.69 5.10	2.76 4.12 8.25 5.43	1.95 8.77 18.27 5.54
	0	p_{SCmax} [%] G_{er} [%] λ_r [%] K [-]	3.60 113.00 15.67 3.40	1.90 30.00 8.85 5.95	5.99 10.01 6.97 5.47
M_{OP} [kN · m]		400	500	600	700
n [min ⁻¹]				700	750

Table 2. The adequacy measure rates adopted for the engine of partial technical fitness for use

Measurement Number	3.7	p_{SCmax} [%] G_{er} [%] λ_r [%]		4.06 4.05 4.94	3.85 0.81 7.80
	2.96	p_{SCmax} [%] G_{er} [%] λ_r [%]		0.36 8.74 7.41	3.89 2.37 5.77
	2.2	p_{SCmax} [%] G_{er} [%] λ_r [%]	3.86 4.55 1.41	4.32 0.63 7.69	0.12 1.68 9.94
	0	p_{SCmax} [%] G_{er} [%] λ_r [%]	5.50 106.25 41.18	0.95 14.93 11.87	8.67 20.81 3.28
	M_{OP} [kN · m]		400	500	600
n [min ⁻¹]			700	700	750

Part of the measure values in case of both the entirely fit for use engine and defective engine exceeds the assumed values (measures marked in yellow in Tables 1 and 2). This proves the inadequacy of the model within the range of operation of the engine without the torque load. Despite the fact that the values of adequacy measures were exceeded it has been found that the developed model is adequate both in quantitative and qualitative terms within the limited range of loads. Decision was made that in case of the research described in this article the adequacy of the mathematical model of the engine is sufficient to pass on to the subsequent stage of the research program, i.e. to the modelling of a Diesel generator unit.

Operation of the engine without load, in case of Diesel generator units may only and exclusively take place at its starting up moment and continues until the operational parameters are reached that makes it possible to load the generator with the receivers. Moreover, the fact is to be taken into consideration that the average crankshaft revolutions of the engine driving the generator change within a very much narrow range (because of the necessity to generate electrical power of an assumed frequency of either 50 Hz or 60 Hz). Also during the engine operation without the torque load numerous factors occur influencing the accuracy of measurements taken on the real object. The most essential include:

- lack of repeatability of the working cycle, particularly in case of low rates of the torque load,
- disturbances caused by the flow ducts of the indicator valves (occurrence of waving) [16]. These ducts are selected in such a manner to ensure the credible measurements of the indicated pressure for an engine operated at nominal revolutions with the nominal torque load,
- large length of the exhaust gas ducts causing the delays in recording the air excess factor,
- low accuracy of the measuring instrument used for measuring the fuel consumption rate (within the no-load operation range of the engine). This instrument was selected in such a manner, to ensure the performance of measurements for the whole range of admissible engine crankshaft revolutions and for the torque loads,
- the marine piston type internal combustion engines represent a high unrepeatability of operational parameters of individual cylinders. This is caused by differences in the manufacturing of the fuel injection apparatus components (the fuel rate is selected for the nominal operating conditions of the engine), cylinder head liners and a number of other components [12].

8. Conclusion

Both the research on models and the empirical tests carried out have proven the fact that the developed mathematical model is adequate within a wide range of crankshaft revolutions and engine indicated power. Excess of the adopted adequacy measures occurs only and exclusively in case when the engine operates with no load. The high adequacy of the model has allowed to commence the second

stage of the research program (Fig. 4). Moreover, based upon the analysis of the pressure curves shown in Fig. 5 (the model research and results obtained from the empirical tests) a conclusion may be drawn up that the application of the developed model may be decidedly wider than that used in our research. The high level of adequacy and versatility

of the said model (possibility to model practically any four-stroke type Diesel engine) and also possibility to simulate selected conditions of a partial technical fitness for use make this model a useful tool for the development of other parametric methods for evaluation of technical fitness of the marine engines.

Bibliography

- [1] BOGDANOWICZ, A., KNIAZIEWICZ, T., ZACHAREWICZ, M. The use of a mathematical model of marine diesel engine in a computer program. *New Trends in Production Engineering*. 2018, **1**(1), 453-460. <https://doi.org/10.2478/htpe-2018-0056>
- [2] CAVINA, N., BUSINARO, A., ROJO, N. et al. Combustion and intake/exhaust systems diagnosis based on acoustic emissions of a GDI TC engine. *Energy Procedia*. 2016, **101**, 677-684. <https://doi.org/10.1016/j.egypro.2016.11.086>
- [3] CHIATTI, G., CHIAVOLA, O., RECCO, E. et al. Accelerometer measurement for MFB evaluation in multi-cylinder diesel engine. *Energy*. 2017, **133**, 843-850. <https://doi.org/10.1016/j.energy.2017.04.148>
- [4] CHŁOPEK, Z., PIASECZNY, L. Badania procesów szybkozmiennych zachodzących w silniku spalinowym. *Zeszyty Naukowe AMW*. 2004, **2**(157), 5-28.
- [5] CWALINA, A., KNIAZIEWICZ, T., ZACHAREWICZ, M. Problems of mathematical modelling of the marine diesel engine working cycle for the diagnostic purposes. *Solid State Phenomena*. 2015, **236**, 212-219. <https://doi.org/10.4028/www.scientific.net/ssp.236.212>
- [6] KLUCZYK, M., GRZADZIELA, A. Vibration diagnostics of the naval propulsion systems. *Scientific Journal of Polish Naval Academy*. 2017, **1**(208), 15-29. <https://doi.org/10.5604/0860889x.1237619>
- [7] KNIAZIEWICZ, T., ZACHAREWICZ, M. Ocena adekwatności modelu okrętowego tłokowego silnika spalinowego opracowanego na potrzeby badań diagnostycznych. *Zeszyty Naukowe Akademii Morskiej w Gdyni*. 2018, **108**, 67-80.
- [8] KORCZEWSKI, Z., ZACHAREWICZ, M. Alternative diagnostic method applied on marine diesel engines having limited monitoring susceptibility. *Transaction of the Institute of Measurement and Control. SAGE*. 2012, **34**, 937-946. <https://doi.org/10.1177/0142331211426170>
- [9] KORCZEWSKI, Z., ZACHAREWICZ M. The method of diagnosing warships engines with a limited capability of measuring indicating pressures based on the results of the gasdynamic processes in the turbocharging system. *Polish Naval Academy*. Gdynia 2008. Research project: OT00B02129.
- [10] ŁUTOWICZ, M. Reverse IIR filter as a tool for cylinder indicating channel patency impact correction on measured cylinder pressure waveform. *Journal of KONES*. 2013, **20**, 253-259.
- [11] PAWLETKO, R., POLANOWSKI, S. Evaluation of current developments and trends in the diagnosis of marine diesel engines based on the indicator diagrams analysis. *Journal of KONES Powertrain and Transport*. 2014, **21**(4), 389-396. <https://doi.org/10.5604/12314005.1130492>
- [12] PIASECZNY, L. Technologia napraw okrętowych silników spalinowych. *Wydawnictwo Morskie*. Linkoping 1992.
- [13] POLAŃSKI, Z. Planowanie doświadczeń w technice. *PWN*. Warszawa 1984.
- [14] WITKOWSKI, K. The issue of the indicator diagram analysis for the purpose of diagnosis of marine diesel engines. *Journal of KONES Powertrain and Transport*. 2015, **22**(2), 293-298. <https://doi.org/10.5604/12314005.1165456>
- [15] ZACHAREWICZ, M. A method of diagnosing working spaces of a marine engine based on gas-dynamic parameters in the duct supplying the turbo-charger. *Polish Naval Academy*. Dissertation. 2009.
- [16] ZACHAREWICZ, M. Possibilities of parametric evaluation of the technical condition of a marine combustion engine of a low diagnostic susceptibility. *Polish Naval Academy*. Gdynia 2019.
- [17] ZACHAREWICZ, M., CWALINA, A. Research on energetic processes in a marine diesel engine driving a synchronous generator for diagnostic purposes. PART 1 – Physical model of the processes. *Journal of POLISH CIMAC*. 2013, **8**(1), 97-104.
- [18] ZACHAREWICZ, M., KNIAZIEWICZ, T. Research on energetic processes in a marine diesel engine driving a synchronous generator for diagnostic purposes. Part 2 mathematical model of the processes, *Journal of POLISH CIMEAC*. 2016, **11**(1), 199-209.
- [19] ZACHAREWICZ, M., KNIAZIEWICZ, T., CWALINA, A. Assessment of technical condition of marine auxiliary diesel engine on the basis of electrical measurements of synchronous generator. *Combustion Engines*. 2015, **3**(162), 170-176.
- [20] ŻÓŁTOWSKI, B., ŻÓŁTOWSKI, M. Vibration signals in mechanical engineering and construction. *ITE-PIB*. Radom 2015.

Tomasz Kniaziewicz, DSc., DEng. – Faculty of Mechanical and Electrical Engineering, Polish Naval Academy.

e-mail: T.Kniaziewicz@amw.gdynia.pl



Marcin Zacharewicz, DSc. DEng. – Faculty of Mechanical and Electrical Engineering, Polish Naval Academy.

e-mail: M.Zacharewicz@amw.gdynia.pl



Thermodynamic cycles variability of TJI gas engine with different mixture preparation systems

Gas engines are a viable source of propulsion due to the ecological indicators of gas fuels and the large amount of the needed natural resources. Combustion of lean homogeneous gas mixtures allows achieving higher thermal efficiency values, which is a key factor in current engine development trends. Using the spark-jet ignition system (also called as Turbulent Jet Ignition or two-stage combustion) significantly improves the efficiency and stability of the combustion process, especially in the part-load operation on lean or very lean mixtures. This paper presents the impact of using two different fuel injection methods: Port Fuel Injection or mixer on the operation stability of a gas engine designed for LDVs.

Comparative studies of two different mixture preparation systems were carried out on a single-cylinder AVL 5804 test engine. By recording the cylinder pressure for a significant number of engine cycles, it became possible to determine the repeatability of engine operation and to correlate the results with the mixture formation system and the air-fuel ratio. In the performed research the beneficial effect of the mixer system application on the engine operation stability in the part-load conditions was found.

Key words: CNG engine, cycle variations, Turbulent Jet Ignition, two-stage combustion, gas mixture formation

1. Introduction

Actually the most common energy sources supplied to internal combustion engines are liquid fuels derived from crude oil. This reliance on one type of resource encourages the search for alternative motor fuels, which are characterized by wide availability, low production costs and better ecological indicators. Natural gas seems to be an attractive alternative, whose reserves are estimated to be more than twice as high as the crude oil reserves [9]. The composition of natural gas strongly depends on where it was extracted from [2, 5]; however, regardless of this, the main component is always natural gas (methane, CH₄). Natural gas can be obtained from several sources, and its production is profitable due to the low production cost [10].

Methane has a low C/H ratio, thanks to which CO₂ emissions during combustion are reduced by about 25% when considered in TTW, along with a significant decrease in particulate emissions compared to gasoline [9].

An effective method of improving the ecological and energy indicators of a single-fuel gas engine is the use of lean mixtures combustion. However, such mixtures require large ignition energy, which can be obtained, for example, by using a divided combustion chamber or spark-jet ignition [13, 14, 21].

Gaseous fuel can be supplied to the engine through a mixer, fuel injection to the intake port (PFI) or using direct injection (DI). As a rule, mixer systems are being installed in heavy duty engines, while multi-point injection systems (PFI-type) are being used in LDVs. Each system has a different method of creating the mixture, which directly translates into different engine performance [8].

Research carried out in the scope of the repeatability of gas engine working cycles with a conventional ignition system indicated a decrease in work stability with an increasingly leaner mixture [15]. Singotia et al. [18] also noted a decrease in operation stability when increasing the engine speed, but when the load increased so did the stability.

Comparison of direct and indirect fuel injection solutions [19] indicated the essential role of the injection tim-

ing, which directly translates into the amount of time available for mixture formation. A lower COV_{IMEP} value was obtained in the whole analyzed range of fuel injection timing (330–120°CA bTDC) when using PFI injection. The disadvantage of this solution is the decrease in volumetric efficiency. Further research [11] conducted for lean gas combustion ($\Phi = 1/\lambda = 0.75\text{--}1.00$), indicated a more stable engine operation and greater thermal efficiency when using indirect injection for high engine loads. Direct injection provides better indicators when operating on partial loads.

Patel et al. [12] compared the direct CNG injection and the throttle body integrated mixer in relation to the engine speed. Higher thermal efficiency was achieved by using the mixer in the low engine speed range, while direct injection proved better when over 1500 rpm.

The impact of mixer design on the cycle operation repeatability in a six-cylinder in-line engine was discussed in [3]. Supplying of gas through cross beams placed perpendicular to the mixer axis was compared, relative to the circumferential arrangement in the case of lean combustion ($\lambda = 1.7$). The lower mean coefficient of cycle variation in all cylinders was observed for the mixer with nozzles placed radially.

A two-stage combustion system, which was also the subject of this paper, has been in development since the 1920s all the way to the present day. The main purpose of its application is to obtain large ignition energy, which is particularly important when burning lean mixtures. Due to the prospects of implementing the solution on a large scale, various construction variants have been proposed [22].

The use of this type of system allows increasing the limits of stable engine operation (COV_{IMEP} < 5) in conditions of lean mixtures combustion as compared to a conventional system with open geometry combustion chamber [16]. In addition, it significantly intensifies the combustion process, which is particularly important due to the slower laminar flame speed of natural gas compared to gasoline [1, 4].

2. Aim and scope of research

The use of a spark-jet ignition system in a single-fuel gas engine results in a change of the nature of the combustion process when compared to the conventional (SI) solution. In the analyzed case, the engine was fed with a pre-mixed fuel-air mixture. The degree of mixture homogeneity depends mainly on the method of its preparation. Hence, various methods of gaseous fuel injection are used. The purpose of the research described in this paper is to assess the impact of various CNG supply methods on the operation stability of an engine with an additionally supplied pre-chamber.

The scope of research reported here includes conducting an experiment on a test stand equipped with a single-cylinder test engine. In the tests engine parameters with two different CNG injection systems were recorded: gas delivery by PFI system and by gas-air mixer, as described later in chapter 3.3. In both cases however, the small ignition gas quantity was supplied by jet igniter mounted in small pre-chamber located in the center of cylinder head (s.c. active pre-chamber).

3. Methodology of research

3.1. Test stand

To measure the impact of the combustible mixture homogeneity on the gas engine operation stability, a test stand equipped with a single-cylinder AVL 5804 engine was used, with its technical data listed in Table 1. The modernization of the engine cylinder head, which was previously used as a dual fuel system, allowed the use of a Turbulent Jet Ignition system. The jet igniter (Fig. 1) consists of a small volume pre-chamber, a housing with a spark plug and a direct gas injection system. Gas is dispensed to the ignition chamber through the injector connected to the pre-chamber with a tube ended with a check valve. The chamber has 10 nozzles, 7 were placed radially, while 3 were placed in the cylinder axis.

The engine was connected to an asynchronous brake operating in the range of -50–300 Nm and ensuring that the engine operates at as constant a speed as possible. The cooling and lubrication system (AVL 577) works independently of the engine speed. It allows obtaining stable thermal conditions up to the water and oil temperature of 150°C.

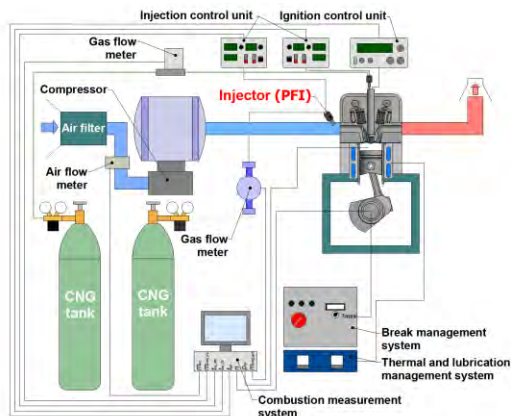


Fig. 2. Schematic of single cylinder engine test stand with port fuel injection system (PFI)

During the tests, the test stand was used in two configurations described in Figs 2 and 3. The difference concerned the system for creating the main combustible mixture. In the first test series, gas injection to the intake manifold (PFI) was used, while in the second, the mixer (M) was used. The intake system was equipped with a supercharging device that allowed smooth pressure regulation in the intake manifold. It consisted of an electric motor driven mechanical compressor and an expansion tank. The exhaust system did not contain any aftertreatment systems.

The CNG tank consisted of two cylinders with pressure reducers, which supplied with gas the igniter and main chamber independently. This made it possible to obtain different injection pressures for those two. Two independent manually adjusted controllers were used to control the injection system operation. They allowed regulating of the start time and duration of fuel injection in a wide range. The ignition time and coil charging current were also adjusted manually.

Table 1. Engine technical data

Engine	single cylinder AVL 5804
Displacement volume	510.7 cm ³
Bore × stroke	85 × 90 mm
Pre-chamber volume	1.8 cm ³
Compression ratio	15.2
Piston bowl shape	omega ω
Cooling system	liquid
Boosting system	mechanically driven supercharger

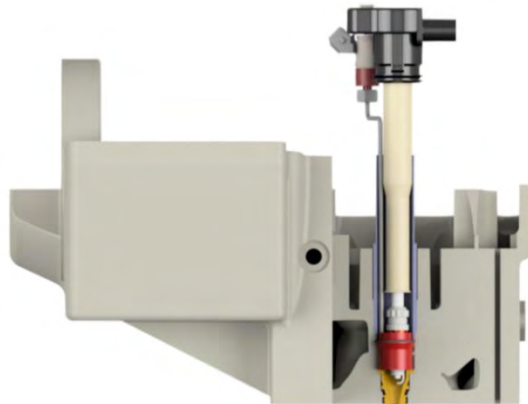


Fig. 1. Cross-section view of jet igniter mounted in AVL 5804 cylinder head

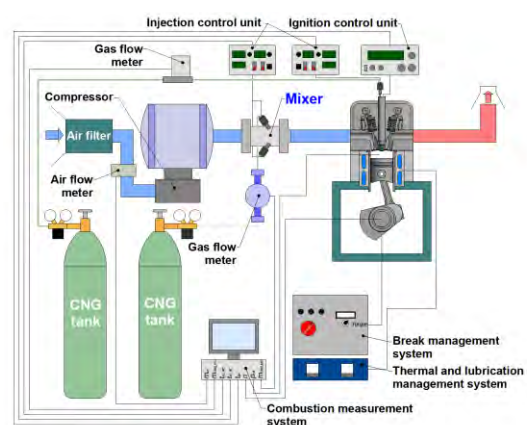


Fig. 3. Schematic of single cylinder engine test stand with mixer (M) injection system

3.2. Methodology and research conditions

The AVL IndiSmart fast variable parameter registration system was used in the research. The data was processed on an ongoing basis using the AVL IndiCom software. The pressure was measured using an AVL GH14D piezoelectric transducer with a measuring range of 0–250 bar mounted in the engine cylinder head. The engine speed was recorded using an optical crank angle marker AVL 364C. The mass air and CNG flow rates were measured by three flow meters with different working ranges, whose exact parameters were provided in Table 2. Based on the data of the amount of CNG supplied, the fuel doses per cycle dispensed to the cylinder (q_{oMC}) and to the pre-chamber (q_{oPC}) were determined. The air-fuel equivalence ratio λ was calculated according to formula (1). Its value was adjusted by changing the pressure in the intake system, which led to a change in the mass air flow rate. Fuel injection time and ignition time were read using clamp meters.

$$\lambda = \frac{m_{air}}{(m_{fuel_PC} + m_{fuel_MC}) \times L_t} \quad (1)$$

Tests for both injection systems were carried out under the same conditions. The parameter that changed during the engine operation was the value of the air-fuel equivalence ratio, as it varied in the range 1.2–1.55. Data was recorded for three engine operating points at 1500 rpm. The total amount of fuel per cycle was constant during testing and the load was about 7 bar of IMEP. The gas injection start time for both chambers was the same at 300°CA bTDC in the intake stroke. Ignition was determined individually at individual work points. The ignition timing was adjusted so that the COC was located 8°CA aTDC. The COC was assumed to be the camshaft angle for which 50% of the fuel dose was burned, MBF50%, and was calculated based on the integral of heat released.

Table 2. Mass flow meters technical data

Parameter	Name	Specification
Air mass flow	Sensycon Sensyflow	0–720 kg/h ($\pm 1\%$)
Main chamber fuel mass flow	Emerson mCMFS	0.1–2 kg/h ($\pm 0.25\%$)
Pre-chamber fuel mass flow	Bronkhorst 111B	0.1–100 g/h ($\pm 0.5\%$)

During the tests, the parameters for 100 following engine cycles were recorded at a frequency of 0.1°CA. To qualitatively determine the repeatability of engine operation from cycle to cycle, COV values were determined according to formula (2). It determined the measure of the degree of variation in the value of the measured variable.

$$COV_{value} = \frac{\sigma_{value}}{\mu_{value}} \quad (2)$$

where σ_{value} is the standard deviation:

$$\sigma_{value} = \sqrt{\frac{\sum_{i=1}^N (x_i - \bar{x})^2}{N}} \quad (3)$$

and μ_{value} is the arithmetic average:

$$\mu_{value} = \frac{1}{N} \sum_{i=1}^N x_i \quad (4)$$

3.3. Injection methods

A gas engine with an additional combustion chamber requires at least two fuel supply systems. In the analyzed case, direct fuel injection into the ignition chamber was used, as well as either an external PFI or a mixing system. The specification of the solutions used during the tests was shown in Table 3. In order to obtain a low dose of q_{oPC} a choking system was installed between the injector and the pipe supplying fuel to the pre-chamber.

Table 3. Gas injection systems specification

Apply	Type	Injector quantity	Injection pressure	Fuel dose [mg/inj]
PC	DI	1	6 bar	0.38
MC	PFI	1	9 bar	19.9
MC	Mixer	4	9 bar	19.9

PFI injection was carried out using a single dedicated electromagnetic injector for CNG supply. It was placed so that the fuel was injected into one of the cylinder head's inlet port. The second system used a mixer built into the intake system at a considerable distance from the engine head. Mixer (Fig. 4) consisted of the housing (2), in which four injectors (3), fuel supply rails (4) and throttle (1) were placed. The body had a network of channels supplying fuel to the nozzle located circumferentially and in crossed beams.



Fig. 4. View of 3D mixer model used in research

4. Discussion of results

Depending on the literature sources, researchers performing similar work used different numbers of recorded engine cycles [7, 17]. Due to the low level of values dispersion for the measured parameters, 100 cycles were deemed a sufficient number for the considered engine tests. The obtained data was presented in a general way as statistical data as well as in a more detailed way. The studies compared external systems for creating an air-fuel mixture, ensuring different quality of the obtained mixture. The air-fuel equivalence ratio λ varied in the range 1.2 to 1.55 during the performed tests. This is due to the specific benefits of lean mixtures combustion.

Figure 5 presents a series of recorded pressure curves for the cylinder as a function of crankshaft angle at the maximum value of the air-fuel equivalence ratio $\lambda = 1.55$. Data for the PFI system are marked in red, and data for the

mixer system (M) are blue. The maximal and minimal peak of pressure for all cycles is specified as a P_{\max} and P_{\min} . Greater divergence of values was found for the fuel injection into the intake duct. This system ensures worse mixing of the gaseous fuel with air, if only due to the smaller amount of time available. A significant part of the mixture formation process takes place directly in the cylinder during the intake and compression strokes. In comparison, while applying the mixer system the formation of the mixture begins in the intake system at a considerable distance from the engine head and much more time is available for better mixture homogenization. In addition, gas and air diffusion was supported by the mixer geometry.

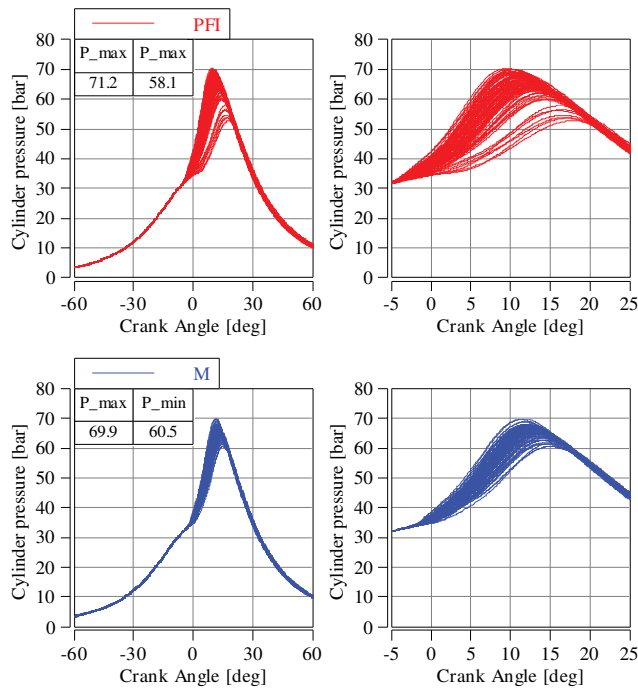


Fig. 5. Dispersion of in cylinder pressure trace for equivalence ratio $\lambda = 1.55$, PFI marked in red, mixer system in blue

The parameter most commonly used to determine the engine operation stability is the coefficient of variation of the indicated mean effective pressure COV_{IMEP} [20], the results of which were shown in Fig 6. The limit value above which the engine is operating incorrectly is being accepted 5% [6]. In the case of gas engines, this is a particularly important parameter when determining the effective flammability limits of an air-fuel mixture. In the analyzed case, the lowest value was achieved for $\lambda = 1.35$; below and above this value the COV_{IMEP} increases. This is probably related to the dependence of the laminar flame velocity on the composition of the combustible mixture.

One should keep in mind that the fuel dose delivered to the ignition chamber was small due to this being the most energy efficient way. As one can observe in the Fig. 6, in the whole analyzed range, more stable operation was obtained using a mixer.

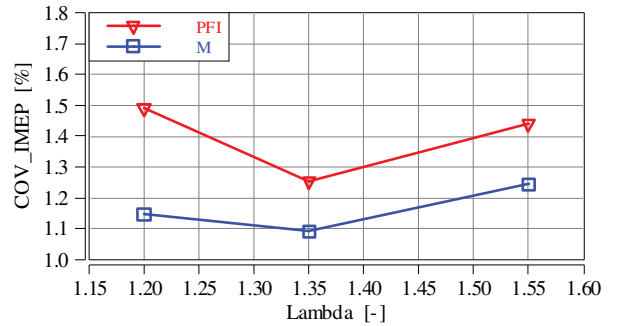


Fig. 6. Effects of injection system on coefficient of variation of indicated mean effective pressure (IMEP) for different charge composition

Figure 7 shows the distribution of the number of cycles in which IMEP falls within a given range for three selected λ values. In the case of the leanest mixture, larger IMEP values were obtained by using injection before the intake valve. Then, along with the decreasing value of λ , the IMEP value increased in favor of the mixer system. This is probably due to the loss of the fresh fuel dose generated by the mixer when the timings overlapped. The air-fuel equivalence ratio increased by increasing the pressure in the intake system, which promoted the flow of fresh fuel dose remaining from the previous cycle directly to the exhaust system.

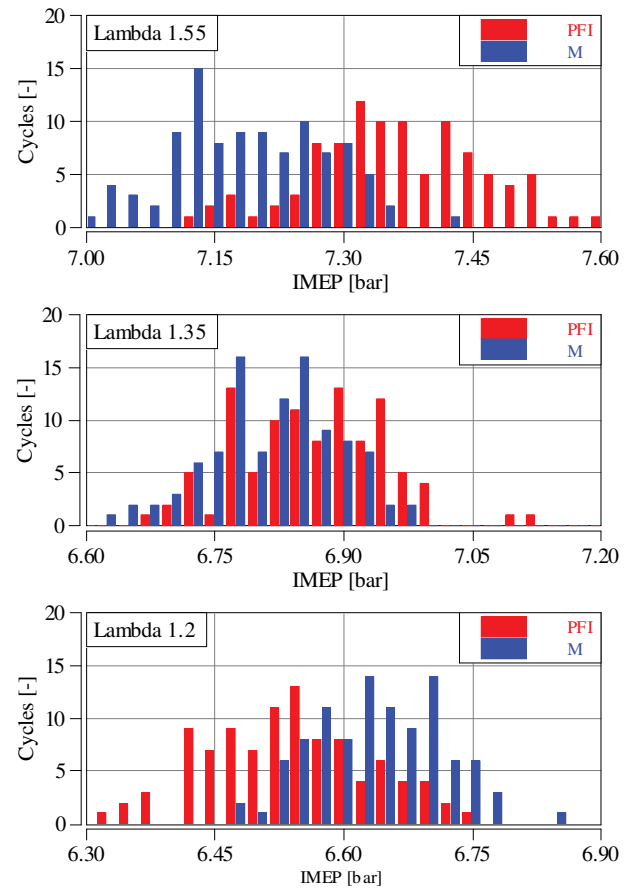


Fig. 7. Histogram of indicated mean effective pressure for three different lambda values

The maximum pressure in the cylinder was then taken into account, as well. This is one of the important indicators

of the intensity and regularity of the combustion process. According to the results presented in Fig. 8, in the entire λ range, as it was in the case of COV_{IMEP} , gas injection through the mixer provides greater engine operation stability. The characteristic shape of both curves varied. In the case of the PFI system, as the dose becomes leaner, the COV increases, i.e. the repeatability of individual work cycles decreases. The use of the mixer significantly stabilizes the combustion process especially in the range of $\lambda = 1.2\text{--}1.35$. The largest difference of 3% was recorded for the leanest mixture.

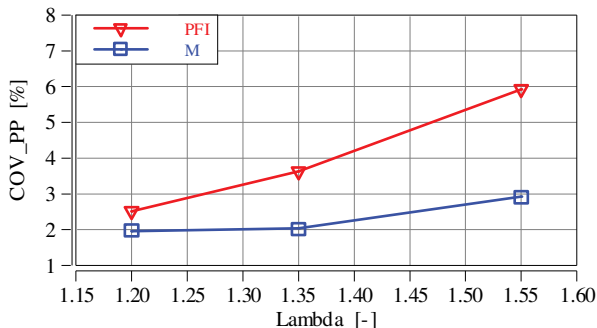


Fig. 8. Effects of injection system on coefficient of variation of peak pressure (PP) for different charge composition

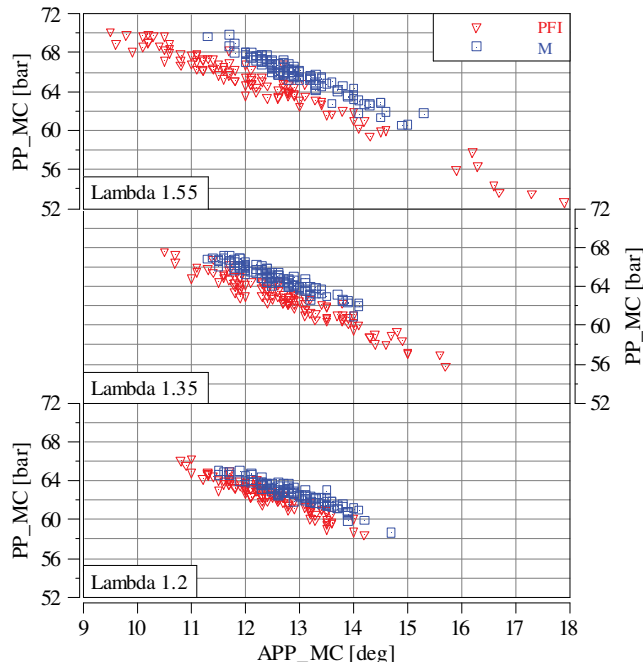


Fig. 9. Distribution of peak pressure points for three different lambda values

A more accurate analysis of the maximum combustion pressure is presented in the form of point maps, Fig. 9. The vertical axes show the maximum pressure values, the horizontal axis is the crankshaft angle CA at which the maximum pressure occurred. The later the pressure reached its maximum, the lower was its recorded value. This is due to the change in cylinder volume during the combustion stroke. The spread of data points increased with the increase of λ , this is especially visible with the PFI system.

The mixture richer in fuel has lower ignition requirements in relation to the lean mixtures. Despite the use of a high-efficiency ignition mechanism in the PFI system, there still are data points where the combustion was abnormal ($\lambda = 1.35\text{--}1.55$). This was probably due to insufficient mixing of the fuel and air, leading to the creation of local areas that were very difficult to ignite.

Data regarding the combustion process duration refers to the amount of MBF relative to the crankshaft rotation angle. The results of the variable nature of the combustion process were shown as $\text{COV}_{\text{MBF}50\%}$ (Fig. 10) representing the center of combustion and $\text{COV}_{\text{MBF}90\%}$ (Fig. 11) representing the end of combustion. In both cases, the observed trends were the same as those previously discussed. The $\text{COV}_{\text{MBF}90\%}$ value over the entire engine operating range was less than for $\text{COV}_{\text{MBF}50\%}$. This proves that the process had higher repeatability in the second phase of combustion.

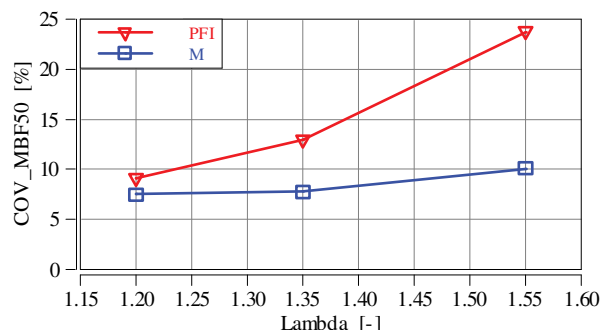


Fig. 10. Effects of injection system on coefficient of variation of 50% mass burned friction (MBF50%) for different charge composition

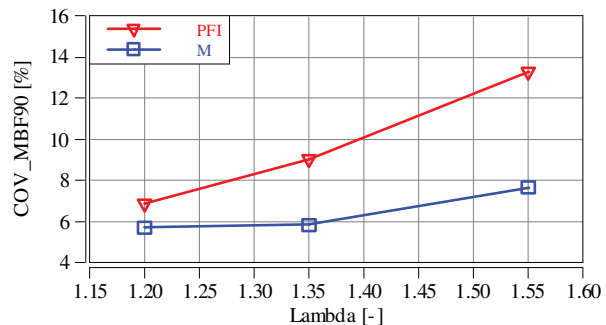


Fig. 11. Effects of injection system on coefficient of variation of 90% mass burned friction (MBF90%) for different charge composition

As previously mentioned, the parameter relative to which the ignition timing was regulated for each test point was the center of combustion COC. The ignition timing was adjusted so that MBF50% was 8°CA aTDC. Figure 12 shows the distribution of the MBF50% values for the 100 registered engine cycles. While recording the engine operating parameters, the ignition system controller was set to generate a spark trigger signal at a constant time. A larger spread of values can be found when using the PFI system. In the conditions of lean mixture combustion, the difference between the minimum and maximum MBF50% reached up to 9°CA compared to the 3.7°CA for the tested mixing system.

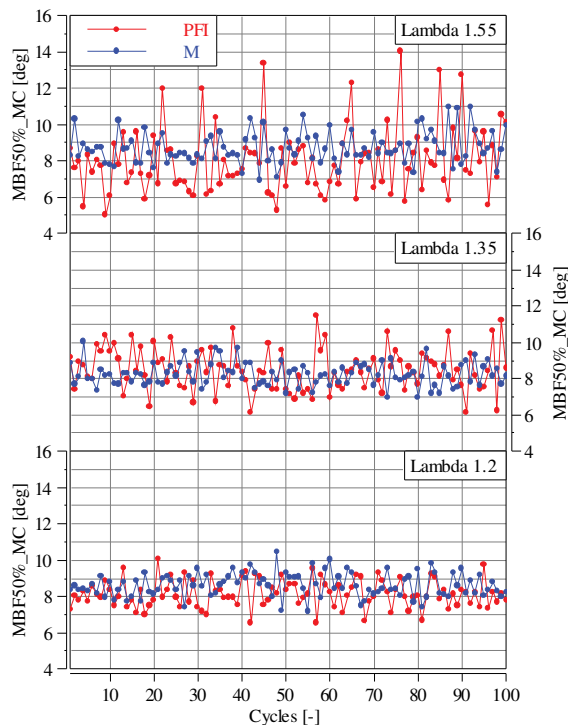


Fig. 12. Cycle by cycle variability of MBF50% for three different lambda values

5. Conclusion

The results of research on the stability of a gas engine operation equipped with a modern two-stage combustion system have been presented in the paper. The analyzed solution was dedicated to LDV vehicles. The large amount of energy generated by the TJI (or spark-jet) ignition system allows to effectively ignite lean mixtures, which can be interpreted directly as a possibility of improving the engine's operating indicators. An important element affecting the engine operation is the mixture creation system. There-

fore, two different methods of gaseous fuel injection were compared in this study.

The compared injection systems were characterized by different degrees of homogeneity of the created air-fuel mixtures. The use of CNG injection into the intake duct shortened the time available for mixing fuel with the air. As a result, the mixture is less homogeneous than the one obtained through the use of a mixer placed in the intake system.

The conducted research indicates the beneficial effects of combustion using more homogeneous mixtures on the repeatability of engine operation from one work cycle to the next. Lower COV_{IMEP} value for mixer fuel supply throughout the whole engine operating range was obtained from a statistical analysis of the results. In each of the analyzed cases, COV_{IMEP} was well below the value considered as a limit for stable engine operation. In the case of combustion of the mixture at $\lambda = 1.2$ the difference was 23% while for $\lambda = 1.55$ it was 14%. The same trends were observed for the other indicators (COV_{PP}, COV_{MBF50%}, COV_{MBF90%}). In addition, the use of a gas-air mixing support system allowed avoiding abnormal combustion in individual engine operating cycles. The disadvantage, however, was the presence of gaseous fuel in a significant volume of the intake system. This creates a risk of backfire as well as fuel leak directly to the exhaust system during the valve overlap timing.

Acknowledgements

This work was partially supported by the EU – Horizon 2020 (grant number 652816) performed within the years 2014-2019 and the investigations were extended with the support of the Subvention of Polish Ministry of Higher Education, project DS-PB 05/52/SBAD/0297.

Nomenclature

CA	crank angle
CNG	compressed natural gas
COV	coefficient of variation
COC	center of combustion
DI	direct injection
IMEP	indicated mean effective pressure
LDV	light duty vehicle
MBF	mass burned fraction
MC	main chamber

PC	pre-chamber
PFI	port fuel injection
PP	peak pressure
SI	spark ignition
TJI	turbulent jet ignition
TTW	tank to wheel
λ	air excess ratio
Φ	equivalence ratio ($1/\lambda$)

Bibliography

- [1] BUESCHKE, W., SKOWRON, M., WISŁOCKI, K., SZWAJCA, F. Comparative study on combustion characteristics of lean premixed CH₄/air mixtures in RCM using spark ignition and turbulent jet ignition in terms of orifices angular position change. *Combustion Engines*. 2019, **176**(1), 36-41. <https://doi.org/10.19206/CE-2019-105>
- [2] CADAVID, Y., AMELL, A. The effect of natural gas composition and atmospheric humidity on premixed combustion across the regions of Colombia. *Thermal Science and Engineering Progress*. 2019, **10**, 198-207. <https://doi.org/10.1016/j.tsep.2019.01.015>
- [3] CHEOLWOONG, P., SUNGWON, L., GIHUN, L. et al. Effect of mixer type on cylinder-to-cylinder variation and performance in hydrogen-natural gas blend fuel engine. *International Journal of Hydrogen Energy*. 2013, **38**, 4809-4815. <https://doi.org/10.1016/j.ijhydene.2013.01.079>

- [4] CHIODI, M., FERRARI, A., MACK, O. et al. A way towards remarkable reduction of CO₂-emissions in motor-sports: the CNG-engine. *SAE Technical Paper* 2011-37-0006. 2011. <https://doi.org/10.4271/2011-37-0006>
- [5] FARAMAWY, S., ZAKI, T., SAKR A.A.-E. Natural gas origin, composition, and processing: a review. *Journal of Natural Gas Science and Engineering*. 2016, **34**, 34-54. <https://doi.org/10.1016/j.jngse.2016.06.030>
- [6] GALLONI, E. Analyses about parameters that affect cyclic variation in a spark ignition engine. *Applied Thermal Engineering*. 2009, **29**(5-6), 1131-1137. <https://doi.org/10.1016/j.applthermaleng.2008.06.001>
- [7] HUNICZ, J. Cycle-by-cycle variations in autonomous and spark assisted homogeneous charge compression ignition combustion of stoichiometric air-fuel mixture. *International Journal of Spray and Combustion Dynamics*. 2018, **10**(3), 231-243. <https://doi.org/10.1177/1756827718763564>
- [8] JI, S., LAN, X., CHENG, Y. et al. Cyclic variation of large-bore multi point injection engine fuelled by natural gas with different types of injection systems. *Applied Thermal Engineering*. 2016, **102**, 1241-1249. <https://doi.org/10.1016/j.applthermaleng.2016.03.082>
- [9] KRAMER, U., FERRERA, M., KUNNE, H. et al. Natural gas/methane fuels: European automotive fuel quality and standardization requirements. *Gas Powered Vehicles Conference*. Stuttgart 2015.
- [10] LYONS, W.C., PLISGA, G.J., LORENZ, M.D. Standard handbook of petroleum and natural gas engineering. Chapter 7: Petroleum economic evaluation. *Gulf Professional Publishing* 2016. <https://doi.org/10.1016/B978-0-12-383846-9.00007-2>
- [11] MOON, S. Potential of direct-injection for the improvement of homogeneous-charge combustion in spark-ignition natural gas engines. *Applied Thermal Engineering*. 2018, **136**, 41-48. <https://doi.org/10.1016/j.applthermaleng.2018.01.068>
- [12] PATEL, R., BRAHMBHATT, P. Performance characteristics comparison of CNG port and CNG direct injection in spark ignition engine. *European Journal of Sustainable Development Research*. 2018, **2**(2), 26. <https://doi.org/10.20897/ejosdr/82058>
- [13] PIELECHA, I., BUESCHKE, W., CIEŚLIK, W. et al. Turbulent spark-jet ignition in SI gas fuelled engine. *MATEC Web of Conferences*. 2017, **118**, 00010-1-00010-10. <https://doi.org/10.1051/matecconf/201711800010>
- [14] PIELECHA, I., BUESCHKE, W., SKOWRON, M. et al. Prechamber optimal selection for a two stage turbulent jet ignition type combustion system in CNG-fuelled engine. *Combustion Engines*. 2019, **176**(1), 16-26. <https://doi.org/10.19206/CE-2019-103>
- [15] REYES, M., TINAUT, F., GIMENEZ B. et al. Characterization of cycle-to-cycle variations in a natural gas spark ignition engine. *Fuel*. 2015, **140**, 752-761. <https://doi.org/10.1016/j.fuel.2014.09.121>
- [16] SCHUMACHER, M., WENSING, M. A gasoline fuelled pre-chamber ignition system for homogeneous lean combustion processes. *SAE Technical Paper* 2016-01-2176. 2016. <https://doi.org/10.4271/2016-01-2176>
- [17] SHI, J., WANG, T., ZHAO, Z. et al. Cycle-to-cycle variation of a diesel engine fueled with Fischer-Tropsch fuel synthesized from coal. *Applied Sciences*. 2019, **9**, 2032. <https://doi.org/10.3390/app9102032>
- [18] SINGOTIA, P.K., SARASWATI, S. Cycle-by-cycle variations in a spark ignition engine fueled with gasoline and natural gas. *IOP Conference Series: Materials Science and Engineering*. 2019, **691**, 012061. <https://doi.org/10.1088/1757-899X/691/1/012061>
- [19] SONG, J., CHOI M., PARK, S. Comparisons of the volumetric efficiency and combustion characteristics between CNG-DI and CNG-PFI engines. *Applied Thermal Engineering*. 2017, **121**, 595-603. <https://doi.org/10.1016/j.applthermaleng.2017.04.110>
- [20] STONE, R. Introduction to internal combustion engines. *Macmillan International Higher Education*. 2012. 135.
- [21] SYROVATKA, Z., VITEK, O., VAVRA, J. et al. Scavenged pre-chamber volume effect on gas engine performance and emissions. *SAE Technical Paper* 2019-01-0258. 2019. <https://doi.org/10.4271/2019-01-0258>
- [22] TOULSON, E., SCHOCK, H., ATTARD, W. A review of pre-chamber initiated jet ignition combustion systems. *SAE Technical Paper* 2010-01-2263. 2010. <https://doi.org/10.4271/2010-01-2263>

Filip Szwajca, MEng. – Faculty of Civil and Transport Engineering, Poznan University of Technology.

e-mail: Filip.Szwajca@put.poznan.pl



Prof. Krzysztof Wislocki, DSc., DEng. – Faculty of Civil and Transport Engineering, Poznan University of Technology.

e-mail: Krzysztof.Wislocki@put.poznan.pl





INSTYTUT TECHNICZNY WOJSK LOTNICZYCH

ul. Księcia Bolesława 6, 01-494 Warszawa, skr. poczt. 96

tel.: 261 851 300; faks: 261 851 313

www.itwl.pl

e-mail: poczta@itwl.pl

SYSTEM DIAGNOSTYKI TRIBOLOGICZNEJ

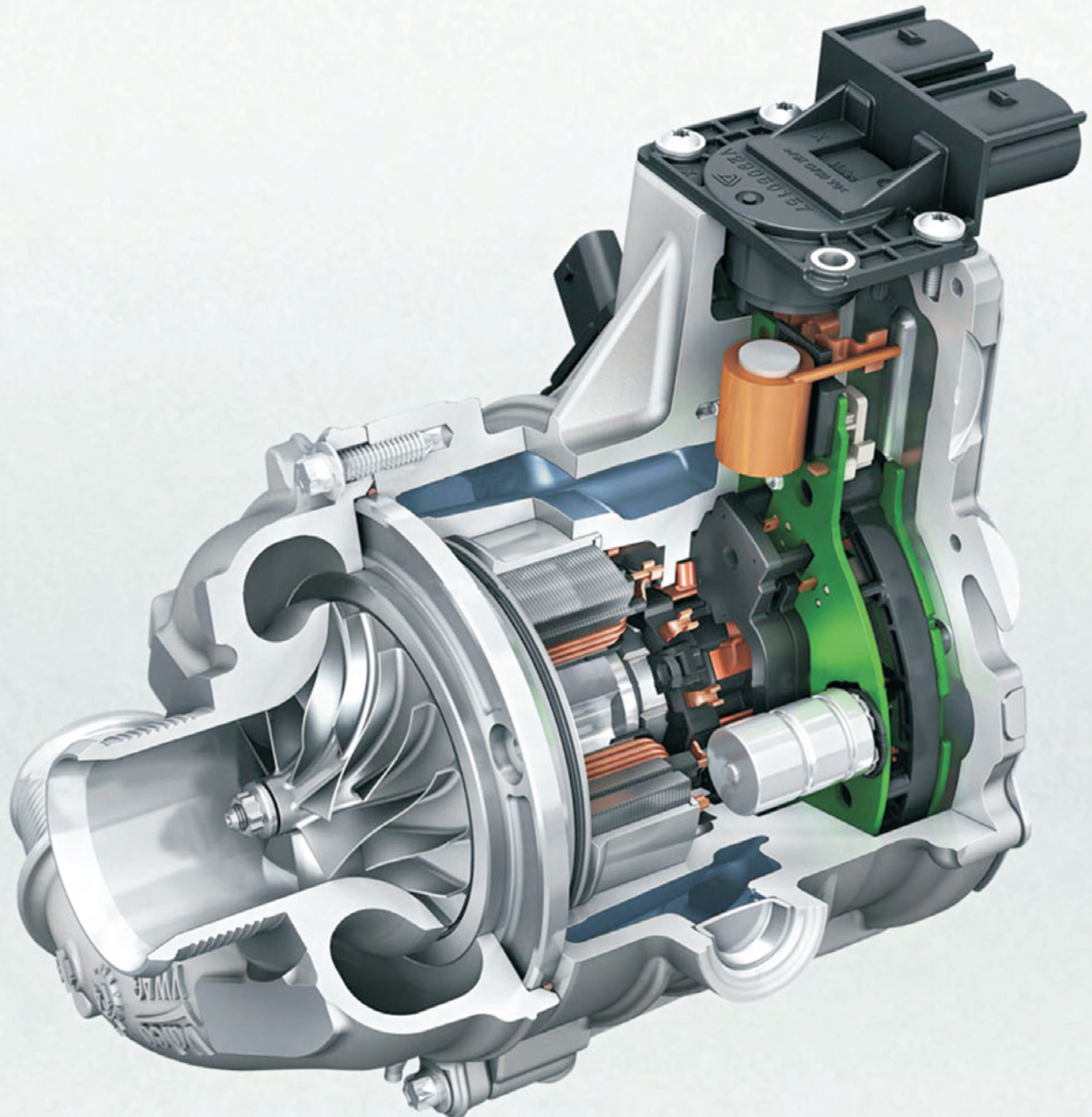


System Diagnostyki Tribologicznej (SDT), opracowany w Instytucie Technicznym Wojsk Lotniczych, przeznaczony jest do wspierania eksploatacji obiektów technicznych.

Na podstawie wyników badań próbek oleju pobranych z układów tribologicznych prowadzi się ocenę i prognozowanie stanu technicznego obiektów technicznych (statki powietrzne, pojazdy mechaniczne, statki wodne, maszyny robocze i inne).



INSTYTUT TECHNICZNY WOJSK LOTNICZYCH
ZAKŁAD SILNIKÓW LOTNICZYCH
Akredytowane laboratorium:
Laboratorium Diagnostyki Systemów Tribologicznych



Publisher:

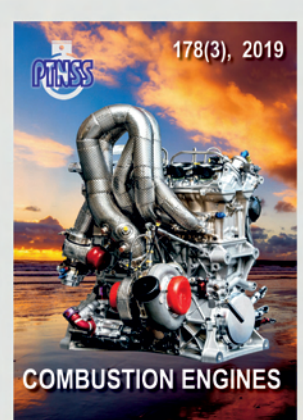
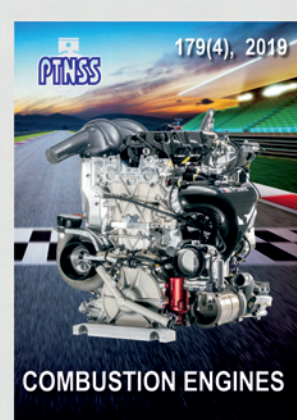
Polish
Scientific
Society
of Combustion
Engines



ISSN: 2300-9896
eISSN: 2658-1442

Combustion Engines

Polskie Towarzystwo Naukowe Silników Spalinowych



www.combustion-engines.eu